Gravitational self-force and the weak Cosmic Censorship

by Marta Colleoni

A thesis presented for the degree of

Doctor of Philosophy

Faculty of Social and Human Sciences

Mathematical Sciences

University of Southampton

June 2016

University of Southampton

ABSTRACT

Faculty of Human and Social Sciences

Mathematical Sciences

Doctor of Philosophy

GRAVITATIONAL SELF-FORCE AND THE WEAK COSMIC CENSORSHIP

by Marta Colleoni

We study the scenario in which a massive, non-spinning, uncharged particle is captured by a rapidly rotating Kerr black hole, so that the final state does not contain an event horizon—in what would be a violation of weak cosmic censorship. We work in black-hole perturbation theory, and focus on particles sent in on equatorial orbits.

We first identify the complete parameter-space region in which overspinning occurs when back-reaction effects from the particle's self-gravity are ignored. Gravitational self-force effects may prevent particles with suitable parameters from ever entering the black hole—by radiating away a sufficient amount of the particle's angular momentum ("dissipative effect") and/or by increasing the effective centrifugal repulsion ("conservative effect").

We analyze the full effect of the self-force and derive a necessary and sufficient "censorship" condition that includes the effect of the full, first-order self-force. Our criterion involves certain self-force quantities calculated on the one-parameter family of unbound critical orbits in the extremal limit.

A self-force computation along such orbits is currently unavailable in Kerr spacetime. However, we argue that it is possible to reformulate the problem in terms of variables computed on circular orbits, relying on a certain variational law that goes under the name of "first law of binary black-hole mechanics". We obtain the required self-force data, and present strong evidence to suggest that captured particles never drive the black hole beyond its extremal limit and can at most saturate it. To entirely rule out such a possibility would require information about higher-order self-force corrections.

Here we also start developing the computational methods required to perform calculations of the self-force along unbound orbits, in order to eventually allow a rigorous test of our results. As a first example, we develop method and code to compute the self-force along a marginally bound critical orbit in *Schwarzschild* spacetime. We compute the shift in the frequency of the innermost bound circular orbit, and the shift in the critical value of the angular momentum of a zero-binding-energy critical orbit. Both calculations require knowledge of the gravitational self-force along a parabolic-like orbit. We show that the frequency shift computed by integrating the self-force along a marginally bound orbit is consistent with the result obtained applying the first law. Thus, our calculation provides reassurance that our reformulation of the overspinning condition is indeed correct; it also paves the way to the computation of new self-force invariants in the high-energy regime, such as deflection angles for hyperbolic-like orbits.

Contents

List of Figures

Declaration of authorship

I, Marta Colleoni, declare that the thesis entitled:

Gravitational self-force and the weak Cosmic Censorship

and the work presented in the thesis are both my own, and have been generated by me as the result of my own original research. I confirm that:

- This work was done wholly or mainly while in candidature for a research degree at this University;
- Where any part of this thesis has previously been submitted for a degree or any other qualification at this University or any other institution, this has been clearly stated;
- Where I have consulted the published work of others, this is always clearly attributed;
- Where I have quoted from the work of others, the source is always given. With the exception of such quotations, this thesis is entirely my own work;
- I have acknowledged all main sources of help;
- Where the thesis is based on work done by myself jointly with others, I have made clear exactly what was done by others and what I have contributed myself;
- Parts of this work have been published as:

  1. M. Colleoni and L. Barack, "Overspinning a Kerr black hole: the effect of self-force", *Phys. Rev. D*, vol. 91, p. 104024, May 2015.
  2. M. Colleoni, L. Barack, A. G. Shah and M. van de Meent, "Self-force as a cosmic censor in the Kerr overspinning problem ", *Phys. Rev. D*, vol. 92, p. 084044, October 2015.

Signed: Date:

Acknowledgements

I would like to thank my supervisor, Leor Barack, for offering me the opportunity to work in the Southampton self-force group. Without his continuous guidance, this work would have not been possible.

I would like to thank my examiners, David Ian Jones and Thomas Sotiriou, for reading this manuscript and for all the useful comments they provided.

Special thanks go to all the past and present Southampton "self-forcers", Adam Pound, Maarten van De Meent, Abhay G. Shah, Charalampos Markakis, Sarp Akcay, Jeremy Miller and Paco Giudice, for the many times they endured hours-long discussions about my research. I would like to especially thank my "brother in self-force", Cesar Antonio Merlin Gonzalez.

I am grateful to the Capra community, for providing a friendly environment to discuss about my PhD project.

I also wish to thank Niccolo' Sesana, Alessandra Casati, Cristian Consonni and Giacomo Germani for keeping in touch throughout the years I have spent far from them.

It is for me imperative to thank my officemates and friends Yafet E. Sanchez[2], Greg Ashton, Liana Kontogeorgaki and Vanessa Graber, for the many fun hours spent together. I would also like to thank Sam Mugel, who brightened up the office while he was around (and offered me countless cups of coffee).

Finally, I would like to thank my parents and Federico Demartin, for supporting me with their love and affection during the toughest moments of this four years long adventure.

List of acronyms

GW	Gravitational waves
EMRI	Extreme mass-ratio inspiral
(G)SF	(Gravitational) self-force
WCCC	Weak cosmic censorship conjecture
ISCO	Innermost stable circular orbit
IBCO	Innermost bound circular orbit
MBMS	Marginally bound marginally stable (orbit)
EOB	Effective one-body (model)

Chapter 1

Introduction

On February 11th 2016, the LIGO collaboration made a historic announcement: for the first time, gravitational waves (GW) had been detected by the interferometers located in Livingston and Hanford [1]. The signal was sourced by a binary system composed of two black holes, with initial masses $\sim 36M_\odot$ and $\sim 29M_\odot$, which coalesced into a black hole of mass $\sim 62M_\odot$ releasing a stunning $\sim 3M_\odot c^2$ in gravitational radiation's energy.

The detection not only represents the first direct measurement of GW (whose existence had been previously inferred indirectly from the study of the Hulse-Taylor system); it also heralds the beginning of a new era in astronomy. The information encoded in GW might shed light on many astrophysical problems: it could allow, for instance, to characterise neutron stars' equation of state [2], constrain models of formation and evolution of compact stars and black holes [3], and test fundamental aspects of General Relativity, such as the weak cosmic censorship conjecture [4].

Advanced LIGO can only detect signals emitted by compact objects of at most a few solar masses; events involving massive and supermassive black holes sit outside its frequency range, as their signals are overpowered by seismic noise. It is hoped that these phenomena will be detected in the near future by the space-borne interferometer eLISA, whose launch is currently scheduled for 2034. A preliminary mission, LISA pathfinder, was successfully launched in December 2015 and is currently being used as a test bed for eLISA's technologies.

Among eLISA's main targets, of particular interest are extreme mass-ratio inspirals (EMRIs), where a stellar-mass compact object of mass μ slowly spirals towards a massive black hole of mass $M \sim 10^5 M_\odot - 10^8 M_\odot$. During the inspiral, the compact object typically emits $O(10^5)$ cycles of GW, thus providing a detailed map of the strong-field

region around massive black holes. EMRIs are therefore excellent probes of fundamental aspects of General Relativity. Based on the GW's phase evolution during the inspiral, for instance, it should be possible to constrain with good precision the mass, spin and quadrupole moment of the central object [5]. This would provide a test of uniqueness theorems and possibly discriminate between Kerr and quasi-Kerr solutions [6, 7]. In fact, the mass and current multipoles of a Kerr black hole with spin parameter a satisfy the relation $M_l + i\,S_l = M(ia)^l$ [8]. Thus, a measurement of the mass, spin and quadrupole moment would provide a consistency check of no hair. It has also been pointed out [9] that an analysis of GW's propagation would allow to distinguish between General Relativity and some modified theories that allow massive modes, which are absent in the classical theory [1].

From a theoretical perspective, a natural framework to study EMRIs is that of the self-force approximation, which models back-reaction effects in terms of a perturbative expansion in the small parameter μ/M, around a background geometry determined by the central black hole. In this work we will rely on the first-order self-force formalism to address a fundamental issue in General Relativity, namely how the cosmic censorship conjecture is enforced in an EMRI-like system, where the central object is a nearly-extremal Kerr black hole. By 'first-order' we mean that only perturbative corrections $O(\mu/M)$ will be considered (this statement will become clearer in Sec. 1.1.2). After providing some basic notions about the self-force formalism (Sec. 1.1) as well as an overview of the weak cosmic censorship conjecture (Sec. 1.2) we will describe how one can "overspin" a Kerr black hole, and thus expose a naked singularity, by throwing in a test mass with suitable orbital parameters (Ch. 2). We will then provide a mathematical condition for the gravitational self-force (GSF) to prevent overspinning (Ch. 3). In Ch. 4, we will then evaluate such condition using state-of-the-art self-force codes. We will show that, generically, back-reaction contributes to preserve cosmic censorship, although there is a subset of orbits that can saturate the black hole's spin.

Our "no-overspinning" conditions will involve some integrals of the gravitational self-force along unbound, critical orbits (i.e. orbits sitting on the threshold between capture and scattering). However, since a direct numerical computation of these quantities in Kerr spacetime is not available yet, we will reduce the problem to that of calculating the self-force along circular orbits, by taking advantage of a certain variational law that goes under

[1] In their recent work [10], the LIGO collaboration estimated an upper limit on the graviton's mass $m_{grav} < 10^{-22} eV$.

the name of "first law of binary black-hole mechanics". The law holds when the perturbed spacetime is helically symmetric [11, 12], and therefore it is applicable to circular orbits.

An interesting feature of the first law is that it provides simple expressions to compute the first-order corrections to the binding energy and total angular momentum of the binary, which can prove useful to establish comparisons among different frameworks (in fact, conserved energies and angular momenta are commonly computed both in the post-Newtonian approximation and Numerical Relativity).

So far, a numerical computation of globally conserved quantities had never been tackled within the self-force scheme, where notions of globally conserved energy or angular momentum are not usually introduced [2]. However, it was suggested [13] that unbound orbits should offer a natural way to compute the binary's conserved energy and angular momentum: intuitively, it should be possible to extract these quantities from the self-force corrected orbital parameters when the small mass μ is at an infinite distance from the central object.

In this work, we will lay the foundation to accomplish this goal. We will focus on the special family of marginally bound, marginally stable (MBMS) orbits in Schwarzschild spacetime. In Ch. 5 we will characterise these orbits, first at the geodesic level (Sec. 5.1), and subsequently in the context of the first-order self-force approximation (Sec. 5.2). We will also present results for the conservative corrections [3] to the azimuthal frequency of the innermost bound circular orbit and to the critical angular momentum of a MBMS orbit.

Our work aims at paving the way for self-force calculations in the high-energy regime, where one could establish new cross-comparisons with other frameworks currently used to model compact binaries, such as the post-Newtonian approximation and Numerical Relativity. Cross-validations among these schemes are crucial to establish confidence in our mathematical modelling of binaries and progress towards a more reliable and efficient generation of gravitational waveforms. A future development of the work described here might be, for instance, the computation of deflection angles for hyperbolic-like encounters [14]. Furthermore, we will show how our calculation can be used to calibrate the conservative sector of the effective-one-body model (EOB), a semi-analytical framework which is widely used to generate gravitational waveforms [15]. We will cover this topic in Sec. 5.6.

[2] Note that the geodesic constants of motion cease to be conserved in the perturbative problem.

[3] As we will explain later, the term "conservative" refers to the backreaction from the time-symmetric part of the metric perturbation.

1.1 Self-force preliminaries

In this section we introduce relevant results from the theory of self-forced motion, which will be used in Ch. 3 to derive conditions for capture and overspinning under the full GSF effect.

Early derivations of the first-order self-force aimed at extending the validity of the point-particle approximation beyond the geodesic level. It is clear, in fact, that neglecting the internal structure of the small body should simplify the treatment of the problem; however, the non-linear nature of Einstein's field equations implies that distributional stress energy-tensors are not allowed in the full theory [16], and thus the point-particle approximation is not justified in that context. Work by Mino, Sasaki and Tanaka [17],and subsequently by Quinn and Wald [18] showed that, at first order, it is still mathematically meaningful to model the source as a distribution. As the physical retarded solution to the linearised Einstein's field equations diverges at the particle's location, one has to properly take care of such singularities. We will briefly explain how this can be achieved in the next subsection.

While the derivation provided by Quinn and Wald assumed the validity of the point-particle picture, Mino, Sasaki and Tanaka adopted a different perspective, which is both more rigorous and directly applicable to higher orders in perturbation theory: they derived the equations for the self-forced motion using matched asymptotic expansion [19, 20] (see Subsec. 1.1.2). This approach provides solid justification to the use of the point-particle approximation in the linearised theory, without assuming a priori its validity. The upshot of the analysis is that, at first post-geodesic order, the motion of the small mass μ can be interpreted as an accelerated motion in the background spacetime, subject to an effective GSF ($\propto (\mu/M)^2$). In Subsec. 1.1.3 we will describe a practical method to numerically compute the finite, local self-force acting on the particle. We will then explain how this local force can be used to model radiative losses of energy and angular momentum, as well as non-dissipative effects related to backreaction (Subsec. 1.1.4).

1.1.1 First-order self-forced motion: early derivations

We have already mentioned that a formula for the GSF at linear order in perturbation theory was first derived by Mino, Sasaki and Tanaka, and subsequently by Quinn and Wald. Let us assume that the metric tensor describing the perturbed spacetime is of the

form

$$\tilde{g}_{\mu\nu} = g_{\mu\nu} + h_{\mu\nu},$$

where $g_{\mu\nu}$ represents the metric of the unperturbed background and $h_{\mu\nu}$ encodes the effects due to the presence of the small mass μ. Then the linearised Einstein's equations, in Lorenz gauge, read

$$E_{\mu\nu}[\bar{h}] := \nabla^\alpha \nabla_\alpha \bar{h}_{\mu\nu} + 2R^\sigma_{\ \mu\ \nu}^{\ \ \tau} \bar{h}_{\sigma\tau} = -16\pi\mu \int_{-\infty}^{\infty} \frac{1}{\sqrt{|g|}} \delta^4(x - x'(\tau)) \hat{u}_\mu(\tau) \hat{u}_\nu(\tau) d\tau, \quad (1.1)$$

$$L_\beta[\bar{h}] := \nabla^\alpha \bar{h}_{\alpha\beta} = 0, \quad (1.2)$$

where x denotes a generic field point, $x'(\tau)$ and $\hat{u}^\mu$ are the particle's position and four-velocity in the perturbed spacetime, g is the determinant of the background metric and we have introduced the trace-reversed metric perturbation $\bar{h}_{\mu\nu} := h_{\mu\nu} - 1/2 g_{\mu\nu} h^\alpha_\alpha$. Note also that the differential operator ∇^α is taken with respect to the background metric. Both the advanced and retarded solutions to the above equation diverge along the worldline, due to the presence of a point-like source. The singular structure of the solution can be studied via an Hadamard expansion of the Green's function associated to (1.1) [4]: such an analysis leads to the conclusion that the full metric perturbation can be split into a *direct* field, coming from the intersection of the past light cone of x with the worldline Γ (see Fig. 1.1.1) and a *tail* field, which is determined by the entire past history of the particle's motion:

$$\bar{h}^{ret}_{\alpha\beta} = \bar{h}^{dir}_{\alpha\beta} + \bar{h}^{tail}_{\alpha\beta}. \quad (1.3)$$

The last term is given by the tail integral

$$\bar{h}^{tail}_{\alpha\beta}(x'(\tau_0)) = 4\mu \lim_{\epsilon\to 0} \int_{-\infty}^{\tau_0 - \epsilon} \left(G_{+\alpha\beta\alpha'\beta'}(x, x') - \frac{1}{2} g_{\alpha\beta} G^\gamma_{+\ \gamma\alpha'\beta'}(x, x') \right) \hat{u}^{\alpha'} \hat{u}^{\beta'} d\tau, \quad (1.4)$$

where primed quantities refer to the particle's location, $G_{+\alpha\beta\alpha'\beta'}(x, x')$ is the retarded Green's function and the integral is cut off at a proper time $\tau_0 - \epsilon$ smaller than the retarded time u. The first-order self-acceleration is then expressed in terms of the above "tail" field,

[4] We refer here to the expansion of a certain biscalar $V(x, x')$, which represents the "tail" part of the Green's function, in powers of the so-called Synge's world-function $\sigma(x, x')$, which is proportional to the squared geodesic distance between x and x'.

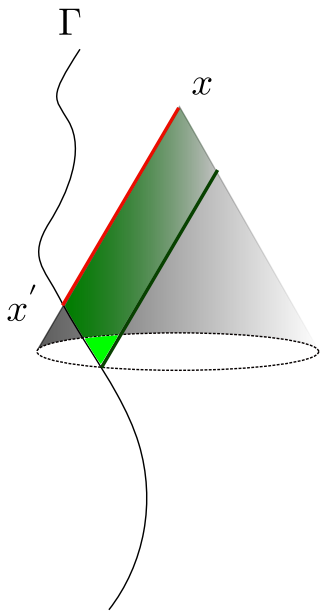

Figure 1.1: The direct field has support only on the light cone (highlighted in red), whereas the tail field is sourced by all the points along Γ that lie inside the light cone. Tail effects arise due to back-scattering of gravitational waves off the spacetime curvature.

in the so-called MiSaTaQuWa equation

$$F^{\alpha}_{self} := \hat{u}^{\beta}\nabla_{\beta}\hat{u}^{\alpha} = -\left(g^{\alpha\beta} + \hat{u}^{\alpha}\hat{u}^{\beta}\right)\left(\nabla_{\sigma}h^{tail}_{\beta\gamma} - \frac{1}{2}\nabla_{\beta}h^{tail}_{\sigma\gamma}\right)\hat{u}^{\sigma}\hat{u}^{\gamma}. \tag{1.5}$$

It should be noticed that $h^{tail}_{\alpha\beta}$ is not smooth along the worldline and is not a solution to the homogeneous field equations (similarly, $h^{dir}_{\alpha\beta}$ does not satisfy the inhomogeneous linearised Einstein's field equations). In Lorenz gauge, the singular field is akin to a Coulomb-like field, which is isotropic and moves with the particle, without exerting any force on it. The tail field is instead a free radiation field, and as such can exert a force on the particle exactly like any other external field.

In order to recover an interpretation of the back-reacted motion closer to the spirit of the Equivalence Principle, Detweiler and Whiting [21] devised an alternative splitting of the metric perturbation

$$\bar{h}^{ret}_{\alpha\beta} = \bar{h}^{S}_{\alpha\beta} + \bar{h}^{R}_{\alpha\beta}, \tag{1.6}$$

where the first term, the singular field, is constructed from a singular Green's function with no support either on the future or past light-cone of x (see Figure 1.2) and the second term, the regular field, is defined as the residual of the subtraction $\bar{h}^{ret}_{\alpha\beta} - \bar{h}^{S}_{\alpha\beta}$. Unlike $h^{tail}_{\alpha\beta}$, the Detweiler-Whiting regular field has the property of being a homogeneous

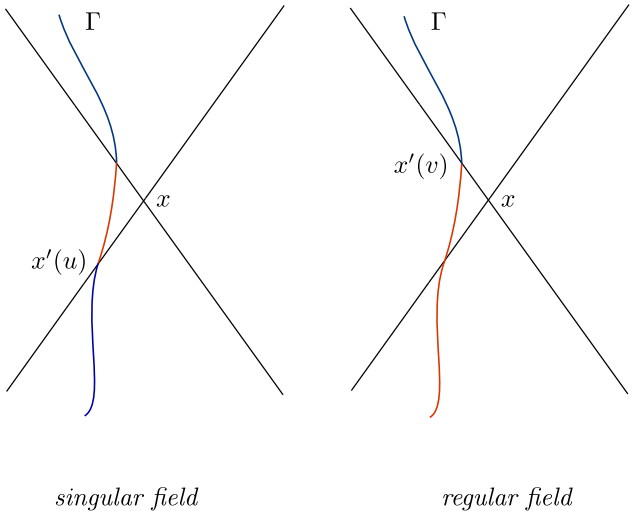

Figure 1.2: In the Detweiler-Whiting decomposition, both the singular and regular field depend on points along Γ that are spacelike separated from x; in addition, the regular field also depends on points along Γ that lie inside the past light cone of x.

solution to the linearized Einstein's field equations. Therefore, in this formalism, one can interpret the motion of the small mass as being geodesic in the perturbed "effective" metric $\tilde{g}_{\alpha\beta} := g_{\alpha\beta} + h^R_{\alpha\beta}$. Furthermore, it can be shown that the self-acceleration with respect to $g_{\alpha\beta}$ can be written once again in the form of Eq. (1.5), with the replacement $h^{tail}_{\alpha\beta} \to h^R_{\alpha\beta}$. This is not in contradiction with our previous statement that the small mass moves along a geodesic in $\tilde{g}_{\alpha\beta}$: in fact, it can be shown that the MiSaTaQuWa equation reduces to the geodesic equation (up to $O(\mu^2)$ corrections) when re-expressed in terms of the proper time measured in $\tilde{g}_{\alpha\beta}$ [22].

1.1.2 Construction of the SF via matched asymptotic expansions

There now exists a rigorous formulation of the equations of motion for compact objects in curved spacetime, valid through first post-geodesic order in perturbation theory—see [23, 23–25] and references therein, and [19, 20] for recent reviews. We will be concerned mainly with results regarding the first order self-force: an extension of the formalism to second order [5] involves additional technical difficulties, and work to numerically implement it is under way [26].

Such formulation relies on the technique of matched asymptotic expansions. The key

[5] Such extension is not a merely academic problem, but it is motivated by the need to generate accurate templates for gravitational waveforms. In fact, a first-order approximation introduces systematic errors in the orbital phase that will accumulate in the course of the inspiral and eventually result in an $O(1)$ dephasing.

idea is to construct two different asymptotic solutions to the Einstein's field equations. The first of these solutions is given by an inner expansion, valid in the region $r \ll M$, (where r is a suitable coordinate that measures the distance from the small body) expressed in terms of some rescaled coordinates $\bar{x}^a := x^a/\mu$ [6]

$$g^{int}_{\alpha\beta}(\bar{x}, \mu) = g^{0,int}_{\alpha\beta}(\bar{x}^a) + \sum_{n=1}^{\infty} \eta^n H^{(n)}_{\alpha\beta}(\bar{x}), \tag{1.7}$$

where $\eta := \mu/M$ and $g^{0,int}_{\alpha\beta}$ is the metric sourced by the small object in vacuum. The second solution is represented by an outer expansion in some coordinates x, valid in the region $r \gg \mu$, of the form

$$g^{ext}_{\alpha\beta}(x, \mu) = g^{0,ext}_{\alpha\beta}(x) + \sum_{n=1}^{\infty} \eta^n h^{(n)}_{\alpha\beta}(x), \tag{1.8}$$

where $g^{0,ext}_{\alpha\beta}$ is a vacuum solution sourced by the massive black hole and higher order corrections capture the gravitational effects produced by the small mass μ. Since we are working under the assumption that $\mu/M \ll 1$, there will be a buffer region, $\mu \ll r \ll M$, where both expansions will be approximations of the same solution to the field equations. In this region, the inner expansion can be expanded for $r \gg \mu$ and the outer one for $r \ll M$: the two expansions can then be matched order by order in r and η. We will now sketch how the matching procedure works, following [22]. First, one expands the metric perturbation of the outer solution

$$\eta^n h^{(n)}_{\alpha\beta}(x) = \eta^n \sum_k r^k h^{(n)k}_{\alpha\beta}(n^i), \tag{1.9}$$

where $n^i := x^i/r$. In the buffer region, the above expansion needs to be matched to the inner solution, expressed in some rescaled coordinates. Note that, by requiring regularity of the metric in the limit $\mu \to 0$, one can deduce that the most negative power of r in Eq. (1.9) must be r^{-n} (in fact, $r^{-n} = \bar{r}^{-n}\mu^{-n}$, and therefore more negative terms would give a divergent expansion in the limit $\mu \to 0$).

The iterative scheme to solve Einstein's field equations in the buffer region schematically proceeds as follows [7]: the Ricci tensor is expressed as a sum of terms of increasing order in $h_{\alpha\beta}$: $R_{\mu\nu} = \delta R_{\mu\nu}[h] + \delta^2 R_{\mu\nu}[h, h] + ...$ Then, using the definition of the operator $E_{\mu\nu}$

[6] This rescaling has the effect of "zooming in" on the particle: in fact, in the limit $\mu \to 0$, all the distances $r \gg \mu$ are sent to infinity and the geometry is determined only by the small compact object.

[7] Crucially, since the field equations are solved in the buffer zone, i.e. in vacuum, there are no issues related to the mathematical representation of the small object's stress-energy tensor, in contrast with the point-particle approximation described earlier.

given in (1.1), one gets

$$E_{\mu\nu}[\bar{h}^{(1)}] = 0, \tag{1.10}$$

$$E_{\mu\nu}[\bar{h}^{(2)}] = 2\delta^2 R_{\mu\nu}[h^{(1)}, h^{(1)}], \tag{1.11}$$

$$...$$

$$E_{\mu\nu}[\bar{h}^{(n)}] = S[h^{(1)}, ..., h^{(n-1)}], \tag{1.12}$$

where by S we denote an effective source given by all the non-linear terms in $R_{\mu\nu}$ involving lower orders of the metric perturbation. The above equations need to be supplemented by similarly expanded gauge conditions (see Eq.(1.2)).

At each perturbative order n, the metric perturbation is then expanded into symmetric, trace-free multipole moments (see Eq. (1.9)) and Eqs. (1.10)-(1.12) are solved order by order in r. It can be shown that, by matching the inner and outer expansions in the buffer zone, some of these multipole moments can be identified with the multipoles of the small object (i.e., with its mass, mass dipole and so on). The remaining multipole moments are either higher order products of the small object's multipoles or arbitrary functions that can be fixed by imposing boundary conditions.

The metric perturbation $h_{\alpha\beta}$ obtained following the above procedure can then be split into a singular and regular piece $h_{\alpha\beta} = h^R_{\alpha\beta} + h^S_{\alpha\beta}$, consistently with the Detweiler-Whiting decomposition. In doing so, one finds that it is possible to define a regular field such that the small body moves along a geodesic in the effective metric $h^{eff}_{\alpha\beta} := g^{0,ext}_{\alpha\beta} + h^R_{\alpha\beta}$, with $h^{eff}_{\alpha\beta}$ being a vacuum solution to the Einstein's field equations. The upshot of this analysis is that, at first order, one recovers once again the MiSaTaQuWa equation, with the R-field replacing the tail field. Unlike the axiomatic derivation of Quinn and Wald, the method described in this subsection is directly applicable to second order and it is thus best suited to study the self-forced motion, especially in view of applications to gravitational wave astronomy.

Gauge dependence of the SF

It is important to keep in mind that the self-force is a gauge-dependent notion and it does not carry any physical information per se: a meaningful description of the system must include knowledge of the metric perturbation $h_{\alpha\beta}$.

Under a gauge transformation of the form $x^\mu \to x'^\mu = x^\mu + \xi^\mu$, where ξ^μ is an infinites-

imal displacement vector, Barack and Ori [27] showed that, at first order, the gravitational self-force changes by an amount

$$\delta F^{\alpha} = -\mu \left[\left(g^{\alpha\lambda} + \hat{u}^{\alpha}\hat{u}^{\lambda} \right) \hat{u}^{\mu}\hat{u}^{\nu}\nabla_{\mu}\nabla_{\nu}\xi_{\lambda} + R^{\alpha}_{\mu\lambda\nu}\hat{u}^{\mu}\xi^{\lambda}\hat{u}^{\nu} \right], \tag{1.13}$$

where $g^{\alpha\lambda}$ is the inverse background metric and $R^{\alpha}_{\mu\lambda\nu}$ is the Riemann tensor computed with respect to $g_{\alpha\beta}$; note that, in the above expression, the perturbed metric can always be replaced with the background one, as $O(\mu^2)$ terms are being neglected.

1.1.3 The mode-sum scheme

The main outcome of the previous subsection is that it is possible to write the first-order GSF in terms of a certain regular metric perturbation:

$$F^{\beta}_{self}(x') = \mu \bar{\nabla}^{\beta\gamma\delta} \bar{h}^{R}_{\gamma\delta}(x'), \tag{1.14}$$

where, to be more concise, we rewrote the operator in Eq. (1.5) as

$$\bar{\nabla}^{\beta\gamma\delta} = 1/2 \left(g^{\beta\sigma}\hat{u}^{\gamma} - 2g^{\beta\gamma}\hat{u}^{\sigma} - \hat{u}^{\beta}\hat{u}^{\gamma}\hat{u}^{\sigma} \right) \hat{u}^{\delta}\nabla_{\sigma}. \tag{1.15}$$

In practice, $h^{R}_{\alpha\beta}$ is computed by subtracting from the retarded field $h^{ret}_{\alpha\beta}$ the singular field $h^{S}_{\alpha\beta}$, whose local structure in a neighbourhood of the particle is known analytically. Thus, a numerical computation of the gravitational self-force has to deal with the problem of computing the finite quantity F^{α}_{self} starting from fields that diverge along the worldline:

$$F^{\beta}_{self}(x') = \lim_{x \to x'} \left(F^{\beta}_{ret}(x) - F^{\beta}_{S}(x) \right) = \mu \lim_{x \to x'} \left(\bar{\nabla}^{\beta\gamma\delta} \bar{h}^{ret}_{\gamma\delta}(x) - \bar{\nabla}^{\beta\gamma\delta} \bar{h}^{S}_{\gamma\delta}(x) \right). \tag{1.16}$$

To overcome this difficulty, Barack and Ori devised a scheme that goes under the name of "mode-sum method", which relies on the observation that, although the total singular and retarded self-force are infinite at the particle's location, their individual multipole modes are finite. Thus, the self-force can be computed as follows

$$F^{\alpha}_{self}(x') = \sum_{\ell=0}^{\infty} \left(F^{\alpha\ell}_{ret/\pm}(x') - F^{\alpha\ell}_{S/\pm}(x') \right), \tag{1.17}$$

where the $\pm$ sign reminds that, although finite at x', the modes of the retarded and singular fields are generically discontinuous there and their value depends on the direction

the worldline is approached from (in particular, adopting Boyer-Lindquist coordinates, a plus/minus sign denotes $r \to r'^{\pm}$, keeping the remaining coordinates fixed).

The retarded and singular modes of the self-force diverge as $\sim \ell$ when $\ell \to \infty$, whence the idea of introducing some "regularisation" functions $H^{\alpha\ell} := \pm(\ell+1/2)A^\alpha + B^\alpha + C^\alpha/(\ell+1/2)$, such that the sum over ℓ of the quantity $F^{\alpha\ell}_{ret/\pm} - H^{\alpha\ell}_{\pm}$ is finite. One can then write

$$F^\alpha_{self}(x') = \sum_{\ell=0}^{\infty} \left(F^{\alpha\ell}_{ret/\pm}(x') - H^{\alpha\ell}_{\pm}(x') \right) - D^\alpha_{\pm}, \tag{1.18}$$

where we defined $D^\alpha_{\pm} := \sum_{\ell=0}^{\infty} \left(F^{\alpha\ell}_{S/\pm}(x') - H^{\alpha\ell}_{\pm}(x') \right)$. This sum also converges if the first sum in the above equation does. The regularisation parameters $A^\alpha_{\pm}, B^\alpha, C^\alpha, D^\alpha$ have been obtained analytically by Barack and Ori for arbitrary geodesics in Kerr spacetime, for scalar, electro-magnetic and gravitational self-forces [28]. Their calculation relied on a local analysis of the multipolar expansion of the singular force and also showed that $D^\alpha = C^\alpha = 0$ in Lorenz gauge [29] (and in gauges that can be obtained from it by sufficiently regular transformations).

It should be stressed that the Barack-Ori regularisation parameters act on the spherical harmonic modes of the full force. This implies, for instance, that the gravitational self-force, which is normally expanded in tensor harmonics in numerical evolutions, needs to be re-expanded into scalar harmonics modes before applying the mode-sum regularisation scheme. As a consequence of this re-expansion, a single scalar mode of the force bears contributions from multiple tensorial modes: in Schwarzschild spacetime, for instance, a single scalar mode ℓ takes input from all the tensorial modes $\ell - 3 \leq l \leq \ell + 3$; the situation is even more complicated in Kerr, where the coupling involves an infinite number of modes. This constitutes a disadvantage from a computational perspective. Recently, tensorial regularisation parameters have been calculated for circular orbits on a Schwarzschild background [30], but an extension to generic orbits and/or Kerr spacetime is yet to come. We also note in passing that the efficiency of the mode-sum scheme can be improved by including higher-order regularisation parameters [31], which accelerate the convergence rate of the sum in Eq. (1.18).

As we briefly mentioned earlier, the mode-sum scheme applies only to a specific class of gauges (among them, the Lorenz gauge, which we will be adopting in our numerical implementation in Sec. 5.3). The extension of Eq.(1.18) to other gauges used in the self-force literature, such as the radiation gauge, is highly non-trivial and requires a careful analysis of the local structure of the singular field in the gauge that is being used. We refer

the reader to [32] for a thorough treatment of this problem.

1.1.4 Conservative and dissipative self-force

For reasons that will be clarified below, it is convenient to split the total self-force into a dissipative (time antisymmetric) and conservative (time symmetric) piece, as follows

$$F^{\alpha}_{cons} := \frac{1}{2}\left(F^{\alpha}_{ret} + F^{\alpha}_{adv}\right), \tag{1.19}$$

$$F^{\alpha}_{diss} := \frac{1}{2}\left(F^{\alpha}_{ret} - F^{\alpha}_{adv}\right). \tag{1.20}$$

In the above equations, $F^{\alpha}_{ret/\,adv}$ denote the self-forces constructed from the retarded (advanced) metric perturbations (see Eq.(1.16)). The two pieces affect the orbital motion in different manners. The dissipative self-force encodes information about radiation-reaction effects, such as energy and angular momentum losses, which accumulate in the course of the evolution; the conservative piece instead shifts the orbital phases from their geodesic value. Example of physical effects produced by the conservative self-force are the periastron advance for eccentric binaries [33] and spin precession [34]. Other conservative corrections have been investigated as they constitute useful tools of comparisons with post-Newtonian results: these include the self-force corrections to the frequency of a circular orbit [35, 36] and tidal effects for quasi-circular orbits [37]. In the next subsection, we will provide further details about a number of conservative effects that are going to play an important role in our analysis.

Constructing the dissipative and conservative pieces of the self-force in the time-domain, which is the numerical framework we will be using later on (Ch.5), is rather straightforward for equatorial or circular orbits. Due to the symmetry of the Kerr metric under the isometry $t \to -t, \phi \to -\phi$ and to the properties of diffeomorphisms [38] one has

$$F^{\mu}_{ret}\left(-\hat{u}_t, \hat{u}_r, \hat{u}_\theta, -\hat{u}_\phi; \tau\right) = \epsilon_\mu F^{\mu}_{ret}\left(\hat{u}_t, \hat{u}_r, \hat{u}_\theta, \hat{u}_\phi; \tau\right), \tag{1.21}$$

where there is no summation over μ on the right hand side and $\epsilon_\mu = (-1, 1, 1, -1)$. Moreover, by definition one has

$$F^{\mu}_{ret}\left(-\hat{u}^{\mu}; \tau\right) = F^{\mu}_{adv}\left(\hat{u}^{\mu}; \tau\right), \tag{1.22}$$

whence it follows that

$$F^{\mu}_{adv}\left(\hat{u}_t,\hat{u}_r,\hat{u}_\theta,\hat{u}_\phi;\tau\right)=\epsilon_\mu F^{\mu}_{ret}\left(\hat{u}_t,-\hat{u}_r,-\hat{u}_\theta,\hat{u}_\phi;\tau\right). \tag{1.23}$$

At the same time, by inspecting the equations of motion for geodesics in the equatorial plane, and denoting by τ the proper time elapsed from a turning point of the motion (i.e. a point where $dr/d\tau=0$), it is readily verified that

$$F^{\mu}_{ret/adv}\left(\hat{u}_t,\hat{u}_r,\hat{u}_\theta,\hat{u}_\phi;-\tau\right)=F^{\mu}_{ret/adv}\left(\hat{u}_t,-\hat{u}_r,-\hat{u}_\theta,\hat{u}_\phi;\tau\right) \tag{1.24}$$

so that

$$F^{\mu}_{ret/adv}(\tau)=\epsilon_\mu F^{\mu}_{adv/ret}(-\tau). \tag{1.25}$$

Combining all the above results, one can conclude that the conservative and dissipative pieces of the self-force along equatorial orbits can be constructed as follows

$$F^{\mu}_{cons}(\tau)=\frac{1}{2}\left(F^{\mu}_{ret}(\tau)+\epsilon_\mu F^{\mu}_{ret}(-\tau)\right); \tag{1.26}$$

$$F^{\mu}_{diss}(\tau)=\frac{1}{2}\left(F^{\mu}_{ret}(\tau)-\epsilon_\mu F^{\mu}_{ret}(-\tau)\right). \tag{1.27}$$

Notice also that, by applying the mode-sum scheme to Eqs. (1.26)-(1.27), one obtains

$$F^{\mu}_{cons}=\sum_{l=0}^{\infty}\left(F^{\mu\ell}_{cons\pm}\mp(\ell+\frac{1}{2})A^{\mu}-B^{\mu}\right), \tag{1.28}$$

$$F^{\mu}_{diss}=\sum_{l=0}^{\infty}F^{\mu\ell\pm}_{diss}, \tag{1.29}$$

whence it follows that the dissipative self-force, as computed from the retarded field, does not need to undergo any regularization procedure.

1.1.5 Effects of the conservative self-force

In this subsection we will focus on some effects produced by the conservative GSF which will be relevant for later discussions. Following work by Detweiler [39], physical conservative effects have been increasingly studied to establish comparisons between numerical self-force results and a number of analytical predictions formulated in the context of the post-Newtonian approximation and other frameworks [40, 41]. Clearly, due to the gauge-dependence of the self-force, such cross-comparisons need to be based on suitable gauge-invariant quantities.

Circular orbits are particularly suited for this purpose, as the circularity assumption significantly reduces the level of complexity of the calculations. We should note though that EMRIs will be in general eccentric and thus circular orbits are mainly stepping stones towards more realistic systems. In what follows we will introduce some conservative corrections that will be relevant for our discussion of the overspinning problem, as well as for our numerical study of MBMS orbits.

As shown by Detweiler [39], in the case of quasi-circular motion, each component of the small body's four-velocity is gauge-invariant, whence it follows that the orbital frequency observed by an asymptotic observer $\Omega := \hat{u}^\phi/\hat{u}^t$ is also invariant, as long as one works in a gauge that respects the helical symmetry of the system, generated by the Killing vector $k^\alpha = \partial_t + \Omega\partial_\phi$.

Another conserved gauge invariant quantity (at first order) is given by the contraction $-k^\alpha \hat{u}_\alpha = E - \Omega L = 1/\hat{u}^t$, where the last equality simply follows from the fact that $\hat{u}^\alpha = \hat{u}^t k^\alpha$. In the self-force literature, this variable is commonly referred to as the redshift $z := 1/\hat{u}^t$: The name originates from the fact that z corresponds to the redshift of a light signal emitted by a source comoving with the small mass, as measured by a distant observer along the z-axis, in a fictitious metric $h^R_{\alpha\beta}$:

$$z = \frac{E_\infty}{E_p}, \tag{1.30}$$

where E_∞, E_p denote the photon's energy at infinity and at the particle's position respectively[8].

We will now show how the conservative self-force affects the frequency Ω: this information will prove useful in Ch. 5. Let us consider a circular orbit of radius R in the *perturbed* spacetime and let us assume that the particle's four-velocity is normalised with respect to the background metric. Then, the equations for the self-forced motion $F^\alpha_{self} = \hat{u}^\beta \nabla_\beta \hat{u}^\alpha$, together with the four-velocity normalisation condition $\hat{u}^\alpha \hat{u}_\alpha = -1$, imply that the first-order GSF-corrected azimuthal frequency reads [42]

$$\Omega = \sqrt{\frac{M}{R^3}} \left(1 - \frac{R^2 \left(R - 3M\right)}{2\mu M \left(R - 2M\right)} F^r(R) \right), \tag{1.31}$$

Using Eq.(1.13), one can verify that the shifts in δR and $F_r(R)$ induced by a gauge trans-

[8] Although Ω and z are gauge invariant, it is important to bear in mind that any comparison between different gauges must take into account the intrinsic ambiguity in the choice of coordinates that characterize the perturbative problem. Stated otherwise, fixing the particle's coordinates in the background geometry is not sufficient to specify unambiguously an orbit in the perturbed spacetime.

formation exactly cancel out, confirming that Ω is indeed a gauge invariant quantity.

The conservative self-force also shifts the total, conserved energy and angular momentum of a binary system, for a fixed azimuthal frequency. These shifts can be computed using the first law of black hole binary mechanics [12]. The first law has known several reformulations: we will mention here only one, which will feature later on in our analysis of the overspinning problem. Let us consider a binary system composed of point particles with masses m_i, corotating at a fixed frequency Ω. Assuming that the particles are non-spinning, the first law relates infinitesimal variation in the individual masses of the point particles to those of the total Bondi energy E_B and angular momentum J of the system:

$$\delta E_B - \Omega \delta J = \sum_i z_i \delta m_i, \tag{1.32}$$

where $z_i = 1/\hat{u}_i^t$. Although the above equation was originally derived by differentiation of high order post-Newtonian expansions [12], it is in fact a specialization of a broader result obtained by Friedman et al. [11], which applies to perfect fluid spacetimes endowed with a global helical symmetry. Further details will be given in Sec. 3.9, where we will apply the first law in the context of the overspinning problem.

1.2 The weak cosmic censorship conjecture

In 1939 Oppenheimer and Snyder pioneered the idea that black holes can form in astrophysical contexts as a result of gravitational collapse [43]. Although their analysis assumed spherical symmetry, theorems by Hawking, Penrose and Geroch later established that singularities can occur in completely generic spacetimes [44,45]. These findings raised a fundamental question: would these singularities ever be visible to distant observers? In order to exclude this possibility, which would undermine the predictive power of General Relativity, Penrose conjectured that singularities are always cloaked by event horizons [46]. This conjecture, which is known as the weak cosmic censorship conjecture (WCCC), has gradually become a cornerstone of classical General Relativity. It is typically invoked, for instance, in proofs of uniqueness theorems for four-dimensional, asymptotically flat spacetimes [9]

Despite being strongly motivated on physical grounds, the WCCC's precise extent of

[9] We stress the fact that, in this work, we will never be concerned with the strong cosmic censorship conjecture, which postulates that maximal Cauchy developments for the Einstein equations are inextendible (the conjecture is thus relevant only for those spacetimes that admit non globally-hyperbolic analytic extensions, such as the Kerr and Reissner-Nordström solutions). The precise degree of such "inextensibility", i.e. the regularity of the metric extension across the Cauchy horizon, has been extensively studied, most recently, by Dafermos [47].

validity remains unclear. Over the past decades, several counter-examples have been investigated in order to make the statement of the conjecture more precise. Naked singularities have been found in the collapse of dust and null fluid shells [48]; however, these occurrences are not generally considered problematic, as they are not regarded as realistic representations of gravitational collapse.

It was later shown that they can also be produced in the presence of scalar matter fields, via careful fine-tuning of the initial conditions. This interesting feature first emerged in numerical evolutions of the spherically symmetric Einstein-Klein-Gordon equations [49], and was later proved analytically in a number of papers by Christodoulou (see [50] and references therein). Crucially, Christodolou showed that small perturbations of initial data evolving to a spacetime containing a naked singularity result in a perfectly regular final state. In other words, the occurrence of naked singularities appears to be non-generic.

In order to account for the aforementioned exceptions, a more precise, and yet still provisional, formulation of the weak cosmic censorship conjecture is the following:

Weak cosmic censorship conjecture. *Generic, asymptotically flat initial data for a solution to the Einstein's field equations, involving suitable matter fields, have maximal future developments possessing a complete future null infinity [51, 52].*

In a spacetime containing naked singularities, some of the geodesics reaching future null infinity are incomplete, i.e. they interact with the singularity during their past history (this can be clearly seen, for instance, by looking at the Carter-Penrose diagram of a Schwarzschild spacetime with negative mass). Therefore, in non-rigorous terms, the above conjecture requires that no singularities can be visible from infinity: if a singularity is present, it must be hidden behind an horizon, where all future causal curves get trapped. Notice that the possible counter-examples mentioned earlier do not actually violate the above formulation of the conjecture: the singularities explored by Choptuik and Christodolou are not generic in nature; also, one can argue that dust and null fluids should not be considered suitable forms of matter, but rather approximations of physical fields.

As it is far from settled whether further restrictions should be applied to the conjecture, thought experiments represent valuable tools to improve our understanding of the WCCC and refine its formulation. In this work, we will focus on a scenario where a particle is sent into a nearly-extremal rotating black hole, in an attempt to drive it beyond extremality. The first use of this framework as a test bed for cosmic censorship can be found in a paper by Wald [53], where an exactly extremal Kerr–Newman black hole was considered. Wald

examined whether the capture of a test mass could bring the final system to a new Kerr–Newman spacetime with mass $M_{\rm f}$, charge $Q_{\rm f}$ and spin $J_{\rm f}$ satisfying $M_{\rm f}^2 < (J_{\rm f}/M_{\rm f})^2 + Q_{\rm f}^2$: In this case a naked singularity would be exposed, in direct violation of WCCC. Wald showed that under his assumptions the naked-singularity scenario is ruled out: Electrostatic and centrifugal repulsion would prevent a particle carrying sufficient charge and/or angular momentum from entering the black hole. The same conclusion was shown to hold true also for a spinning test particle dropped from rest at infinity along the symmetry axis of an extremal Kerr black hole, with its spin aligned along the axis. In this case, it is the repulsion force from spin-spin coupling that prevents suitable particles from ever entering the black hole. Whether the equations of classical GR permit the occurrence of naked singularities in similar scenarios, under relaxation of the extremality condition, has since been subject of much investigation. It is usually assumed that the particle's energy and electric charge are much smaller than those of the black hole, which then places the problem within the realm of black-hole perturbation theory.

In fact, later work has demonstrated that over-extremality is achievable when the initial black hole is taken to be *nearly* extremal—if back-reaction effects on the particle's trajectory are ignored. This was first shown by Hubeny [54] for a nearly extremal Reissner-Nordström black hole, and more recently by Jacobson and Sotiriou [55] for a nearly extremal Kerr black hole ("overcharging" and "overspinning" scenarios, respectively). The nearly extremal Kerr-Newman case was subsequently studied in Ref. [56]. In all cases, all orbits identified as capable of driving the black hole beyond the extremal limit lie very close, in the relevant parameter space, to the separatrix between orbits that are captured by the black hole and ones that are scattered off it. In Hubeny's analysis of a radially falling electric charge, electrostatic repulsion only marginally fails to prevent the particle from falling into the hole: The particle's radial velocity upon crossing (what would have been) the event horizon is proportional to the ratio $\tilde{\eta} \ll 1$ between the particle's energy and the black hole's mass. The amount of post-capture excess charge, $Q_{\rm f} - M_{\rm f}$, is found to be *quadratic* in $\tilde{\eta}$. Similarly, in Ref. [55]'s analysis of equatorial-plane captures, overspinning particles clear the peak of the effective potential barrier with radial velocities $\propto \tilde{\eta}$, and the post-capture excess spin, $J_{\rm f} - M_{\rm f}^2$, is quadratic in $\tilde{\eta}$.

This suggests that back-reaction effects cannot be ignored and may well change the outcome of the gedanken experiment. Heuristically, effects of the (electromagnetic and/or gravitational) self-force enter the analysis in two ways. First, the dissipative piece of the self-force continually removes some of the particle's energy and angular momentum, send-

ing them to infinity and down the event horizon in gravitational waves. In the Kerr case, dissipative effects may accumulate as the particle "lingers" over the peak of the effective potential on a nearly circular orbit. Second, the conservative piece of the self-force might supply just the right amount of additional repulsive force to prevent would-be overcharging/overspinning particles from ever entering the black hole. For particles sent in from infinity in the Kerr case, this second effect may be formulated in terms of a shift in the critical impact parameter for capture: If the GSF shifts the critical impact parameter inward by a sufficient amount (for a given energy-at-infinity), then would-be overspinning particles may end up being scattered away rather than captured.

There have been several recent attempts to quantify the effect of back-reaction in the problem. Focusing on the Reissner-Nordström case, Isoyama, Sago and Tanaka [57] argued that the full effect can be properly taken into account by considering the quasi-equilibrium configuration of a charged particle placed precisely on the capture-scatter separatrix. An exact solution is known for this configuration—the static double Reissner-Nordström spacetime—and the authors calculated that its total energy is always greater than its total charge. They have also established that radiative losses during the final plunge are negligible, hence concluding that (under the assumption that the true capture system does indeed go through a quasi-equilibrium state) the final configuration cannot be a naked singularity.

In a later work, Zimmerman, Vega and Poisson [58] took up the challenge of directly calculating the charged particle's trajectory including the full effect of the electromagnetic self-force. Analyzing numerically a large sample of orbits within the domain identified by Hubeny, the authors found no example of successful overcharging: all particles with a combination of charge and energy suitable for overcharging the black hole were found to be repelled before reaching the horizon. This analysis, however, neglected the potentially important effect of back-reaction from the gravitational perturbation sourced by the particle's electromagnetic energy-momentum. A complete analysis would require calculation of the corresponding GSF, but techniques for calculating self-forces in the coupled problem are only now starting to be developed [59, 60].

In that respect, the Kerr setup provides a cleaner environment, in which the perturbative problem is purely gravitational (at the obvious cost of abandoning spherical symmetry). Barausse, Cardoso and Khanna [61, 62] studied the dissipative GSF effect in the Kerr overspinning problem, focussing on ultra-relativistic particles on equatorial orbits (but excluding fine-tuned orbits that get trapped on the separatrix sufficiently long that they

radiate away a large portion of their initial energy). Using analytic arguments backed by numerical calculations of the energy and angular-momentum fluxes, they showed that dissipation averts the overspinning for some but not all of Jacobson–Sotiriou's orbits. If the initial spin of the black hole is sufficiently high, the dissipative effect is always negligible and cannot prevent overspinning. This result highlights the importance of accounting for the full effect of GSF. To reach a definitive conclusion necessitates an actual calculation of the full local GSF acting on the captured particles.

In the next chapter, we will review basic properties of Kerr geodesics and identify the complete "window" in the parameter space in which overspinning occurs if the GSF is ignored. We will then formulate a condition for this window to be eliminated by the effect of the full GSF. The condition will take the form of an inequality that is required to hold for each member of a certain 1-parameter family of geodesics, and it will involve the GSF calculated along such orbits.

Chapter 2

Overspinning with geodesics

Our initial configuration involves a Kerr black hole of mass M and angular momentum $J = a\,M < M^2$. A point-like test particle of rest mass $\mu \ll M$ is sent in on a geodesic orbit of the background Kerr geometry. As in [55], we restrict our attention to prograde orbits in the equatorial plane, so that the orbital angular momentum is aligned with the spin of the black hole (this configuration is *a priori* most favourable for successful overspinning).

Notice also that we will consider only non-spinning particles. Including spin poses a number of challenges. At the geodesic level, finite-size effects need to be taken into account (Jacobson and Sotiriou found that only deeply-bound, oblate bodies can overspin in this case [55]). Beyond the geodesic approximation, the situation is even more delicate. An analysis of spin-curvature coupling effects on generic Kerr orbits has been recently performed [63]. For compact objects, such effects enter the equations of motion at the same order as the gravitational self-force. Models including both the GSF and the spin-orbit coupling are under development, but so far they have been applied only to simplified scenarios, such as quasi-circular orbits in Schwarzschild spacetime [64, 65]. In order to simplify our analysis of the self-force effects later on, we chose to focus on particles carrying exclusively *orbital* angular momentum.

We denote the particle's specific energy and angular momentum by E and L, respectively; these are constants of the motion. For the geodesic approximation to make sense, we must assume $\mu E \ll M$ and $\mu L \ll J$. Then, clearly, overspinning could only be possible, in principle, if the black hole is nearly extremal. We write

$$a/M = 1 - \epsilon^2, \tag{2.1}$$

where $\epsilon \ll 1$.[1]

Below we study the overspinning scenario in the above setup, but we begin with a survey of some essential properties of timelike Kerr geodesics in the equatorial plane.

2.1 Relevant results for Kerr geodesics

Let u^α denote the particle's four-velocity. In Boyer-Lindquist coordinates $\{t, r, \theta, \phi\}$ we have $u^\theta \equiv 0$, and

$$\dot{u}_t = 0, \qquad \dot{u}_\phi = 0, \tag{2.2}$$

where an overdot denotes differentiation with respect to proper time along the geodesic. The last two equalities express the conservation of energy $E = -\xi^\alpha_{(t)} u_\alpha = -u_t$ and angular momentum $L = \xi^\alpha_{(\phi)} u_\alpha = u_\phi$, where $\xi^\alpha_{(t)} := \partial^\alpha_t$ and $\xi^\alpha_{(\phi)} := \partial^\alpha_\phi$ are Killing vectors associated with the time-translation and rotational symmetries of the Kerr background. The pair $\{E, L\}$ parametrizes the family of equatorial geodesics (up to initial conditions).

The normalization $u_\alpha u^\alpha = -1$ now gives the radial equation of motion, which we write in the form

$$\dot{r}^2 \;=\; B(r)\,[E - V_-(L,r)]\,[E - V_+(L,r)]\,. \tag{2.3}$$

Here r is the Boyer-Lindquist radius of the particle, $B(r) := 1 + a^2(r+2M)/r^3$, and (for $MaL \neq 0$)

$$V_\pm(L,r) := \frac{2MaL}{Br^3}\left(1 \pm \sqrt{1 + \frac{Br^3[L^2(r-2M) + r\Delta]}{4M^2a^2L^2}}\right), \tag{2.4}$$

with $\Delta := r^2 - 2Mr + a^2$. For prograde orbits, the potential V_- is manifestly negative definite, so the factor $B(r)(E - V_-)$ in Eq. (2.3) is manifestly *positive* definite. Thus, V_+ plays the role of an effective potential for the radial motion: motion is allowed for $E \geq V_+(L,r)$, with an equality identifying radial turning points.

Stationary points of $V_+(L,r)$ outside the black hole, when they exist, correspond to circular orbits. These satisfy the simultaneous conditions

$$E = V_+, \qquad \partial_r V_+ = 0 \quad \text{(circular orbits)}. \tag{2.5}$$

Substituting from Eq. (2.4) and solving for E and L in terms of the circular-orbit radius,

[1] Note, to avoid confusion, that in [55, 61, 62] one has instead $a/M = 1 - 2\epsilon^2$.

$r = R$, gives $E = E_c(R)$ and $L = L_c(R)$, with

$$E_c(R) = \frac{1 - 2\tilde{R}^{-1} + \tilde{a}\tilde{R}^{-3/2}}{\sqrt{1 - 3\tilde{R}^{-1} + 2\tilde{a}\tilde{R}^{-3/2}}}\,, \tag{2.6}$$

$$\tilde{L}_c(R) = \frac{\tilde{R}^{1/2}(1 - 2\tilde{a}\tilde{R}^{-3/2} + \tilde{a}^2\tilde{R}^{-2})}{\sqrt{1 - 3\tilde{R}^{-1} + 2\tilde{a}\tilde{R}^{-3/2}}}. \tag{2.7}$$

Here an overtilde denotes a-dimensionalization using M, i.e., $\tilde{R} := R/M$, $\tilde{a} := a/M$ and $\tilde{L} := L/M$; we shall adopt this notation from now on. Timelike circular-orbit solutions exist only for $R > R_{\rm ph}(a)$, the radius of a photon's unstable circular orbit ("light ring"). $R_{\rm ph}(a)$ is the (unique) root of $1 - 3\tilde{R}^{-1} + 2\tilde{a}\tilde{R}^{-3/2} = 0$ greater than the event horizon's radius, $\tilde{R}_{\rm eh}(a) = 1 + (1 - \tilde{a}^2)^{1/2}$.

The number of stationary points of V_+ and their location depend on L. There are none outside the black hole when L is below a certain critical value $L_{\rm isco}(a)$, and there are two for $L > L_{\rm isco}(a)$: a maximum representing an unstable circular orbit, and, further out, a minimum representing a stable one. The critical value $L_{\rm isco}(a)$ marks the innermost stable circular orbit (ISCO). It is given by $L_{\rm isco} = L_c(R_{\rm isco})$, where the ISCO radius $R_{\rm isco}$ is found by solving Eqs. (2.5) simultaneously with $\partial_r^2 V_+(L, r) = 0$. The ISCO may also be said to represent the outer boundary of unstable circular orbits. (This statement becomes somewhat subtle in the extremal limit, $\tilde{a} \to 1$, as we discuss below.)

The radii of unstable circular geodesic orbits span the interval $R_{\rm ph}(a) < R < R_{\rm isco}(a)$. This 1-parameter family of orbits will feature dominantly in our analysis, because it defines the capture–scatter threshold where much of the relevant physics occurs. Members of the family may be parametrized by either E or L, both being monotonically decreasing functions of R between $R_{\rm ph}$ (where $E, L \to \infty$) and $R_{\rm isco}$ for any $\tilde{a} < 1$. This monotonicity can be readily established from Eqs. (2.6) and (2.7). Hence, the radius R itself is also a valid parameter.

To each unstable circular orbit there correspond non-circular critical geodesic orbits that join the circular orbit asymptotically in either their infinite past or their infinite future, or both. Nearly-critical orbits exhibit a "zoom-whirl" behavior [66]: an episode of prolonged rotation ("whirl") about the location of the associated unstable circular orbit. We will see that all orbits relevant to the overspinning problem fall in that category. Unstable circular orbits may be divided into "bound" ($E < 1$) and "unbound" ($E > 1$). The radius of the innermost bound circular orbit (IBCO) is obtained by solving $E_c(R) = 1$, giving $\tilde{R}_{\rm ibco} = [1 + (1 - \tilde{a})^{1/2}]^2$.

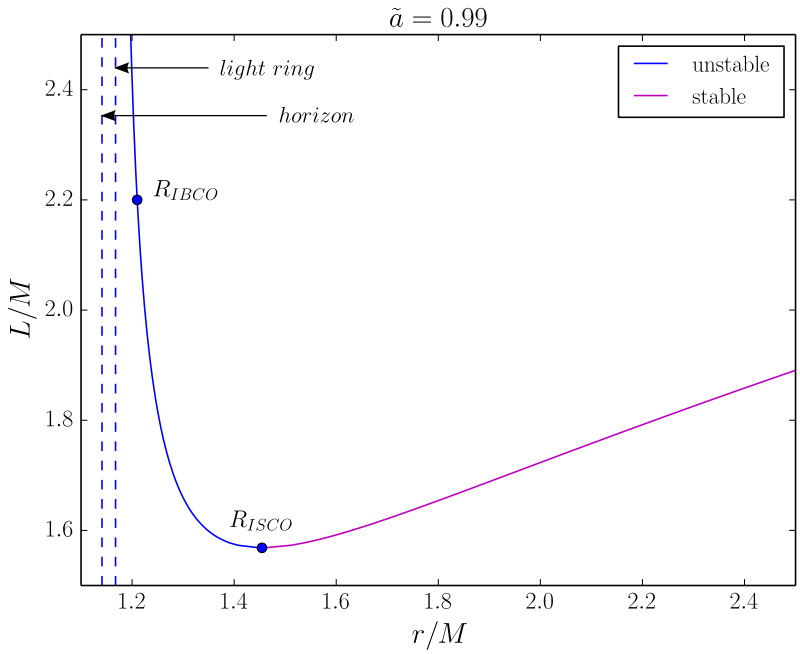

Figure 2.1: Circular equatorial orbits around a nearly extremal Kerr black hole, shown here for $a = 0.99M$. The plot shows specific angular momentum versus Boyer-Lindquist radius. Orbits with $r > R_{\rm isco}$ (magenta) are stable, while these with $r < R_{\rm isco}$ (blue) are unstable. Also indicated are the innermost bound circular orbit (IBCO, $E = 1$) and the photon orbit ("light ring", $E, L \to \infty$). In the extremal limit, $a \to M$, the radii $R_{\rm isco}$, $R_{\rm ibco}$ and $R_{\rm ph}$ all coincide with the horizon radius $R_{\rm eh}$.

Figure 2.1 illustrates the range of stable and unstable circular orbits, and the location of the various special orbits mentioned, in a particular example ($\tilde{a} = 0.99$). For easy later reference, we note here the ordering

$$R_{\rm eh} < R_{\rm ph} < R_{\rm ibco} < R_{\rm isco}, \tag{2.8}$$

which applies for any $\tilde{a} < 1$.

Let us now specialize to a near-extremal Kerr background with spin as in Eq. (2.1). One finds

$$\tilde{R}_{\rm eh} = 1 + \sqrt{2}\,\epsilon + O(\epsilon^2)\,, \tag{2.9}$$

$$\tilde{R}_{\rm ph} = 1 + \sqrt{8/3}\,\epsilon + O(\epsilon^2)\,, \tag{2.10}$$

$$\tilde{R}_{\rm ibco} = (1+\epsilon)^2 \quad \text{(exact)}\,, \tag{2.11}$$

$$\tilde{R}_{\rm isco} = 1 + (2\epsilon)^{2/3} + O(\epsilon^{4/3})\,. \tag{2.12}$$

The function $E_c(R)$ in Eq. (2.6) can be inverted perturbatively in ϵ to obtain the radius of an arbitrary unstable circular orbit in terms of its energy E. We find

$$\tilde{R} = 1 + \epsilon\rho_1(E) + \epsilon^2\rho_2(E) + O(\epsilon^3), \tag{2.13}$$

where the first two coefficients, needed below, read

$$\rho_1 = \frac{2\sqrt{2}E}{\sqrt{3E^2-1}}, \quad \rho_2 = \frac{2(2E^4-E^2+1)}{(3E^2-1)^2}. \tag{2.14}$$

Equation (2.11) is the special case of (2.13) with $E = 1$, giving $\rho_1 = 2$ and $\rho_2 = 1$.

It follows that, in the extremal limit $\epsilon \to 0$, the Boyer-Lindquist radii of the light-ring and the ISCO both coincide with the horizon radius, and so do the radii of all unstable circular orbits enclosed between them. Also peculiar is the fact that the ratio of coordinate differences $(\tilde{R}_{\rm isco} - \tilde{R}_{\rm eh})/(\tilde{R}_{\rm ibco} - \tilde{R}_{\rm eh})$ diverges as $\epsilon \to 0$. A careful inspection [67] reveals that the light ring, IBCO and ISCO remain well separated from the horizon, and from each other, when examined on a Boyer-Lindquist t=const slice. On that slice, the proper radial distance between the light-ring and the horizon is finite, and so is the distance between any finite-E unstable circular orbit and the light ring. On the other hand, the proper radial distance between the ISCO and any unstable circular orbit *diverges* on the t=const slice, and so does the distance between the ISCO and any circular orbit of radius $R > R_{\rm isco}$; the geometry of the t=const hypersurface appears to "stretch" infinitely around the ISCO location [67]. The situation, however, is rather different when examined on a horizon-crossing time slice. As emphasized recently by Jacobson [68], on any such slice, the light ring, IBCO and ISCO all actually coincide with horizon generators, so from that perspective they—and all unstable orbits in between them—are "at the same place" in the extremal limit.

These subtleties will not affect our analysis directly: ϵ will be kept small but nonzero, and the strict ordering (2.8) will therefore apply on any time slice. However, we must take note of the degeneracy of R as a parameter for unstable circular orbits when $\epsilon \to 0$. The energy E, on the other hand, remains a good parameter even in this limit, spanning the entire range $\infty > E > \frac{1}{\sqrt{3}}$. We will thus generally adopt E for labelling unstable circular orbits, with the added benefit of it allowing us a gauge-invariant description of the overspinning conditions in the self-force case. Given E, the angular momentum $L_c(R(E))$, which we henceforth write as $L_c(E)$, is obtained by substituting Eqs. (2.1) and (2.13) in

Eq. (2.7) and then expanding in ϵ. The result is

$$\tilde{L}_c(E) = 2E + (6E^2 - 2)^{1/2}\epsilon + O(\epsilon^2). \tag{2.15}$$

We note that to determine the $O(\epsilon)$ term here required the explicit values of both ρ_1 and ρ_2 of Eq. (2.14).

2.1.1 Exclusion of deeply bound orbits

Heuristically, if we assume our point particle represents a compact object—say, a Schwarzschild black hole—then its effective proper "diameter" is $\sim \mu$. Below it will become clear that a successful overspinning requires $\mu \sim \epsilon$, and so relevant objects have proper diameters $\sim \epsilon$. Now consider placing such an object in a deeply bound orbit with an *outer* turning point at $r < R_{\rm isco}$ [and with $L > L_c(E)$]. Such an object (it can be checked) will plunge through the horizon within a proper time of $O(\epsilon)$ (at most), comparable to its own "light-crossing time". It is not clear whether the object can be made to initially "fit" in its entirety outside the hole. At the very least, it is not clear if the simple model of a point particle and a stationary horizon provides a faithful description of the physics in this case.

To avoid such subtleties, we wish to exclude deeply bound orbits from our analysis. We achieve this by requiring that, if the orbit possesses an outer radial turning point at some $r = r_{\rm out}$, then

$$r_{\rm out} > R_{\rm isco}(\epsilon). \tag{2.16}$$

It can be checked that, under this condition, the proper-time interval along any timelike equatorial geodesic connecting $r = r_{\rm out}$ to $r = R_{\rm eh}$ is finite (nonzero) even in the limit $\epsilon \to 0$ (taken with fixed E, L). The condition (2.16) demands that eligible particles must clear the peak of the effective potential as they plunge into the black hole. This requirement excludes from the analysis orbits starting off between the peak of the potential and the horizon, for which finite-size effects are expected to be non-negligible.

2.2 Overspinning domain

Given the restriction (2.16), a necessary and sufficient condition for a falling particle of specific energy E to be captured by the black hole is

$$L < L_c(E). \tag{2.17}$$

A captured particle would overspin the black hole if and only if

$$(M + \mu E)^2 < aM + \mu L. \tag{2.18}$$

Using $\tilde{a} = 1 - \epsilon^2$ and introducing the small mass ratio $\eta := \mu/M$, this condition becomes

$$\epsilon^2 + \eta W + \eta^2 E^2 < 0\,, \tag{2.19}$$

where we have introduced[2]

$$W := 2E - \tilde{L}. \tag{2.20}$$

Note that Eq. (2.19) sets an upper bound on L (for given E, η, ϵ), while Eq. (2.17) sets a lower bound. Also note that Eq. (2.19) implies the necessary condition $W < 0$ for overspinning to occur.

Our goal now is to identify the complete domain in the space of $\{\eta, E, L\}$ for which the conditions (2.17) and (2.19) are simultaneously satisfied, assuming $\epsilon \ll 1$ and the condition (2.16). For easy reference, let us call this domain "OS", for "overspinning".

We first show that orbits with $L \leq L_{\rm isco}$ all fall *outside* OS. To this end, consider first the ISCO itself, where $W = 2E_{\rm isco} - \tilde{L}_{\rm isco} =: W_{\rm isco}$. Using Eqs. (2.6), (2.7) and (2.12) we obtain $W_{\rm isco} = -\hat{c}\epsilon^{4/3} + O(\epsilon^2)$, where $\hat{c} = 2^{1/3}\sqrt{3} > 0$. Thus, $W_{\rm isco}$ is negative as required, but it can be easily checked that (2.19) is always violated for sufficiently small ϵ: Replacing $W \to -\hat{c}\epsilon^{4/3}$ in Eq. (2.19) and considering the left-hand side as a quadratic function of η, we find this function is positive definite for any $\epsilon < (2E_{\rm isco}/\hat{c})^3$. [Since $E_{\rm isco}$ is bounded from below by $E_{\rm isco}(\epsilon = 0) = \frac{1}{\sqrt{3}}$, we find that (2.19) is always violated for $\epsilon < \frac{4}{27}$.] This rules out the ISCO itself, and it immediately rules out also all orbits with $\{E > E_{\rm isco}, L = L_{\rm isco}\}$, for which $W > W_{\rm isco}$. Orbits with $\{E < E_{\rm isco}, L_{\rm isco}\}$ *can* potentially satisfy Eq. (2.19), but they are always deeply bound in the sense of failing to satisfy Eq. (2.16): For any $E < E_{\rm isco}$, the orbit has an outer radial turning point at a radius $r_{\rm out} < R_{\rm isco}$.

The upshot is that orbits with $L = L_{\rm isco}$ are all outside OS. For orbits with $L < L_{\rm isco}$ we would need to require $E < E_{\rm isco}$ in order for W to be sufficiently negative. But, once again, such orbits are excluded on account of their being deeply bound. We conclude that orbits with $L \leq L_{\rm isco}$ are all outside OS.

Let us focus therefore on orbits with $L > L_{\rm isco}$. For such an orbit to be in OS, we

[2]Heuristically, $W/2$ may be interpreted as the specific energy in a co-rotating frame with $\tilde{\Omega} = 1/2$, i.e., the common angular velocity of all unstable circular geodesics in the extremal limit.

require that (given E, η, ϵ) L is bounded from above by $L_c(E)$ and simultaneously from below via Eq. (2.19):

$$\epsilon^2 + 2\eta E + \eta^2 E^2 < \eta \tilde{L} < \eta \tilde{L}_c(E;\epsilon). \tag{2.21}$$

We have made here the ϵ dependence of L_c explicit, for clarity. The span of the permissible range is $\eta\Delta_L := -\epsilon^2 - \eta[2E - \tilde{L}_c(E;\epsilon)] - \eta^2 E^2$, or, using Eq. (2.15),

$$\eta\Delta_L = -\epsilon^2 + \eta\epsilon\sqrt{6E^2 - 2} - \eta^2 E^2, \tag{2.22}$$

where we have omitted terms of $O(\eta\epsilon^2)$. OS is populated if and only if we can find E, η, ϵ for which $\Delta_L > 0$.

A few conclusions can be drawn immediately. First, considering $\eta\Delta_L$ in Eq. (2.22) as a quadratic function of η, we find it has a maximum value

$$\max_{\eta} \eta\Delta_L = \frac{\epsilon^2(E^2 - 1)}{2E^2}. \tag{2.23}$$

This is positive only for $E > 1$. Therefore, all orbits with $E \leq 1$ fall outside OS. *Bound orbits cannot overspin.*

Second, for any $E > 1$, we can obtain $\Delta_L > 0$ by choosing the mass ratio η from within the interval

$$\epsilon\eta_-(E) < \eta < \epsilon\eta_+(E), \tag{2.24}$$

where

$$\eta_\pm = \frac{1}{\sqrt{2}\,E^2}\left[\sqrt{3E^2 - 1} \pm \sqrt{E^2 - 1}\right]. \tag{2.25}$$

In other words, *overspinning can be achieved for any $E > 1$, as long as η satisfies (2.24).* Since the condition $\Delta_L > 0$ is both necessary and sufficient, the converse also holds: All orbits in OS satisfy $E > 1$ with Eq. (2.24).

Third, from Eq. (2.24) it follows that η must be chosen to be of $O(\epsilon)$ (assuming $E \ll 1/\epsilon$). One can check that η_+ has a maximal value of

$$\max_{E} \eta_+ = \sqrt{3/2}, \tag{2.26}$$

obtained for $E = 2/\sqrt{3}$. Therefore, *the range $\eta \geq \sqrt{3/2}\,\epsilon$ lies outside OS.* The bandwidth

of admissible mass ratios, for given E and ϵ, is

$$\Delta_\eta := \epsilon\eta_+ - \epsilon\eta_- = \epsilon\sqrt{2(E^2-1)}/E^2, \tag{2.27}$$

which is maximal for $E = \sqrt{2}$. Figure 2.2 depicts the permissible range of η/ϵ as a function of E.

Fourth, from Eqs. (2.23) and (2.27) we learn that an $E = \text{const}(> 1)$ slice of OS has maximal dimensions $\Delta_L \sim \epsilon^2/\eta \sim \epsilon$ and $\Delta_\eta \sim \epsilon$. OS is thus a narrow "tube" in the $\{E, L, \eta\}$ parameter space, of a cross section $\sim \epsilon \times \epsilon$, whose boundary is tangent to the surface of unstable circular orbits, $L = L_c(E)$.

To summarize, we have found that OS is a narrow tube-like region of the $\{E, L, \eta\}$ space, described by $E > 1$, $L_c(E;\epsilon) - \Delta_L(E,\eta;\epsilon) < L < L_c(E;\epsilon)$ and $\epsilon\eta_-(E) < \eta < \epsilon\eta_+(E)$, where Δ_L and $\eta_\pm$ are given in Eqs. (2.22) and (2.25), respectively. A neater description of the OS window is obtained in terms of the quantity W defined in Eq. (2.20): Rearranging Eq. (2.21) and using (2.15), we find

$$\epsilon W_-(E) < W < \epsilon W_+(E, \eta/\epsilon), \tag{2.28}$$

where

$$W_- = -\sqrt{6E^2-2}, \qquad W_+ = -\left(\frac{\epsilon}{\eta} + \frac{\eta}{\epsilon}E^2\right). \tag{2.29}$$

This domain is illustrated in Figure 2.3 for a sample of η/ϵ values. To overspin a black hole of given M and $\epsilon \ll 1$, one should pick an E greater than 1, choose any η from within the interval (2.24), and then choose W (hence L) from within the interval (2.28).

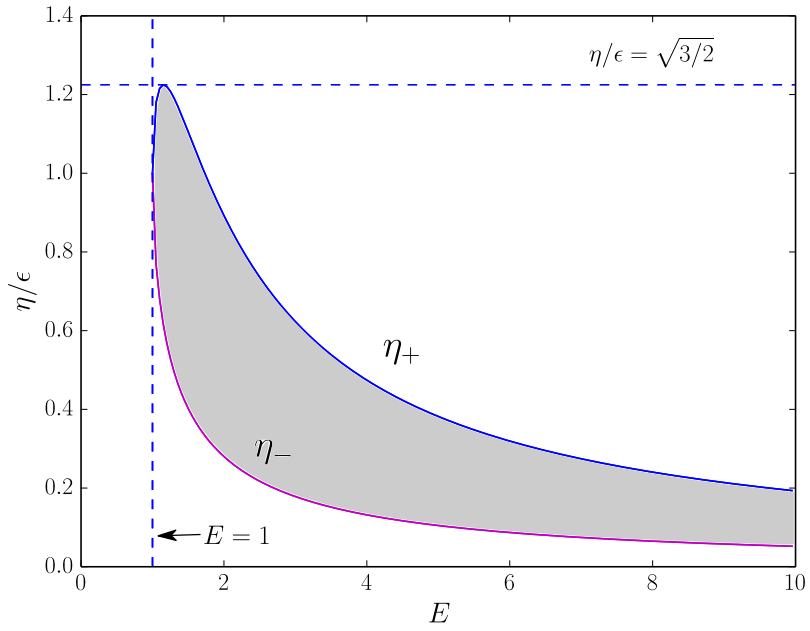

Figure 2.2: Domain of mass ratios η for which overspinning is possible in the geodesic approximation. η is shown divided by the near-extremality parameter $\epsilon = (1 - a/M)^{1/2}$, and E is the particle's specifi c energy. The boundaries $\eta_\pm(E)$ are given in Eq. (2.25). Overspinning is not possible for $E < 1$ or $\eta > \sqrt{3/2}\,\epsilon$. However, for any value $E > 1$ there is a range of η for which the black hole may be overspun. This happens if the particle's angular momentum is chosen from within the range indicated in Eq. (2.24).

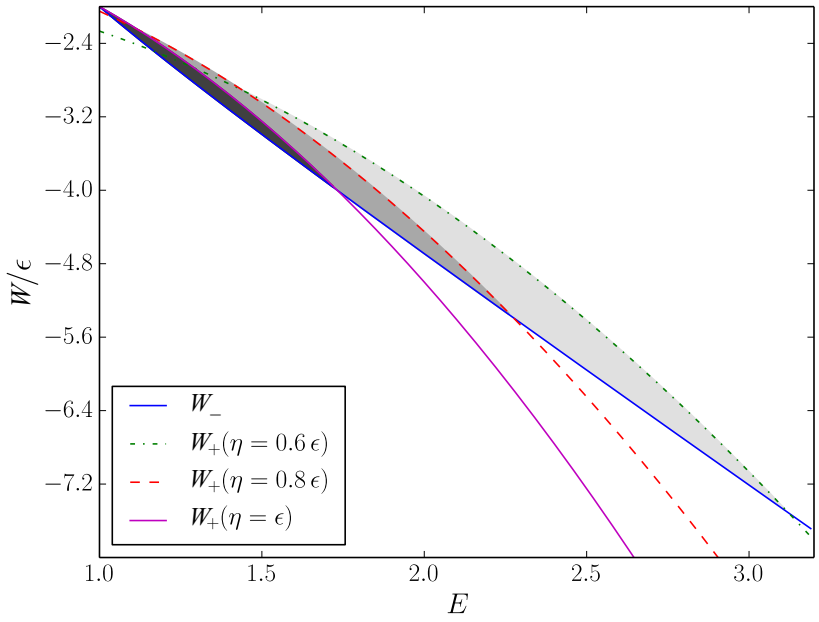

Figure 2.3: The overspinning window, shown in the plane of E, W (where $W = 2E - L/M$) for several values of η/ϵ. Note W is shown divided by ϵ. The boundaries $W_\pm$ are given in Eq. (2.29). The lower boundary $W_-(E)$ (which does not depend on η) arises from the requirement that the particle is captured by the black hole. The upper boundary $W_+(E, \eta/\epsilon)$ comes from the requirement that the final object is an over-extremal black hole. Overspinning is possible with any $E > 1$, provided η is chosen from within the range shown in Eq. (2.28).

Chapter 3

Overspinning with the full self-force

Because the width of the overspinning window is of $O(\eta)$, self-gravity effects may potentially shut this window close, and they must therefore be included in the analysis. Specifically, the gravitational self-force modifies the capture condition (2.17) by changing the functional relation $L_c(E)$ at $O(\eta)$. It also modifies the overspinning condition (2.18) by dissipating away some of the system's initial energy and angular momentum. The key results of this chapter will be given in Sec. 3.4, where we will provide conditions for capture and overspinning under the full GSF effect.

As we explained in the introduction, the equations of motion including the leading-order GSF, may be written in the form

$$\mu \hat{u}^\beta \nabla_\beta \hat{u}^\alpha = F^\alpha. \tag{3.1}$$

Here $\hat{u}^\alpha$ is the particle's four-velocity, tangent to the (accelerated) trajectory in the background spacetime (Kerr, in our case) and normalized using

$$g_{\alpha\beta}\hat{u}^\alpha \hat{u}^\beta = -1, \tag{3.2}$$

where $g_{\alpha\beta}$ is the background (Kerr) metric. The covariant derivative in (3.1) is taken with respect to $g_{\alpha\beta}$, and F^α is the first-order GSF, proportional to μ^2. The GSF is normal to the four-velocity, $g_{\alpha\beta}\hat{u}^\alpha F^\beta = 0$, so that the rest mass μ remains constant [1].

[1] The situation is different for a scalar charge, where the inclusion of the self-force can source a time-dependent shift in the particle's mass. A study of this phenomenon in cosmological spacetimes can be found in [69].

Now consider a particle sent in along the equator of the Kerr black hole, i.e. with $\theta = \pi/2$ and $\hat{u}^\theta = 0$ at the initial moment, where hereafter τ is proper time along the self-accelerated orbit in $g_{\alpha\beta}$. In any reasonable gauge, the component F^θ would vanish from symmetry and the motion will remain equatorial. Let us then define

$$\hat{E} := -\hat{u}_t, \qquad \hat{L} := \hat{u}_\phi, \tag{3.3}$$

in analogy with E and L of the geodesic case. Here, however, $\hat{E}$ and $\hat{L}$ are not constants of the motion. Rather, Eq. (3.1) tells us they evolve (slowly) according to

$$\mu\frac{d\hat{E}}{d\tau} = -F_t, \qquad \mu\frac{d\hat{L}}{d\tau} = F_\phi, \tag{3.4}$$

where $F_\alpha = g_{\alpha\beta}F^\beta$. With these definitions, Eq. (3.2) produces the radial equation of motion

$$\dot{r}^2 = B(r)\left(\hat{E} - V_-(\hat{L}, r)\right)\left(\hat{E} - V_+(\hat{L}, r)\right), \tag{3.5}$$

whose form is identical to that of Eq. (2.3)—except that here $\hat{E}$ and $\hat{L}$ are slow functions of τ along the orbit.

The results of the previous section lead us to focus attention on particles sent in from infinity, i.e., ones with $r(\tau \to -\infty) \to \infty$. For such particles, we define

$$E_\infty := \hat{E}(\tau \to -\infty), \qquad L_\infty := \hat{L}(\tau \to -\infty). \tag{3.6}$$

From Eq. (3.4) we have

$$\hat{E}(\tau) = E_\infty + \Delta E(\tau), \qquad \hat{L}(\tau) = L_\infty + \Delta L(\tau), \tag{3.7}$$

where

$$\mu\Delta E(\tau) = -\int_{-\infty}^{\tau} F_t\, d\tau, \qquad \mu\Delta L(\tau) = \int_{-\infty}^{\tau} F_\phi\, d\tau. \tag{3.8}$$

In principle, the coupled set (3.5) with (3.7) determines the self-accelerated orbit, given the initial values E_∞, L_∞ and a method for calculating the GSF along the orbit.

3.1 Conservative and dissipative GSF for quasi-circular orbits

Using Eqs.(1.26)-(1.27), one can immediately conclude that, for circular orbits, for which $F^\alpha(r,\dot{r}) = F^\alpha(r,-\dot{r})$, F^t, F^ϕ are purely dissipative while F^r is purely conservative. In general, however, each component has both dissipative and conservative pieces. Of particular interest to us will be nearly-circular orbits with $|\dot{r}| \ll 1$. Along such orbits we may write, to leading order in $|\dot{r}|$,

$$F^\alpha_{\rm cons} \simeq \dot{r} F^\alpha_1(r), \qquad F^\alpha_{\rm diss} \simeq F^\alpha_0(r) \tag{3.9}$$

for $\alpha = t, \phi$, and

$$F^r_{\rm cons} \simeq F^r_0(r), \qquad F^r_{\rm diss} \simeq \dot{r} F^r_1(r), \tag{3.10}$$

where F^α_0 and F^α_1 are some functions of r only.

Equations (1.26)–(1.27) and (3.9)–(3.10) are applicable, at leading order in η, even for an orbit that is slowly evolving under the GSF effect. In that case the GSF depends also on the instantaneous self-acceleration, but that dependence appears only at subleading order in η.

The GSF integrals ΔE and ΔL can be related, in certain situations, to asymptotic fluxes of energy and angular momentum in gravitational waves. This was established rigorously in Ref. [18] for a trajectory starting and ending at infinity.[2] A similar balance relation has been argued to hold also for adiabatic inspiral orbits around a black hole, subject to a suitable averaging over many orbital periods [70, 71]. In both scenarios, the contribution from $F^\alpha_{\rm cons}$ to the integrals ΔE and ΔL (taken from $\tau = -\infty$ to $\tau = +\infty$) vanishes at leading order, by virtue of the orbital symmetry expressed in Eq. (1.26). This guarantees that the radiated fluxes balance the work done by the *dissipative* piece of the self-force alone, as expected.

3.2 ADM energy and angular momentum

Our analysis in the next section will require knowledge of the total, conserved ADM energy and angular momentum contents of the spacetime in the above setup. Specifically, we will need expressions for $E_{\rm ADM}$ and $L_{\rm ADM}$ in terms of E_∞ and L_∞ (and the two masses, M

[2] The configuration considered in Ref. [18] had no black hole in it, but the authors argue convincingly that a similar conclusion would hold also in the black hole case, if fluxes down the event horizon were accounted for in the balance equation.

and μ), correct through $O(\mu^2)$. A subtlety is that ADM quantities are most conveniently evaluated in a "center-of mass" system (and, at the required order, would include a contribution from the black hole's "recoil" motion), whereas E_∞ and L_∞ are components of the particle's four-velocity, defined in a coordinate system centred around the black-hole.

In our setup, the ADM quantities are most easily evaluated on a hypersurface of constant $t \ll -M$, where the binary separation is $r \gg M$. In the limit $t \to -\infty$ ($r \to \infty$), the gravitational interaction energy vanishes and does not contribute to $E_{\rm ADM}$. Working at that limit, we assume that, for the purpose of calculating ADM quantities, the black hole–particle system may be replaced with that of two relativistic point-like particles in flat spacetime. $E_{\rm ADM}$ is then simply the sum of the two relativistic energies in the center-of-mass frame, and $L_{\rm ADM}$ is similarly the sum of two angular momenta (with respect to the center of mass), plus the spin of the black hole.

Appendix A gives the details of this calculation, which is straightforward. The result is

$$E_{\rm ADM} = M\left[1 + \eta E_\infty - \frac{1}{2}\eta^2(E_\infty^2 - 1)\right] + o(\eta^2), \tag{3.11}$$

$$L_{\rm ADM} = M\left(a + \eta L_\infty - \eta^2 L_\infty E_\infty\right) + o(\eta^2). \tag{3.12}$$

3.3 Critical orbits

In the geodesic case we have introduced the function $L_c(E)$, which we now interpret as the *critical value* of the angular momentum for a given energy: Geodesic orbits with $L > L_c(E)$ scatter back to infinity, while ones with $L < L_c(E)$ fall into the black hole. This type of critical behavior carries over to the GSF case, though radiation losses then introduce a subtlety, since orbits that are initially scattered may fall into the black hole at a subsequent approach. However, we may still speak of a critical threshold for an *immediate* capture, which separates (in the space of initial conditions) between orbits that scatter at first approach and orbits that do not. A detailed analysis of this critical behavior was given in Ref. [72] for orbits in Schwarzschild spacetime (working in the first-order GSF approximation, as here), and in the following discussion we assume the same qualitative behavior applies in the Kerr case too.

In particular, we assume there exists a critical value $L_\infty = L_{\infty,c}(E_\infty)$ that separates between the two possible outcomes. The initial conditions $\{E_\infty, L_{\infty,c}(E_\infty)\}$ thus define a one-parameter family of "critical orbits". Let us denote by $\hat{E}_c(\tau; E_\infty)$ and $\hat{L}_c(\tau; E_\infty)$

the functions $\hat{E}(\tau)$ and $\hat{L}(\tau)$ corresponding to a critical orbit with a given E_∞ [so that $\hat{E}_c(\tau \to -\infty; E_\infty) = E_\infty$ and $\hat{L}_c(\tau \to -\infty; E_\infty) = L_{\infty,c}(E_\infty)$]. Unlike in the geodesic case where critical geodesics of different E are disjoint, in the GSF case all critical orbits join a *global attractor*, which is the perfectly fine-tuned orbit that evolves radiatively along the sequence of unstable circular orbits starting at the light ring and ending at the ISCO, where it plunges into the black hole. Figure 1 in Ref. [72] illustrates the evolution of the critical orbit along the attractor, and see also Fig. 3.1 below.

Let us define the "GSF correction"

$$\delta L_c(\tau; E_\infty) := \hat{L}_c(\tau; E_\infty) - L_c(E_\infty), \tag{3.13}$$

and then

$$\delta L_\infty(E_\infty) := \delta L_c(\tau \to -\infty; E_\infty). \tag{3.14}$$

δL_∞ is the GSF-induced shift in the critical value of L_∞ at a fixed E_∞. It may also be interpreted in terms of a GSF correction to the critical impact parameter.

We assume that the difference $\delta L_c(\tau; E_\infty)$ remains small [$O(\eta)$] during the approach, which should be the case in any reasonable gauge. However, clearly, that difference ceases to remain small as the critical orbit joins the global attractor and evolves along it; then the meaning of $\delta L_c(\tau; E_\infty)$ as a small GSF correction is lost.

For our analysis of overspinning orbits in the next section, we will require an explicit expression for $\delta L_\infty(E_\infty)$ in terms of GSF quantities. It is instructive to derive this relation first with the dissipative piece of the GSF turned off, i.e. replacing the full GSF with its conservative piece (in which case the global attractor disappears, and critical orbits of different E_∞ remain disjoint). Let us call the resulting quantity $\delta L_\infty^{\rm cons}(E_\infty)$. As a second step we will restore dissipation and consider its effect.

3.3.1 Conservative GSF effect

With dissipation turned off, the critical orbit becomes exactly stationary at $\tau \to \infty$, where it joins an unstable (nongeodesic) circular orbit of radius $\hat{R}(E_\infty) = R(E_\infty) + \delta R$. Here $R(E_\infty)$ is the geodesic relation given in Eq. (2.13), and δR is a conservative GSF correction. To obtain $\delta L_\infty^{\rm cons}$ we first substitute $\hat{E}$ and $\hat{L}$ from Eq. (3.7) into the radial equation of motion (3.5), replacing L_∞ with $L_c(E_\infty) + \delta L_\infty^{\rm cons}(E_\infty)$, where $L_c(E_\infty)$ is the geodesic relation given in Eq. (2.15). We then demand $dr/d\tau = 0$ as well as $d^2r/d\tau^2 = 0$ at $r = \hat{R}$ through $O(\eta)$.

At leading order in ϵ this yields two algebraic equations for the two $O(\eta)$ unknowns $\delta L_\infty^{\rm cons}$ and δR, given E_∞ and the GSF. The solution is

$$\delta L_\infty^{\rm cons}(E_\infty) = 2M\Delta E^{\rm cons}(\infty) - \Delta L^{\rm cons}(\infty), \tag{3.15}$$

and $\delta R(E_\infty) = O(\epsilon)O(\eta)$. Here $\Delta E^{\rm cons}$ and $\Delta L^{\rm cons}$ are the same as ΔE and ΔL of Eq. (3.8), but with $F_\alpha \to F_\alpha^{\rm cons}$, and with the GSF integrals evaluated along the critical orbit with energy-at-infinity E_∞. The precise dependence of δR on the GSF will not be needed, but we note that the $O(\epsilon\eta)$ GSF correction to the radius of the critical circular orbit is reassuringly small compared to the $O(\epsilon)$ radial distance to the light ring.

To simplify the appearance of subsequent equations, let us from now on use units in which $M = 1$. This, in particular, makes our "tilde" notation redundant (with $\tilde{L} = L$, etc.) and μ becomes interchangeable with η. Recalling our W notation from Eq. (2.20), we rewrite Eq. (3.15) as

$$\delta L_\infty^{\rm cons}(E_\infty) = \Delta W^{\rm cons}(\infty), \tag{3.16}$$

where $\Delta W^{\rm cons}$ represents the conservative piece of

$$\begin{aligned} \Delta W(\tau) &:= 2\Delta E(\tau) - \Delta L(\tau) \\ &= -\eta^{-1}\int_{-\infty}^{\tau} (2F_t + F_\phi)\, d\tau. \end{aligned} \tag{3.17}$$

The quantity $\Delta W^{\rm cons}(\infty)$ is the limit $\tau \to \infty$ of $\Delta W^{\rm cons}(\tau)$. Does this limit actually exist? The answer is positive, since both $F_t^{\rm cons}$ and $F_\phi^{\rm cons}$ vanish exponentially fast in τ as the orbit approaches the limiting circular orbit at $\tau \to \infty$.

To make this last statement more precise, let us split the τ integral into an "approach" piece, $\int_{-\infty}^{\tau_c}$, and a "quasi-circular" piece, $\int_{\tau_c}^{\infty}$, with τ_c chosen so that $\delta r(\tau_c)$, where $\delta r(\tau) := r(\tau) - \hat{R}$, is already very small. For a small δr we have the form $F_t^{\rm cons} \simeq \dot{r} F_{1t}(r)$ [Eq. (3.9)] and similarly for $F_\phi^{\rm cons}$. Thus $\int_{\tau_c}^{\infty} F_t^{\rm cons} d\tau \simeq -F_{1t}(\hat{R})\delta r(\tau_c)$, and similarly for the ϕ component. A local analysis of Eq. (3.5) near the limiting circular orbit gives $\delta r \sim e^{-\lambda\tau}$, with a Lyapunov exponent $\lambda = M^{-1}(3E_\infty^2 - 1)^{1/2}$ at leading order in ϵ (and ignoring the small effect of the GSF). The choice $\tau_c = -\lambda^{-1}\log\eta$, for example, gives $\delta r(\tau_c) \sim \eta$, and the quasi-circular piece of $\Delta W^{\rm cons}$ does not contribute to $\delta L_\infty^{\rm cons}$ at leading order in η.

Our discussion assumes that $\Delta E(\tau_c)$ and $\Delta L(\tau_c)$ [hence also $\Delta W(\tau_c)$] are $O(\eta)$ quantities, i.e. that the accumulated GSF-induced positional shift in the orbit during the approach is a small, $O(\eta)$ quantity. This should be the case in any reasonable gauge. Under this

assumption, we note that the value of the integral ΔW remains unchanged, at leading order in η, if in Eq. (3.17) we replace the integration along the actual, GSF-perturbed orbit, with an integration along the critical *geodesic* of energy E_∞. This can be exploited to simplify actual calculations: To compute $\delta L_\infty^{\rm cons}$ at leading order in η requires only an evaluation of the GSF along a fixed geodesic, and there is no need to consider the back-reaction from the GSF on the orbital trajectory.

3.4 Full GSF effect

Now restore dissipation. The fine-tuned critical orbit no longer settles into a strictly stationary motion, but rather it continues to evolve radiatively, in an adiabatic fashion, through a sequence of unstable circular orbits of decreasing energies (hence increasing radii). With a perfect fine-tuning, the orbit can reach the ISCO before plunging into the black hole—a scenario illustrated in Fig. 3.1.

A relation between the degree of fine-tuning and the amount of energy loss was derived in Ref. [72] (for the Schwarzschild case): Rewriting their Eq. (124) in terms of angular momentum, we have the scaling $\delta L/L_{\infty,c} \sim \exp[(E_{\rm f}-E_{\rm i})/\eta]$, where δL (not to be confused with the GSF shift δL_∞) is any small perturbation in the value of the initial angular momentum off the critical value $L_{\infty,c}$, and $E_{\rm f}-E_{\rm i}$ is the resulting change in specific energy as the orbit progresses along the global attractor. To achieve an $O(1)$ change in the specific energy requires an "exponentially delicate" fine-tuning, $\delta L/L_{\infty,c} \sim \exp(-1/\eta)$.

For our analysis we do not require knowledge of the perfectly fine-tuned angular momentum at that level. We need $L_{\infty,c}$ through $O(\eta)$ only. Fine-tuning at $O(\eta)$ [corresponding to $\delta L = o(\eta)$] guarantees only $E_{\rm f}-E_{\rm i} = O(\eta\ln\eta)$. Therefore, for the purpose of determining $L_{\infty,c}$ through $O(\eta)$, it is sufficient to restrict attention to the early part of the critical orbit, where ΔE and ΔL (specific values) are still $O(\eta\ln\eta)$ at most, and have not yet accumulated $O(1)$ changes.

Consider a critical orbit parametrized by $E_\infty(\geq 1)$, and an arbitrary moment $\tau = \tau_0$ after the orbit had settled into quasi-circular motion, but before $\Delta E(\tau_0)$ and $\Delta L(\tau_0)$ have accumulated $O(1)$ changes [specifically, assume $\Delta E(\tau_0), \Delta L(\tau_0) = O(\eta\ln\eta)$ at most]. Evaluate the full-GSF radial equation of motion (3.5) at time τ_0, subject to the near-circularity condition $dr/d\tau = O(\eta)$, substituting for $\hat{E}(\tau_0)$ and $\hat{L}(\tau_0)$ from Eq. (3.7), and replacing L_∞ with $L_c(E_\infty) + \delta L_\infty(E_\infty)$. At leading order in η and in ϵ one obtains the

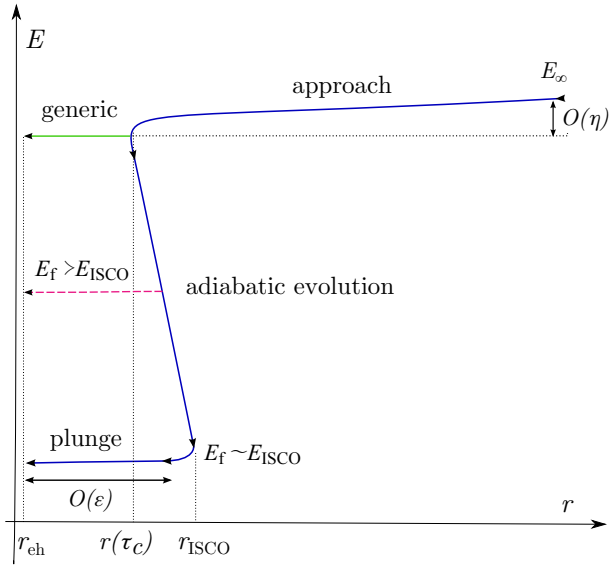

Figure 3.1: Schematic illustration of the evolution of orbital energy along a perfectly fine-tuned critical orbit (solid blue curve). The orbit approaches from infinity, becomes trapped on an unstable circular orbit, and then evolves adiabatically in a quasi-circular fashion before transiting to plunge around the ISCO location. Radiative losses are small during the approach and plunge, but, through fine-tuning, the orbit can be made to lose "all" its energy during the quasi-circular stage. Intermediate values of the final energy E_f may also be obtained by fine-tuning (dashed magenta line). Note the orbital radius *increases* through radiation losses during the quasi-circular stage. In the near-extremal case, $\epsilon \ll 1$, the quasi-circular evolution occurs within a small range of coordinate radii, $\Delta r = O(\epsilon)$.

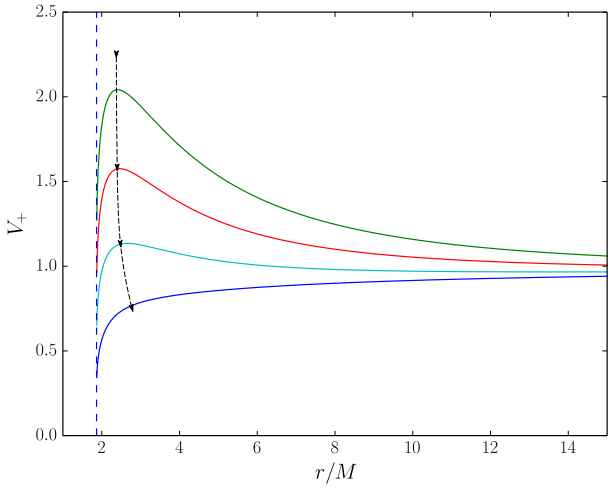

Figure 3.2: Sequence of effective potentials along the global attractor. A strongly fine-tuned orbit (black dashed line) emits energy and angular momentum so that it hovers on the peak of a sequence of effective potentials with decreasing L. Notice that, while L decreases, the location of the peak moves further away from the horizon (vertical dashed blue line) and so does the orbit, as indicated by the arrows. A perfectly fine-tuned orbit follows the global attractor until it reaches the ISCO (blue line on the bottom of the plot), where the curvature of the potential is such that the small mass is then forced to plunge into the black hole. Here we show the effective potential $V_+(L, r)$ of Eq. (2.4) for $a = 0.99$ and a sample of values of $L = L_{ISCO}(a = 0.99) + n$, with $n = 0...3$ (note that the green line represents $L_{ISCO} + 3$).

solution

$$\delta L_\infty(E_\infty) = \Delta W(\tau_0), \tag{3.18}$$

where ΔW is the GSF integral defined in Eq. (3.17). This result can only make sense if (i) the expression on the right-hand side is in fact independent of τ_0 at leading order; and (ii) the quantity $\Delta W(\tau_0) = 2\Delta E(\tau_0) - \Delta L(\tau_0)$ remains of $O(\eta)$ even for τ_0 large enough that the individual terms $\Delta E(\tau_0)$ and $\Delta L(\tau_0)$ are already of $O(\eta \ln \eta)$. We now argue that both conditions are satisfied.

To make the argument, let us split $\Delta W(\tau_0)$ into an "approach" piece $\Delta W(\tau_c)$, and a "quasi-circular" piece

$$\begin{aligned} \Delta W(\tau_c, \tau_0) &:= \Delta W(\tau_0) - \Delta W(\tau_c) \\ &= -\eta^{-1} \int_{\tau_c}^{\tau_0} (2F_t + F_\phi)\, d\tau. \end{aligned} \tag{3.19}$$

Here the end-of-approach time τ_c can be taken to be any moment $\tau_c < \tau_0$ after the orbit had settled into quasi-circular motion, in the sense that $\dot{r}(\tau_c) = O(\eta)$ at most. We will now show that

$$\Delta W(\tau_c, \tau_0) = O(\epsilon) O(\eta \ln \eta) \tag{3.20}$$

at most, for any choice of τ_0 and of τ_c. Assuming $\epsilon |\ln \eta| \ll 1$, this would mean that $\Delta W(\tau_0)$ is dominated by its approach piece $\Delta W(\tau_c)$, so that (i) $\Delta W(\tau_0)$ does not depend on τ_0 at leading order, and (ii) $\Delta W(\tau_0) \simeq \Delta W(\tau_c) = O(\eta)$ as argued above.

To establish the scaling in (3.20), we use the orthogonality relation $\hat{u}^\alpha F_\alpha = 0$ to write $F_t + \Omega F_\phi = -(u^r/u^t) F_r$, where $\Omega = u^\phi/u^t$, and the replacement $\hat{u}^\alpha \to u^\alpha$ does not affect the expression at leading order in η. We wish to evaluate this relation for $\tau_c \le \tau \le \tau_0$, when the orbit is quasi-circular. At leading order in η, $\Omega = \Omega(E; \epsilon)$ is then equal to the angular velocity of an unstable circular geodesic of specific energy $E = \hat{E}(\tau)$. At fixed energy, the angular velocity admits the small-ϵ expansion $\Omega = \frac{1}{2} - \frac{1}{4} b(E) \epsilon + O(\epsilon^2)$ with $b = 6E(6E^2 - 2)^{-1/2}$ [see Eqs. (3.62) and (3.63)]. Thus, omitting terms that are subdominant in ϵ, the integrand in Eq. (3.19) is $2F_t + F_\phi = -2(u^r/u^t) F_r + 1/2(b\epsilon F_\phi)$, or, equivalently,

$$2F_t + F_\phi = -2(u^r/u^t) F_r - b\epsilon F_t. \tag{3.21}$$

Let us denote the contributions to $\Delta W(\tau_0, \tau_c)$ from the first and second terms on the right-hand side of (3.21) by $\Delta W_{(r)}$ and $\Delta W_{(t)}$, respectively. In what follows we consider each of

the two contributions in turn.

Start with $\Delta W_{(r)}$, given by

$$\Delta W_{(r)} = (2/\eta) \int_{r(\tau_c)}^{r(\tau_0)} \left(F_r/u^t \right) dr. \tag{3.22}$$

Note $r(\tau_0) - r(\tau_c) = O(\epsilon)$, since both radii belong to unstable circular geodesics. From Eq. (3.10) we recall that for $|\dot{r}| \ll 1$ the radial component F_r is dominated by its conservative piece, $F_r^{\rm cons} \simeq F_{0r}(r)$, which is approximately constant within the integration domain and may therefore (as we only keep track of the leading term in ϵ) be pulled out of the integral. A simple calculation gives $1/u^t \propto \epsilon$ (at fixed E), and this factor can likewise be taken out of the integral. We thus obtain the scaling $\Delta W_{(r)} \sim \epsilon^2 F_{0r}/\eta$, where F_{0r} is evaluated, e.g., at $r = r(\tau_c)$, the end of approach. It remains to determine the ϵ-scaling of F_{0r}. Numerical evidence suggests the scaling $F_{0r} \sim \epsilon^{-1}$. This is consistent with what one would obtain by assuming that the GSF components in a normalized coordinate basis are finite: $F_{0r} = F_{0\hat{r}}(g^{rr})^{-1/2} \sim \epsilon^{-1}$ (or smaller), assuming the normalized component $F_{0\hat{r}}$ is finite and noting $g^{rr} \sim \epsilon^2$. Assuming, therefore, that F_{0r} does not diverge faster than $\sim \epsilon^{-1}$, and recalling $F_{0r} \propto \eta^2$ as usual, we arrive at

$$\Delta W_{(r)} = O(\epsilon) O(\eta) \tag{3.23}$$

(or smaller).

Next, consider the contribution $\Delta W_{(t)}$:

$$\begin{aligned} \Delta W_{(t)} &= (\epsilon/\eta) \int_{\tau_0}^{\tau_c} b(E) F_t d\tau = -\epsilon \int_{E(\tau_c)}^{E(\tau_0)} b(E) dE \\ &= -\epsilon \sqrt{6E^2 - 2} \Big|_{E(\tau_c)}^{E(\tau_0)}. \end{aligned} \tag{3.24}$$

In the second equality we have used $F_t = -\mu\, dE/d\tau$, and in the third we have substituted for $b(E)$ and integrated explicitly. Since the energy difference $E(\tau_0) - E(\tau_c)$ is at most of $O(\eta \ln \eta)$, we conclude that

$$\Delta W_{(t)} = O(\epsilon) O(\eta \ln \eta) \tag{3.25}$$

(or smaller).

The combination of Eqs. (3.23) and (3.25) leads to the scaling stated in Eq. (3.20). The upshot is that the contribution to $\Delta W(\tau_0)$ from the quasi-circular part, $\Delta W(\tau_c, \tau_0)$, is negligible compared to the contribution from the approach part, $\Delta W(\tau_c) = O(\epsilon^0) O(\eta)$

(assuming $\epsilon|\ln\eta| \ll 1$). In other words, the GSF integral $\Delta W(\tau_0)$ in Eq. (3.18) may be truncated at the end-of-approach time τ_c, with the latter taken to be any instance after the orbit had settled into quasi-circular motion [but before the specific energy has accumulated $O(1)$ changes]. Hence one has

$$\delta L_\infty(E_\infty) = \Delta W(\tau_c) + O(\epsilon)O(\eta\ln\eta), \tag{3.26}$$

in analogy with the "no dissipation" case, Eq. (3.16). Here, $\Delta W(\tau_c)$ is the full-GSF integral shown in Eq. (3.17), evaluated along the orbit from infinity and up to the "end of approach" time τ_c, when the orbit settles into a quasi-circular motion. Crucially, the contribution to ΔW from the quasi-circular part of the orbit is suppressed by a factor of ϵ, so that the precise choice of τ_c does not affect the value of $\Delta W(\tau_c)$ at leading order. This assumes only that $\epsilon \ll |\ln\eta|^{-1}$, so that the error terms in Eq. (3.26) are negligible compared to $\Delta W(\tau_c) = O(\epsilon^0)O(\eta)$. All we require of τ_c is to be sufficiently late that $|\dot{r}|$ is already very small [specifically, $\dot{r}(\tau_c) = O(\eta)$], but sufficiently early that ΔE is $O(\eta\ln\eta)$ at most. In practice, ΔW may again be evaluated along the critical *geodesic* of energy-at-infinity E_∞, with the integral in Eq. (3.26) truncated after, say, 4–5 orbital revolutions. Truncating instead after (e.g.) 10 revolutions should change the result by a negligible amount of only $O(\epsilon)O(\eta)$.

The dissipative piece of $\Delta W(\tau_c)$ [call it $\Delta W^{\rm diss}$, defined by replacing $F_\alpha \to F_\alpha^{\rm diss}$ in Eq. (3.26)] may be expressed in terms of radiated quantities. Let $\mathcal{E}_{\rm (apr)}$ and $\mathcal{L}_{\rm (apr)}$ be the total energy and angular momentum in gravitational waves radiated out to infinity and down the black hole during the approach. We shall assume that the balance relation[3,4]

$$\mathcal{W}_{\rm (apr)} := 2\mathcal{E}_{\rm (apr)} - \mathcal{L}_{\rm (apr)} = -\eta\Delta W^{\rm diss}(\tau_c) \tag{3.27}$$

holds at leading order in η and in ϵ. Equations (3.16) and (3.26) then lead to

$$\delta L_\infty = \delta L_\infty^{\rm cons} - \mathcal{W}_{\rm (apr)}/\eta, \tag{3.28}$$

[3]The balance (3.27) does not follow directly from the theorem of Ref. [18], because the approach part of the critical orbit does not end at infinity. It may be possible to construct a proof by considering a small outward deformation of the orbit (such that the new orbit starts at infinity and scatters back to infinity), then invoking the approximate symmetry about the periapsis, together with the ϵ-suppression of the quasi-circular contribution to $\Delta W^{\rm diss}$. We shall not endeavour to provide the details of such a proof here.

[4]One cannot expect to be able to similarly balance $\mathcal{E}_{\rm (apr)}$ and $\mathcal{L}_{\rm (apr)}$ individually, because the dissipative pieces of $\Delta E(\tau_c)$ and $\Delta L(\tau_c)$, unlike $\Delta W^{\rm diss}(\tau_c)$, *are* sensitive to the choice of τ_c already at leading order. However, such individual balance relations will not be needed in our analysis.

where subleading terms have been omitted. This reexpresses δL_∞ as a sum of conservative and radiative contributions, the motivation for which will become clear in the next section.

Finally, let us further write $\mathcal{E}_{(\rm apr)} = \mathcal{E}^+_{(\rm apr)} + \mathcal{E}^-_{(\rm apr)}$ and similarly for $\mathcal{L}_{(\rm apr)}$ and $\mathcal{W}_{(\rm apr)}$, where hereafter superscripts '+' and '−' denote contributions from fluxes to infinity and down the black hole, respectively. The following argument, based on the first law of black hole mechanics, suggests that $\mathcal{W}^-_{(\rm apr)}$ must vanish in the limit $\epsilon \to 0$. If we assume the black hole is not overspun during the approach, its horizon's area should increase by an amount δA satisfying

$$\frac{\kappa}{8\pi}\delta A = \mathcal{E}^-_{(\rm apr)} - \Omega_H \mathcal{L}^-_{(\rm apr)}, \tag{3.29}$$

where $\kappa = \epsilon/\sqrt{2} + O(\epsilon^2)$ is the horizon's surface gravity, and $\Omega_{\rm H}$ its angular velocity. Since $\Omega_{\rm H} = \frac{1}{2} + O(\epsilon)$, we identify the right-hand side of (3.29) as $\mathcal{W}^-_{(\rm apr)}$ at leading order in ϵ. We thus have, in the $\epsilon \to 0$ limit, $\mathcal{W}^-_{(\rm apr)} \simeq \epsilon(c_1\delta A + c_2\mathcal{L}^-_{(\rm apr)})$, with c_1, c_2 certain numerical coefficients. Since δA and $\mathcal{L}^-_{(\rm apr)}$ must remain bounded even in the $\epsilon \to 0$ limit, we conclude that $\mathcal{W}^-_{(\rm apr)}$ vanishes in that limit. Thus, at leading order in ϵ, Eq. (3.28) becomes

$$\delta L_\infty = \delta L^{\rm cons}_\infty - \mathcal{W}^+_{(\rm apr)}/\eta, \tag{3.30}$$

which now features only outgoing fluxes.

With this we have completed the necessary groundwork for our overspinning analysis, to be presented next.

3.5 General form of the censorship condition and reduction to near-critical orbits

Starting with a near-extremal Kerr geometry with $a/M = 1 - \epsilon^2$, consider a particle sent in from infinity with specific energy E_∞ and specific angular-momentum L_∞ at $t \to -\infty$. The ADM mass and angular momentum of the spacetime are given in Eqs. (3.11) and (3.12) through $O(\eta^2)$. We assume the particle crosses the event horizon[5] at some retarded time u_h, and we let $\mathcal{E}^+$ and $\mathcal{L}^+$ be the total energy and angular momentum radiated to null-infinity up until u_h (with $u_h \to \infty$ if the post-capture geometry relaxes to a Kerr black hole). Then the Bondi mass and angular-momentum of spacetime at retarded time u_h are

[5] More pedantically, we refer here to the crossing of a marginally trapped surface; spacetime need not contain a global horizon.

$E_{\rm ADM} - \mathcal{E}^+$ and $L_{\rm ADM} - \mathcal{L}^+$, respectively. Overspinning is *avoided* if and only if[6]

$$(E_{\rm ADM} - \mathcal{E}^+)^2 \geq L_{\rm ADM} - \mathcal{L}^+. \tag{3.31}$$

To rule out the overspinning scenario, we need to show that this inequality holds for all E_∞, L_∞ and for all η, ϵ. The restriction to orbits coming from infinity follows from our analysis of the geodesic scenario: we will not examine bound orbits, as our implicit assumption is that the self-force should disfavour overspinning. Since we work in first-order perturbation theory, we only demand that (3.31) is satisfied at leading order in η. We also assume $\epsilon \ll 1$ and keep only leading terms in ϵ, but we do not *a priori* restrict the magnitude of ϵ relative to that of η. We shall refer to the inequality (3.31) as the *censorship condition*.[7]

Substituting from Eqs. (2.1), (3.11) and (3.12), the censorship condition becomes

$$\epsilon^2 + \eta W_\infty + \eta^2(1 + L_\infty E_\infty - E_\infty^2) + (\eta E_\infty - \mathcal{E}^+)^2 - \mathcal{W}^+ \geq 0, \tag{3.32}$$

where $W_\infty := 2E_\infty - L_\infty$, $\mathcal{W}^+ := 2\mathcal{E}^+ - \mathcal{L}^+$, and we have omitted subleading terms of $o(\eta^2)$. Note how the various terms here scale with η. The quantities E_∞ and L_∞ (hence also W_∞) are specific values, thus *a priori* they are $O(\eta^0)$. The radiated energy $\mathcal{E}^+$ is generically $O(\eta^2)$, but may accumulate at $O(\eta)$ for orbits that are fine-tuned to evolve along the global attractor; it is to allow for such orbits that we have kept the terms $2\eta E_\infty \mathcal{E}^+$ and $(\mathcal{E}^+)^2$ in Eq. (3.32). The quantity $\mathcal{W}^+$ is likewise $O(\eta^2)$ generically and up to $O(\eta)$ with fine-tuning, but, as will be shown below, in the latter case the $O(\eta)$ term is also proportional to ϵ.

Inspecting Eq. (3.32), we observe that, for all captured orbits that are not sufficiently close to criticality, the term ηW_∞ is $O(\eta)$ and positive, so the censorship condition (3.32) is trivially satisfied at leading order in η and ϵ. Violation of (3.32) (hence overspinning) may only be achieved, potentially, if L_∞ is tuned so that $L_\infty = 2E_\infty + O(\epsilon, \eta)$, giving

[6] We do not know, and for our purpose do not need to know, the future evolution of spacetime beyond retarded time u_h in the hypothetical case where (3.31) is *not* satisfied. The likely scenario involves the formation of a naked singularity and a breakdown of predictability for $u > u_h$ [53]. If (3.31) *is* satisfied, then, by "no-hair" theorems, geometry should relax to a Kerr black hole.

[7] It may be argued that (3.31) is guaranteed to hold (with a strong inequality) by virtue of the third law of black-hole mechanics [73], though some of the third-law's assumptions are not satisfied within our model: for instance, a distributional source does not comply with the hypothesis that the matter considered should have a bounded stress-energy tensor [58]; it was also pointed out that the process leading to the formation of an extremal black hole through the capture of a test body cannot actually take place in a finite time through a continuous process [74]. However, we observe that all these arguments apply only to some approximations to the full non-linear evolution of the system, and thus cannot be considered conclusive. In any case, it is still of interest to explore the *physical mechanism* that enforces the third law in our setup, which is what our study aims to achieve.

$W_\infty = O(\epsilon, \eta)$. It is therefore sufficient to restrict attention to this class of orbits, to be referred to in what follows as "near-critical". Formulated on near-critical orbits, the censorship condition takes the sufficient form

$$\epsilon^2 + \eta W_\infty + \eta^2(1 + E_\infty^2) + (\eta E_\infty - \mathcal{E}^+)^2 - \mathcal{W}^+ \geq 0, \tag{3.33}$$

where we have dropped $O(\epsilon\eta^2, \eta^3)$ terms. This is required to hold for each member of the reduced two-parameter family $\{E_\infty, L_\infty\}$ with $L_\infty - 2E_\infty = O(\epsilon, \eta)$.

To proceed, we need to make more precise the distinction between "weakly fine-tuned" orbits and "strongly fine-tuned" near-critical orbits. Referring to Fig. 3.1, let E_f be the final value of the specific energy with which the particle plunges into the hole; and let $L_{\infty,c}(E_\infty)$ be the perfectly fine-tuned value of L_∞, for which the orbit joins the global attractor and evolves along it to the ISCO. Assuming the universal scaling $L_\infty - L_{\infty,c}(E_\infty) \sim \exp[(E_f - E_\infty)/\eta]$ [72], near-critical orbits as defined above generically have $E_f - E_\infty = O(\eta \ln \eta\epsilon)$ [here we neglect the $O(\eta)$ difference between E_∞ and E_i]. Calibrating L_∞ at higher order in η, ϵ [so that $L_\infty - L_{\infty,c} = O(\eta^n, \epsilon^k)$ with some $n, k > 1$] does not qualitatively change this generic scaling of $E_f - E_\infty$. To achieve $E_f - E_\infty = O(1)$ requires an exponentially accurate tuning, i.e. $L_\infty - L_{\infty,c} \sim \exp(-1/\eta)$. In what follows we use the η scaling of $E_f - E_\infty$ to distinguish between *weakly* and *strongly* fine-tuned members of the near-critical family: The former admit $E_f - E_\infty = O(\eta \ln \eta\epsilon)$, and the latter $E_f - E_\infty = O(1)$. This distinction can also be formulated in terms of the radiated quantities $\mathcal{E}^+$ or $\mathcal{L}^+$:

$$\mathcal{E}^+, \mathcal{L}^+ = O(\eta^2 \ln \eta\epsilon) \quad (\text{"weakly fine-tuned"}), \tag{3.34}$$

$$\mathcal{E}^+, \mathcal{L}^+ = O(\eta) \qquad (\text{"strongly fine-tuned"}). \tag{3.35}$$

3.6 Further reduction to critical orbits

The inequality (3.33) is still a condition on a two-parameter family of orbits. Ignoring fine-tuned orbits for now, it is possible—and beneficial—to reduce it further to a sufficient condition formulated on a one-parameter family. We achieve this by minimizing the left-hand side of Eq. (3.33) over all near-critical orbits for a given E_∞. We argue that the minimizing orbit is one with L_∞ tuned to its critical value at least through $O(\eta, \epsilon)$, namely

$$L_\infty = 2E_\infty + \epsilon\sqrt{6E_\infty^2 - 2} + \delta L_\infty(E_\infty) + o(\eta, \epsilon), \tag{3.36}$$

where we have recalled Eq. (2.15), and $\delta L_\infty(E_\infty)$ is the $O(\eta)$ GSF term derived in the previous section.

To see this, note first that $W_\infty = 2E_\infty - L_\infty$ is trivially minimized by $L_\infty = L_{\infty,c}(E_\infty)$, since $L_{\infty,c}(E_\infty)$ maximizes L_∞ (over all captured orbits of a fixed E_∞) by definition of a critical orbit. This means that, to minimize W_∞ through $O(\eta,\epsilon)$ (higher orders are irrelevant in our approximation) it suffices to demand $L_\infty - L_{\infty,c}(E_\infty) = o(\eta,\epsilon)$. Then also note that the two radiative terms on the left-hand side of (3.33) are insensitive, at relevant order, to variations of L_∞ within the family of nearly-critical orbits for a fixed E_∞. For weakly fine-tuned orbits, the term $(\eta E_\infty - \mathcal{E}^+)^2$ is simply $\eta^2 E_\infty^2$ at leading order, recalling Eq. (3.34). As for the term $-\mathcal{W}^+$, we note that the contribution to that term from the approach part of the orbit, which is already $O(\eta^2)$, is not sensitive, at that order, to $O(\eta,\epsilon)$ variations in L_∞. Meanwhile, the contribution to $\mathcal{W}^+$ from the quasi-circular part of the orbit is of $O(\epsilon)O(\eta^2 \ln \eta\epsilon)$ at most (the occurrence of the factor ϵ will be explained below) and hence negligible in Eq. (3.33), assuming only $\epsilon \ll |\ln \eta|^{-1}$.

Thus, discounting fine-tuned orbits, we find that the entire left-hand side of Eq. (3.33) is minimized by L_∞ as given in Eq. (3.36). A new sufficient version of the censorship condition may therefore be written as

$$\epsilon^2 - \eta\epsilon\sqrt{6E_\infty^2 - 2} - \eta\,\delta L_\infty + \eta^2(1 + E_\infty^2) + (\eta E_\infty - \mathcal{E}^+)^2 - \mathcal{W}^+ \geq 0, \tag{3.37}$$

which, at the relevant, leading order, is a condition on the *one*-parameter family of (generic) critical orbits parametrized by E_∞ alone.

It should now be noted that the condition (3.37) also applies to fine-tuned orbits [whether or not they minimize the left-hand size of (3.33)], simply because such orbits always satisfy Eq. (3.36). However, for fine-tuned orbits the condition still involves *two* parameters, conveniently chosen as E_∞ and E_f. Different values of E_f correspond to a fine-tuning of L_∞ at an exponential level. In principle, any value of E_f in the range $E_{\rm isco} \lesssim E_f \lesssim E_\infty$ may be obtained this way. To rule out overspinning by fine-tuned orbits, the censorship condition (3.37) must hold for all $\{E_\infty, E_f\}$ with E_f in the above range.

Observe that in Eq. (3.37) we have

$$\begin{aligned} \eta\delta L_\infty + \mathcal{W}^+ &= \eta\,\delta L_\infty^{\rm cons} + \mathcal{W}^+ - \mathcal{W}^+_{\rm (apr)} \\ &= \eta\,\delta L_\infty^{\rm cons} + \mathcal{W}^+_{\rm (qc)} + \mathcal{W}^+_{\rm (end)}, \end{aligned} \tag{3.38}$$

where in the first line we have recalled Eq. (3.30), $\mathcal{W}^+_{(\mathrm{qc})}$ is the piece of $\mathcal{W}^+$ coming from the evolution along the quasi-circular part of the orbit, and $\mathcal{W}^+_{(\mathrm{end})}$ is the piece coming from the transition to a final plunge into the black hole and from the plunge itself. It follows that only the *conservative* piece of the shift δL_∞ actually enters our condition:

$$\epsilon^2 - \eta\epsilon\sqrt{6E_\infty^2 - 2} - \eta\,\delta L_\infty^{\mathrm{cons}} + \eta^2(1 + E_\infty^2) + (\eta E_\infty - \mathcal{E}^+)^2 - \mathcal{W}^+_{(\mathrm{qc})} - \mathcal{W}^+_{(\mathrm{end})} \geq 0. \quad (3.39)$$

In this last form, conservative and dissipative terms of the GSF feature separately. The former are associated with the approach leg of the orbit, and the latter accumulate during the adiabatic evolution along the attractor. In Appendix B we combine results by Ori and Thorne [75], Kesden [76] and Mino and Brink [77], to argue that the term $\mathcal{W}^+_{(\mathrm{end})}$ is always subdominant and negligible in Eq. (3.39). We shall therefore omit that term in the rest of our discussion.

In section 3.8 below we will show that the radiative term $\mathcal{W}^+_{(\mathrm{qc})}$ scales as $O(\epsilon)O[\eta(E_\infty - E_f)]$. This term can thus feature at leading order in Eq. (3.39) only for fine-tuned orbits, for which $E_\infty - E_f = O(1)$. Likewise, terms involving $\mathcal{E}^+$ feature only for fine-tuned orbits and are negligible otherwise. On the other hand, the conservative term $\eta L_\infty^{\mathrm{cons}}$ is always $O(\eta^2)$, featuring in the censorship condition regardless of fine-tuning. An important consequence is that *dissipative effects of the GSF enter the censorship condition only for fine-tuned orbits*. This seems consistent with suggestions made in earlier analyses [62,76,78] (in which fine-tuning has not been considered).

Below we further simplify the condition (3.39), and reformulate it explicitly in terms of E_∞ alone (for weakly fine-tuned orbits) or E_∞ and E_f alone (for strongly fine-tuned ones), without reference to η and ϵ. We shall consider separately the cases of weakly and strongly fine-tuned orbits, starting with the former, simpler case.

3.7 Censorship condition for weakly fine-tuned orbits

As mentioned above (and shown in the next section), without strong fine-tuning the radiative terms $\mathcal{E}^+$ and $\mathcal{W}^+_{(\mathrm{qc})}$ become subdominant in Eq. (3.39) and drop out of it. The censorship condition then reduces to

$$\epsilon^2 + \eta\epsilon F + \eta^2 H \geq 0, \quad (3.40)$$

with

$$F := -\sqrt{6E_\infty^2 - 2}\,, \tag{3.41}$$

$$H := 1 + 2E_\infty^2 - \delta\breve{L}_\infty^{\rm cons}. \tag{3.42}$$

Here we have made the η-scaling of $\delta L_\infty^{\rm cons}$ explicit by introducing the shift-per-eta

$$\delta\breve{L}_\infty^{\rm cons} := \eta^{-1}\,\delta L_\infty^{\rm cons}, \tag{3.43}$$

which should have a finite (nonzero) limit $\eta \to 0$. We observe that the conservative self-force modifies the geodesic censorship condition through the term $\delta\breve{L}_\infty^{\rm cons}$. The GSF will disfavour overspinning if $\delta\breve{L}_\infty^{\rm cons} < 0$, which is equivalent to decreasing the upper bound given in Eq. (2.21).

For the overspinning scenario to be ruled out, the inequality (3.40) must be satisfied for all $\eta, \epsilon > 0$ and all $E_\infty \geq 1$. The condition can be written in the equivalent form $\Phi := \alpha^2 + \alpha F + H \geq 0$, with $\alpha := \epsilon/\eta > 0$. At fixed E_∞, Φ is quadratic in α, with a minimum value $\Phi(\alpha = -F/2) = H - F^2/4$. To guarantee $\Phi \geq 0$ for all E_∞ and all $\alpha > 0$ (hence all $\eta, \epsilon > 0$) we must demand $H \geq F^2/4$; if $H < F^2/4$ for some E_∞, then for that E_∞ there exist η, ϵ values for which overspinning is achieved. In that way, $H \geq F^2/4$ is both sufficient and necessary for overspinning to be avoided. Inserting the values of F and H, the censorship condition takes the simple form

$$\delta\breve{L}_\infty^{\rm cons} \leq \frac{1}{2}(E_\infty^2 + 3). \tag{3.44}$$

Overspinning is averted (for orbits that are not fine-tuned) if and only if (3.44) is satisfied for each member of the one-parameter family of critical orbits with $E_\infty \geq 1$, in the limit $\eta, \epsilon \to 0$.

Equation (3.44) states our final result for weakly fine-tuned orbits. As already mentioned, it involves only *conservative* GSF effects, specifically the shift in the critical value of the angular-momentum-at-infinity (at fixed E_∞) due to the conservative piece of the GSF. For easy reference, we give here the explicit formula for $\delta\breve{L}_\infty^{\rm cons}$ in terms of GSF components:

$$\delta\breve{L}_\infty^{\rm cons}(E_\infty) = \lim_{\epsilon\to 0}\frac{1}{\mu^2}\int_{R_\epsilon}^{\infty}\left(2\,M\,F_t^{\rm cons} + F_\phi^{\rm cons}\right)dr/\dot{r}, \tag{3.45}$$

where we have recalled Eqs. (3.16) and (3.17). The integration is carried out along the

critical geodesic of specific energy E_∞ on a background with spin $a/M = 1 - \epsilon^2$, starting at the unstable circular orbit of radius $R_\epsilon = R_\epsilon(\epsilon, E_\infty)$ and ending at infinity.

Inspecting Eq. (3.44), it may seem peculiar that overspinning may be averted even for some *positive* values of $\delta L_\infty^{\rm cons}$: A positive $\delta L_\infty^{\rm cons}$ would seem to mean that the GSF *increases* the critical impact parameter, allowing in particles that would otherwise be scattered away. However, we must recall that the shift $\delta L_\infty^{\rm cons}$ is defined not with respect to the physical, ADM angular momentum, but with respect to the quantity $\hat{L} = \hat{u}_\phi$, which (while convenient to work with in practice) does not have a clear invariant meaning beyond the geodesic approximation. To rewrite (3.44) in a more physically insightful way, let us, then, recast it in terms of ADM quantities, as follows.

First, let us introduce the specific quantities $E^{\rm p}_{\rm ADM}$ and $L^{\rm p}_{\rm ADM}$ defined through

$$\begin{aligned} \mu E^{\rm p}_{\rm ADM} &:= E_{\rm ADM} - M, \\ \mu L^{\rm p}_{\rm ADM} &:= L_{\rm ADM} - Ma, \end{aligned} \tag{3.46}$$

which may be thought of as the particle's contributions to the total ADM energy and angular momentum of the system. Then, denote by $\delta L^{\rm p}_{\rm ADM}(E^{\rm p}_{\rm ADM})$ the shift, due to the conservative GSF, in the critical value of $L^{\rm p}_{\rm ADM}$ for a fixed $E^{\rm p}_{\rm ADM}$. A short calculation, based on Eqs. (3.11) and (3.12), gives

$$\delta L^{\rm p}_{\rm ADM}(E^{\rm p}_{\rm ADM}) = \delta L_\infty^{\rm cons}(E_\infty) - \eta(E_\infty^2 + 1) + O(\eta^2). \tag{3.47}$$

Thus, in terms of $\delta \breve{L}^{\rm p}_{\rm ADM} := \eta^{-1}\, \delta L^{\rm p}_{\rm ADM}$, the censorship condition (3.44) becomes

$$\delta \breve{L}^{\rm p}_{\rm ADM} \leq \frac{1}{2}(1 - E_\infty^2), \tag{3.48}$$

where on the right-hand side E_∞ may be replaced with $E^{\rm p}_{\rm ADM}$ at relevant order.

The alternative form (3.48) is now more intuitive: For unbound orbits ($E_\infty \geq 1$), the GSF averts overspinning if it shifts the critical value of the (ADM-related) angular momentum by a sufficiently negative amount, which depends only on E_∞. In the marginal case of $E_\infty = 1$ (where overspinning is marginally prevented already in the geodesic case), the shift $\delta \breve{L}^{\rm p}_{\rm ADM}$ need only be nonpositive. We are not aware of any *a priori* argument to suggest that $\delta \breve{L}^{\rm p}_{\rm ADM}$ must necessarily be nonpositive for all $E_\infty \geq 1$.

Let us make a few more points about the condition (3.44). First, in its form (3.48) it is manifestly gauge invariant (within a class of suitable asymptotically flat gauges) despite the

gauge dependence of the local GSF featuring in $\delta\breve{L}^{\rm cons}_{\infty}$ [Eq. (3.45)]. The condition involves only quantities that are defined and evaluated at infinite separation, namely the specific energy E_∞ (or $E^{\rm p}_{\rm ADM}$) and angular-momentum shift $\delta\breve{L}^{\rm p}_{\rm ADM}$, each having a clear gauge-invariant physical meaning. The evident invariance of our final condition is reassuring.

Second, as already mentioned, the condition that (3.44) is satisfied for all $E_\infty \geq 1$ is both sufficient and necessary for overspinning to be avoided within the scenario considered here. It is a *sufficient* condition only in the sense that it guarantees no overspinning occurs *for sufficiently small mass-ratio* η; since we work in the first-order self-force approximation, we cannot make the statement any stronger. Equation (3.44) describes a *necessary* condition in the sense that its violation for any E_∞ would mean there exist (small) η values for which overspinning occurs.

Finally, the condition (3.44) involves the single parameter E_∞, and the task of testing whether it is satisfied amounts to evaluating a single function of E_∞, namely $\delta\breve{L}^{\rm cons}_{\infty}(E_\infty)$. The perturbative parameters themselves, η and ϵ, do not feature in the final condition. This is expected, given our first-order perturbative treatment and the fact that GSF effects (including ADM terms) appear in the overspinning condition already at leading order. It is precisely because of this "order mixing" that one cannot neglect the GSF in considering the overspinning problem, and why there is no sense in which the geodesic limit may be said to provide a useful approximation here.

3.8 Censorship condition for fine-tuned orbits

It is not *a priori* clear whether fine-tuning favours the overspinning scenario or disfavours it: The answer depends on the details of the radiative evolution along the attractor. Indeed, for fine-tuned orbits the radiative terms $\mathcal{E}^+$ and $\mathcal{W}^+_{\rm (qc)}$ feature already at leading order in Eq. (3.39), and cannot be neglected. We may again write Eq. (3.39) in the form (3.40), with F and H replaced with, respectively,

$$\begin{aligned} \bar{F} &= -\sqrt{6E_\infty^2 - 2} - \breve{\mathcal{W}}^+_{\rm (qc)}\,, \\ \bar{H} &= 1 + E_\infty^2 + (E_\infty - \breve{\mathcal{E}}^+)^2 - \delta\breve{L}^{\rm cons}_{\infty}. \end{aligned} \tag{3.49}$$

Here we have introduced the rescaled quantities

$$\breve{\mathcal{E}}^\pm := \eta^{-1}\mathcal{E}^\pm, \qquad \breve{\mathcal{W}}^\pm_{\rm (qc)} := (\epsilon\eta)^{-1}\mathcal{W}^\pm_{\rm (qc)}, \tag{3.50}$$

which should have finite (nonzero) limits $\epsilon, \eta \to 0$ for fine-tuned orbits [that $\mathcal{W}^{\pm}_{(\rm qc)} = O(\epsilon)O(\eta)$ will be discussed in the next two paragraphs].

It will prove beneficial to reexpress $\bar{F}$ and $\bar{H}$ in terms of the absorption-related quantities $\breve{\mathcal{E}}^-$ and $\breve{\mathcal{W}}^-_{(\rm qc)}$, in place of $\breve{\mathcal{E}}^+$ and $\breve{\mathcal{W}}^+_{(\rm qc)}$. This is easily done for $\bar{H}$, noting $E_\infty - \breve{\mathcal{E}}^+ = E_f + \breve{\mathcal{E}}^-$ at the relevant, leading order. As for $\bar{F}$, we start by writing $\mathcal{W}^+_{(\rm qc)} = \mathcal{W}_{(\rm qc)} - \mathcal{W}^-_{(\rm qc)}$, where, under the assumption of adiabaticity, the total $\mathcal{W}_{(\rm qc)}$ may be expressed as an integral over the local GSF[8]:

$$\mathcal{W}_{(\rm qc)} = \int_{E_\infty}^{E_f} \left(2F_t^{\rm diss} + F_\phi^{\rm diss}\right) dE/\dot{E}. \tag{3.51}$$

Here we have used Eq. (3.17), changing the integration variable from τ to specific energy E, and assumed a balance relation as in Eq. (3.27). We have also neglected the subdominant $[O(\eta^2)]$ amount of radiated energy during the approach, replacing the initial energy of the quasi-circular motion with E_∞. Then, following similar calculations to the ones that lead to Eq. (3.21) and using $u^\alpha F_\alpha^{\rm diss} = 0$ one obtains

$$F_t^{\rm diss} + F_\phi^{\rm diss}/2 = -(u^r/u^t)F_r^{\rm diss} - \frac{3E}{\sqrt{6E^2-2}}\,\epsilon F_t^{\rm diss}, \tag{3.52}$$

where subdominant terms in ϵ have been omitted. The contribution from the term $\propto F_r^{\rm diss}$ to the integral in (3.51) can be shown to be of only $O(\epsilon)O(\eta^2)$ [see the paragraph containing Eq. (3.22)], and hence entirely negligible. The contribution from the term $\propto F_t^{\rm diss}$ can be evaluated explicitly upon replacing $F_t = \mu\dot{E}$, giving

$$\mathcal{W}_{(\rm qc)} = -\eta\epsilon\left(\sqrt{6E_\infty^2-2} - \sqrt{6E_f^2-2}\right). \tag{3.53}$$

Thus, Eqs. (3.49) are obtained in their alternative form

$$\begin{aligned} \bar{F} &= -\sqrt{6E_f^2-2} + \breve{\mathcal{W}}^-_{(\rm qc)}\,, \\ \bar{H} &= 1 + E_\infty^2 + (E_f + \breve{\mathcal{E}}^-)^2 - \delta\breve{L}^{\rm cons}_\infty. \end{aligned} \tag{3.54}$$

We note that Eq. (3.53) establishes the scaling $\mathcal{W}_{(\rm qc)} = O(\epsilon)O(\eta)$ for fine-tuned orbits. The first-law argument used in the previous section (see the discussion around Eq. (3.29)) can also be used to show $\mathcal{W}^-_{(\rm qc)} = O(\epsilon)O(\eta)$. This then establishes the scaling $\mathcal{W}^+_{(\rm qc)} = O(\epsilon)O(\eta)$ assumed above.

In both Eqs. (3.49) and (3.54), the radiative quantities $\breve{\mathcal{E}}^\pm$ and $\breve{\mathcal{W}}^\pm_{(\rm qc)}$ should be thought

[8] In this section we set $M = 1$ once again, for convenience.

of as functions of E_∞ and E_f only. While $\breve{\mathcal{E}}^+$ is necessarily positive, the absorbed energy $\breve{\mathcal{E}}^-$ may be either positive, or—due to superradiance—negative, depending on E_∞ and E_f. We will elaborate on this point in Sec. 4.4.1. The quantity $\breve{\mathcal{W}}^+_{(\mathrm{qc})}$, on the other hand, is easily shown to be negative definite. In fact, Eqs. (3.59) and (3.64), given below, imply

$$-\breve{\mathcal{W}}^+_{(\mathrm{qc})} > \breve{\mathcal{E}}^+ > 0. \tag{3.55}$$

Note this means that $\bar{F}$ in Eq. (3.49) may change sign, depending on E_∞, E_f.

To proceed, we once again write the condition (3.40) (for the barred quantities) in the form $\bar{\Phi} := \alpha^2 + \alpha\bar{F} + \bar{H} \geq 0$, with $\alpha = \epsilon/\eta$. Here, however, the sign of $\bar{F}$ is not known *a priori*, which somewhat complicates matters. For $\bar{F} < 0$, $\bar{\Phi}$ has its minimum at $\bar{\Phi}(\alpha = -\bar{F}/2) = \bar{H} - \bar{F}^2/4$, so the condition becomes $\bar{H} \geq \bar{F}^2/4$ as before. However, for $\bar{F} \geq 0$ the condition $\bar{\Phi} \geq 0$ is satisfied trivially for all $\bar{H} \geq 0$, and violated trivially for all $\bar{H} < 0$ (by choosing a sufficiently small α). In that case, therefore, a necessary and sufficient condition for $\bar{\Phi} \geq 0$ to hold for any η, ϵ is $\bar{H} \geq 0$. In summary, we obtain

$$\bar{H} \geq (\min\{\bar{F}/2, 0\})^2 \tag{3.56}$$

as a necessary and sufficient condition for overspinning to be averted for all η, ϵ. In this condition, $\bar{F}$ and $\bar{H}$ are both functions of the two independent parameters E_∞ and E_f. To rule out overspinning we must require that (3.56) is satisfied for all $E_\infty > E_f (> E_{\mathrm{isco}})$.

Evaluation of the condition (3.56) requires knowledge of the radiative quantities $\breve{\mathcal{E}}^\pm$ and $\breve{\mathcal{W}}^\pm_{(\mathrm{qc})}$ (in addition to $\delta\breve{L}^{\mathrm{cons}}_\infty$). To conclude our discussion, we now give convenient expressions for these two quantities in terms of a single function of one variable, namely the ratio

$$\mathcal{R}(E) := \frac{\dot{\mathcal{E}}^-(E)}{\dot{\mathcal{E}}^+(E)}, \tag{3.57}$$

where $\dot{\mathcal{E}}^{+/-}(E)$ are the outgoing/incoming fluxes of energy in gravitational waves sourced by a particle on a circular geodesic, evaluated in the $\epsilon \to 0$ limit[9] at a fixed specific energy E. [In deviation from our notation elsewhere, here and in the next two paragraphs an overdot denotes differentiation with respect to (any suitable) coordinate time.] We note $\mathcal{R} < 0$ for $E < \frac{2}{\sqrt{3}}$, the superradiance regime in the extremal limit (see Sec. 4.4.1).

[9]Note that all the numerical results presented in this work are obtained for small, but non-zero values of ϵ. Thus, whenever we mention taking the $\epsilon \to 0$ limit, we only wish to remind that our analysis keeps track of the leading order terms in ϵ.

First, we use the specific energy E as a parameter along the global attractor, to write

$$\breve{\mathcal{E}}^{+} = \int_{E_\infty}^{E_f} \frac{\dot{\mathcal{E}}^{+}}{\eta \dot{E}}\, dE = -\int_{E_\infty}^{E_f} \frac{\dot{\mathcal{E}}^{+}}{\dot{\mathcal{E}}^{+} + \dot{\mathcal{E}}^{-}}\, dE, \tag{3.58}$$

where we assumed the balance relation $\eta \dot{E} = -(\dot{\mathcal{E}}^{+} + \dot{\mathcal{E}}^{-})$ applies during the adiabatic evolution along the attractor. Thus,

$$\breve{\mathcal{E}}^{+}(E_\infty, E_f) = -\int_{E_\infty}^{E_f} \frac{dE}{1 + \mathcal{R}(E)}, \tag{3.59}$$

and, similarly,

$$\breve{\mathcal{E}}^{-}(E_\infty, E_f) = -\int_{E_\infty}^{E_f} \frac{\mathcal{R}(E)}{1 + \mathcal{R}(E)}\, dE, \tag{3.60}$$

which should be evaluated in the extremal limit, $\epsilon \to 0$. Note $\dot{\mathcal{E}}^{\pm} \to 0$ in the extremal limit [62], while the ratio $\mathcal{R}$ admits a finite, nonzero limit, as we will see in Sec. 4.5. Thus, by writing $\breve{\mathcal{E}}^{\pm}$ as in Eqs. (3.59) and (3.60) we have made it possible for the limit $\epsilon \to 0$ to be taken before the integration, which is advantageous in practice.

As for $\mathcal{W}^{\pm}_{(\mathrm{qc})}$, we start by writing

$$\dot{\mathcal{W}}^{\pm}_{(\mathrm{qc})} := 2\dot{\mathcal{E}}^{\pm} - \dot{\mathcal{L}}^{\pm} = -\epsilon b(E) \dot{\mathcal{E}}^{\pm}, \tag{3.61}$$

where $\dot{\mathcal{L}}^{\pm}$ are the angular-momentum fluxes corresponding to $\dot{\mathcal{E}}^{\pm}$, and

$$b(E) := \frac{6E}{\sqrt{6E^2 - 2}}. \tag{3.62}$$

To derive the second equality in (3.61), which is valid to leading order in ϵ, we have used the small-ϵ expansion of the orbital angular velocity at fixed E,

$$\Omega = \frac{1}{2} - \frac{1}{4} b(E)\epsilon + O(\epsilon^2), \tag{3.63}$$

together with the general relation $\dot{\mathcal{E}}^{\pm} = \Omega \dot{\mathcal{L}}^{\pm}$ applicable to the radiation from any circular orbit [79]. Thus, proceeding as with $\breve{\mathcal{E}}^{+}$, we obtain

$$\breve{\mathcal{W}}^{+}_{(\mathrm{qc})} = \lim_{\epsilon \to 0} \int_{E_\infty}^{E_f} \frac{\dot{\mathcal{W}}^{+}}{\epsilon \eta \dot{E}}\, dE = \int_{E_\infty}^{E_f} \frac{b(E)}{1 + \mathcal{R}(E)}\, dE, \tag{3.64}$$

and, similarly,

$$\breve{\mathcal{W}}^{-}_{(\mathrm{qc})} = \int_{E_\infty}^{E_f} \frac{b(E)\mathcal{R}(E)}{1 + \mathcal{R}(E)}\, dE. \tag{3.65}$$

Equations (3.59), (3.60), (3.64) and (3.65) express $\check{\mathcal{E}}^{\pm}$ and $\check{\mathcal{W}}^{\pm}_{(\mathrm{qc})}$ in terms of the single function $\mathcal{R}(E)$, which will be determined numerically in Sec. 4.5.

In the next section, we explore an alternative approach to the determination of $\delta\check{L}^{\mathrm{cons}}_{\infty}$, which offers a practical advantage.

3.9 Reformulation in terms of redshift variable

Our final overspinning conditions (3.44) and (3.56) feature the critical angular-momentum shift $\delta L^{\mathrm{cons}}_{\infty}$, whose evaluation, through equation (3.45), requires an integration of the GSF from infinity along critical geodesics. As we discuss in the next section, this step is the main stumbling block when it comes to evaluating the conditions using currently available GSF codes. The integration from infinity comes about, essentially, because of the need to relate the local properties $\hat{E}$ and $\hat{L}$ of the particle just before it falls into the black hole, to ADM properties of spacetime defined at infinity. This would have been unnecessary if we had available explicit formulas for E_{ADM} and L_{ADM} (or for the corresponding Bondi quantities $E_{\mathrm{ADM}} - \mathcal{E}^{+}$ and $L_{\mathrm{ADM}} - \mathcal{L}^{+}$), correct through $O(\eta^2)$, for the configuration of a particle in an unstable circular orbit around a Kerr black hole. Furthermore, given such formulas we would have been able to relax the requirement that the particle is sent in from infinity, and explore the possibility of overspinning with "bound" orbits. (We recall our result that bound *geodesics* cannot overspin; however, in principle, there remains the possibility that GSF effects change this situation.)

By good fortune, suitable formulas have been proposed very recently, in Ref. [36]. The expressions, to be presented below, were obtained using (and in agreement between) two independent frameworks. One is the Hamiltonian approach of Isoyama and collaborators [80], in which the conservative portion of the orbital dynamics is described (through first order in η beyond the geodesic approximation) in terms of geodesic motion in a certain effective smooth spacetime. The other is based on the recently proposed first law of binary black-hole mechanics (itself a limiting case of the generalized law established in [11]), which relates globally conserved quantities of a helically-symmetric binary system of post-Newtonian particles to the redshift of the particles. Neither framework is *a priori* guaranteed to correctly describe the strong-field dynamics in the black-hole–particle system relevant to us, but some evidence suggests that they might, and indeed we will provide a further confirmation of this expectation in Sec. 5.5.1.

The said results, as they are stated in [36], apply to a particle in a circular equatorial

orbit (stable or unstable) around a Kerr black hole, ignoring the dissipative piece of the gravitational interaction (or, more precisely, time-symmetrizing the gravitational perturbation, so that spacetime admits a global helical symmetry). They express the Bondi[10] energy and angular momentum of that configuration, through $O(\eta^2)$, in terms of Detweiler's redshift variable [70], which we first introduced in Subsec. 1.1.5,

$$\hat{z} := (\hat{u}^t)^{-1}, \tag{3.66}$$

where $\hat{u}^t$ is the t component of the four-velocity on the circular orbit, and overhats, recall, denote properties of the GSF-corrected orbit. The usefulness of such relations is in the fact that a computation of $\hat{z}$ requires only GSF information for circular orbits, and there is no need to integrate from infinity. Such information is essentially accessible to existing GSF codes.

Following [36], let us formally expand the redshift $\hat{z}$ in powers of η, in the form

$$\hat{z} = z_0(\Omega) + \eta z_1(\Omega) + O(\eta^2), \tag{3.67}$$

where $\Omega(= d\phi/dt)$ is the circular orbit's angular velocity,

$$z_0 = (1 - a\Omega)^{1/2} \left[1 + a\Omega - 3(M\Omega)^{2/3}(1 - a\Omega)^{1/3}\right]^{1/2} \tag{3.68}$$

is the geodesic limit of $\hat{z}$, and $\eta z_1(\Omega)$ is the $O(\eta)$ GSF correction, defined for a fixed value of Ω. According to Ref. [36], the Bondi energy and angular momentum of the circular-orbit binary are given, through $O(\eta^2)$, by

$$E_{\rm B}^{\rm sym} = M + \mu E_{\rm B}^{\rm p}, \qquad L_{\rm B}^{\rm sym} = Ma + \mu L_{\rm B}^{\rm p}, \tag{3.69}$$

where

$$E_{\rm B}^{\rm p} = \tilde{z} - \Omega \frac{d\tilde{z}}{d\Omega}, \qquad L_{\rm B}^{\rm p} = -\frac{d\tilde{z}}{d\Omega}, \tag{3.70}$$

with

$$\tilde{z}(\Omega) = z_0(\Omega) + \frac{1}{2}\eta z_1(\Omega) + O(\eta^2). \tag{3.71}$$

The label 'sym' is to remind us that these Bondi properties are defined in a time-symmetrized

[10] First-law literature [12, 81, 82] usually alludes to ADM properties, which are defined even in helical symmetry within the PN context in which these works operate. In the context of black hole perturbation theory, the first-law results should be interpreted as referring to *Bondi* properties. See also [83], where first-law results are formulated directly in terms of Bondi quantities for a black-hole–particle system.

("half-retarded-plus-half-advanced") spacetime. The function $z_1(\Omega)$ explicitly determines $E_{\rm B}^{\rm sym}$ and $L_{\rm B}^{\rm sym}$ through $O(\eta^2)$.

We are now reaching the crux of our discussion. Consider a critical orbit, subject to the conservative GSF alone (dissipation ignored), which asymptotes to a certain unstable circular orbit at $\tau \to \infty$. Let $E_{\rm B}^{\rm sym}(u)$ and $L_{\rm B}^{\rm sym}(u)$ be the Bondi energy and angular momentum of the corresponding time-symmetrized spacetime, with u a suitable retarded-time coordinate. At $u \to \infty$, these quantities must approach the corresponding Bondi quantities of the asymptotic circular-orbit configuration, as given in Eq. (3.69). Furthermore,

$$E_{\rm B}^{\rm sym}(u \to \infty) = E_{\rm ADM}, \qquad L_{\rm B}^{\rm sym}(u \to \infty) = L_{\rm ADM}, \tag{3.72}$$

where on the right-hand side we have the ADM properties of the physical ("retarded") critical-orbit spacetime. [That this must be the case follows from $E_{\rm B}^{\rm sym}(u \to \infty) = E_{\rm ADM}^{\rm sym} - \mathcal{F}^+ = E_{\rm ADM}^{\rm sym} - \mathcal{F}^- = E_{\rm ADM}$, where $\mathcal{F}^+$ and $\mathcal{F}^-$ are the total energies flowing, respectively, outward at future null-infinity and inward at past null-infinity, in the time-symmetrized setup where $\mathcal{F}^+ = \mathcal{F}^-$. In fact, in order to keep the small body on an eternal circular orbit, the same amount of radiation emitted by the system ($\mathcal{F}^+$) must be injected back, in the form of radiation coming from past null infinity ($\mathcal{F}^-$). A similar argument applies to the angular momentum.] As a result, using the first law of binary black hole mechanics, we can write $E_{\rm ADM} = M + \mu E_{\rm ADM}^{\rm p}$ and $L_{\rm ADM} = M + \mu L_{\rm ADM}^{\rm p}$ [as in Eqs. (3.46)], with

$$E_{\rm ADM}^{\rm p} = \tilde{z} - \Omega \frac{d\tilde{z}}{d\Omega}, \qquad L_{\rm ADM}^{\rm p} = -\frac{d\tilde{z}}{d\Omega}. \tag{3.73}$$

These expressions relate the ADM properties of the physical critical-orbit configuration to the redshift of the asymptotic circular orbit when dissipation is ignored.

The conservative GSF shift $\delta L_{\rm ADM}^{\rm p}(E_{\rm ADM}^{\rm p})$ [recall Eq. (3.47)] may now be obtained simply by considering the $O(\eta)$ piece of $L_{\rm ADM}^{\rm p}$ in Eq. (3.73), for a fixed $E_{\rm ADM}^{\rm p}$. Equations (3.73) with (3.77) immediately give us the $O(\eta)$ piece of $L_{\rm ADM}^{\rm p}$ for a fixed *angular velocity*: $\delta^{(\Omega)} L_{\rm ADM}^{\rm p} = -(\eta/2) dz_1/d\Omega$, where we introduced the operator $\delta^{(X)}$ to denote a linear variation with respect to η at fixed X. To obtain the shift at fixed *energy*, $\delta L_{\rm ADM}^{\rm p} \equiv$

$\delta^{(E)}L^{\rm p}_{\rm ADM}$, we write

$$\begin{aligned}\delta L^{\rm p}_{\rm ADM} &= \delta^{(\Omega)}L^{\rm p}_{\rm ADM} + \frac{dL^{\rm p}_{\rm ADM}}{d\Omega}\,\delta^{(E)}\Omega \\ &= \delta^{(\Omega)}L^{\rm p}_{\rm ADM} - \frac{dL^{\rm p}_{\rm ADM}}{dE^{\rm p}_{\rm ADM}}\,\delta^{(\Omega)}E^{\rm p}_{\rm ADM} \\ &= \delta^{(\Omega)}L^{\rm p}_{\rm ADM} - \Omega^{-1}\delta^{(\Omega)}E^{\rm p}_{\rm ADM}, \end{aligned} \tag{3.74}$$

where in the second line we used $\delta^{(E)}\Omega = -(d\Omega/dE^{\rm p}_{\rm ADM})\delta^{(\Omega)}E^{\rm p}_{\rm ADM}$, and in the third line we applied $dL^{\rm p}_{\rm ADM}/dE^{\rm p}_{\rm ADM} = \Omega^{-1}$, which is valid for any circular geodesic (omitting subdominant terms in η). From Eqs. (3.73) and (3.77) we find $\delta^{(\Omega)}E^{\rm p}_{\rm ADM} = (\eta/2)\,[z_1 - \Omega(dz_1/d\Omega)]$, and substituting this with the above result for $\delta^{(\Omega)}L^{\rm p}_{\rm ADM}$, we arrive at the simple expression

$$\delta L^{\rm p}_{\rm ADM} = -\frac{\eta}{2\Omega}\,z_1. \tag{3.75}$$

Note that in the analysis leading to Eq. (3.75) we have not assumed anything about the spin a of the central black hole, so the result should apply in general (and suggests an interesting new interpretation of z_1 in terms of a shift in the critical value of the angular momentum). In the extremal case, $\Omega = 1/2 + O(\epsilon)$, so at leading order in ϵ we obtain

$$\delta L^{\rm p}_{\rm ADM}(E) = -\eta Z_1(E), \tag{3.76}$$

where

$$Z_1(E) := \lim_{\epsilon\to 0} z_1(\Omega(E;\epsilon),\epsilon), \tag{3.77}$$

with the limit taken *at fixed energy* E. Here, for clarity, we have made explicit the functional dependence of z_1 and Ω on ϵ, and have parametrized the circular orbits by their geodesic energy E, noting that the difference between E and $E^{\rm p}_{\rm ADM}$ is subdominant in Eq. (3.76). Indeed, in practice, $Z_1(E)$ may be evaluated by considering a sequence of circular *geodesics* of diminishing ϵ (and a fixed E).

Equation (3.76) may then be used with Eq. (3.47) to obtain the sought-for relation

$$\delta\breve{L}^{\rm cons}_{\infty}(E) = E^2 + 1 - Z_1(E), \tag{3.78}$$

which may then be used in place of (3.45) in both conditions (3.44) and (3.56). The relation (3.78) relieves us from the need to restrict attention to particles coming from infinity, which is why we have used in it the argument E in place of E_∞. The energy may now take any

value $E > E_{\rm isco}(= 1/\sqrt{3})$, and the conditions (3.44) and (3.56) may be evaluated for all corresponding orbits.

We may also use Eq. (3.76) directly in conjunction with Eq. (3.48), to write the censorship condition (in the weakly fine-tuned case) in the remarkably simple form

$$Z_1(E) \geq \frac{1}{2}(E^2 - 1). \tag{3.79}$$

Overspinning is averted if and only if this inequality holds for all $E > E_{\rm isco}$. The evaluation of the condition (3.79) requires only redshift information on unstable circular orbits, evaluated at the extremal limit $\epsilon \to 0$ with E held fixed.

Chapter 4

Evaluation of the overspinning conditions

In the next section we evaluate the censorship condition (3.48), which ignores the possibility of strong fine-tuning. The latter will be considered in Sec. 4.3. If the inequality can be shown to hold for all $E_\infty > E_{\rm isco} = \frac{1}{\sqrt{3}}$, then overspinning is ruled out for all orbits (except, possibly, strongly fine-tuned ones).

The evaluation of (3.48) requires only the function $\delta\check{L}^{\rm p}_{\rm ADM}$, and we shall use Eq. (3.76) to calculate it. As will be shown, the evaluation of the redshift correction $Z_1(E)$ in Eq. (3.77) becomes particularly simple in the limit $\epsilon \to 0$, to the effect that the essential part of the calculation can be done analytically. The only numerical input we shall require is a verification that a certain perturbative quantity has a finite limit $\epsilon \to 0$; the precise numerical value of that limit will not be important to us. Below we first present the analytical part of the calculation, and in subsection (4.2) we discuss the numerical input.

4.1 Weakly fine-tuned orbits: analytical considerations

Isoyama *et al.* [36] show that the first-order GSF correction to the redshift z can be obtained via

$$Z_1(E) = -z^{(0)} H^R \quad \text{where} \quad H^R := \frac{1}{2} h^{R,\rm sym}_{\alpha\beta} \hat{u}^\alpha \hat{u}^\beta. \tag{4.1}$$

In the near-extremal limit,

$$z^{(0)}(E;\epsilon) = \frac{\epsilon}{\sqrt{6E^2-2}} + O(\epsilon^2), \tag{4.2}$$

whence it follows that

$$\delta L^{\rm p}_{\rm ADM}(E) = (6E^2-2)^{-1/2} \lim_{\epsilon\to 0} \left[\epsilon H^R(E;\epsilon)\right]. \tag{4.3}$$

Note that, for $\delta L^{\rm p}_{\rm ADM}(E)$ to be finite and generally nonzero (as expected) requires H^R to blow up like $1/\epsilon$ for $\epsilon \to 0$.

Our calculation of $H^R(E;\epsilon)$ will be based on the strategy and numerical codes developed by A. Shah and M. Van de Meent in Refs. [84–86]. $H^R(E;\epsilon)$ is expressed as a sum of two contribution:

$$H^R = H^R_{\rm recons} + H^R_{\rm compl}. \tag{4.4}$$

The "reconstructed" part $H^R_{\rm recons}$ is obtained numerically, starting from frequency-domain solutions of Teukolsky equation with a circular-geodesic source and retarded boundary conditions, following through a reconstruction of the multipole modes of the metric perturbation, and finally applying a suitable form of mode-sum scheme (see Subsec. 1.1.3) to extract the R part of the perturbation. (A more detailed description will be given in the next section.) In our case of a circular-orbit source, the double contraction of $h^R_{\alpha\beta}$ with $\hat{u}^\alpha$ [recall Eq. (4.1)] automatically picks out the time-symmetric part of $h^R_{\alpha\beta}$, as desired.

The second contribution to H^R in Eq. (4.4) is the "completion" piece $H^R_{\rm compl}$, which (by definition) arises from any part of the metric perturbation that is not captured by the reconstruction procedure. In our problem, this piece corresponds simply to mass and angular-momentum perturbations of the background Kerr geometry (plus pure-gauge perturbations) [84,87]. In the vacuum region $r > R$ outside the particle's orbit, these stationary perturbations can be written analytically, in a "Boyer-Lindquist" gauge, as [84]

$$h^{(\delta M)}_{\alpha\beta} = \mu E \frac{\partial g_{\alpha\beta}}{\partial M}, \qquad h^{(\delta J)}_{\alpha\beta} = \mu L \frac{\partial g_{\alpha\beta}}{\partial J}, \tag{4.5}$$

where $g_{\alpha\beta} = g_{\alpha\beta}(x^\mu; M, J)$ is the Kerr background metric, ∂_M is taken with fixed $J := Ma$, ∂_J is taken with fixed M, and both derivatives are taken with fixed Boyer-Lindquist coordinates x^μ. Our particular regularization procedure (see below) does not require the completion piece for $r < R$. The quantity $H^R_{\rm compl}$ is given by

$$H^R_{\rm compl} = \frac{1}{2}\hat{u}^\alpha \hat{u}^\beta \left(h^{(\delta M)}_{\alpha\beta} + h^{(\delta J)}_{\alpha\beta}\right), \tag{4.6}$$

where the perturbations are evaluated in the sided limit $r \to R^+$ (with $\theta = \pi/2$).

Let us denote by $\delta\mathsf{L}^{\rm cons}_{c,\rm recons}$ and $\delta\mathsf{L}^{\rm cons}_{c,\rm compl}$ the contributions to $\delta L^{\rm p}_{\rm ADM}(E)$ from $H^R_{\rm recons}$ and $H^R_{\rm compl}$, respectively, and proceed to obtain $\delta\mathsf{L}^{\rm cons}_{c,\rm compl}$ analytically. First use Eq. (4.6) with Eq. (4.5) and with $\hat{u}^\alpha = g^{\alpha\beta}\hat{u}_\beta$, where $\hat{u}_\beta = \{-E, 0, 0, L\}$ (in Boyer-Lindquist coordinates). This gives $H^R_{\rm compl}$ in terms of the circular-orbit radius R, its energy E and its angular momentum L. Then substitute the fixed-E expansions (2.13) for R, and $\tilde{L}_c(E)$ from Eq. (2.15) for L, along with $a = 1-\epsilon^2$. Finally, expand the result in ϵ at fixed E. The outcome is

$$H^R_{\rm compl} = \frac{\eta}{2\epsilon}(1-E^2)(6E^2-2)^{1/2} + O(\epsilon^0). \tag{4.7}$$

Notice this is an $O(\epsilon^{-1})$ quantity, so, recalling Eq. (4.3), it gives a finite contribution to $\delta\breve{\mathsf{L}}^{\rm cons}_c$. We find

$$\delta\breve{\mathsf{L}}^{\rm cons}_{c,\rm compl} = \frac{1}{2}(1-E^2), \tag{4.8}$$

where $\delta\breve{\mathsf{L}}^{\rm cons}_{c,\rm compl} := \eta^{-1}\delta\mathsf{L}^{\rm cons}_{c,\rm compl}$.

Remarkably, it follows that the completion contribution, on its own, *precisely saturates* the censorship condition (3.79). In the next section we will demonstrate numerically that the reconstructed part, $H^R_{\rm recons}(E;\epsilon)$, has a *finite* (non-divergent) fixed-E limit $\epsilon \to 0$. This will imply

$$\delta\mathsf{L}^{\rm cons}_{c,\rm recons} = 0, \tag{4.9}$$

and therefore

$$\delta\breve{L}^{\rm p}_{\rm ADM}(E) = \frac{1}{2}(1-E^2). \tag{4.10}$$

The censorship condition (3.79) is precisely saturated. This result and its implications will be discussed in Sec. 6.

4.2 Numerical input

To validate Eq. (4.9), we will demonstrate numerically that the limit

$$\lim_{\epsilon\to 0} H^R_{\rm recons}(E;\epsilon) =: \hat{H}^R(E) \tag{4.11}$$

(taken with fixed E) exists and yields a finite value. It may be possible to establish this mathematically through analysis of the reconstructed solutions in the near-extremal near-horizon approximations (perhaps modelled upon the method of Ref. [88]). Here we content ourselves with a numerical calculation, which, we find, already illustrates the finiteness of

$\hat{H}^R(E)$ rather convincingly.

Two independent numerical calculations have been performed in our group, using two different (albeit related) methods. One of the methods performs best at ϵ values that are not too small, and the other does best for ϵ values that are not too large. The combination of the two methods thus allowed access to a range of ϵ values wide enough to enable taking the limit $\epsilon \to 0$ accurately. The agreement we found between the two sets of results in an overlapping domain of intermediate ϵ values provides reassurance.

Both methods tackle the problem of finding solutions to the inhomogeneous Teukolsky equations, which govern the evolution of generic spin-s fields ψ on a Kerr background:

$$\begin{aligned}
&\left[\frac{\left(r^2+a^2\right)^2}{\Delta} - a^2\sin^2\theta\right]\frac{\partial^2\psi}{\partial t^2} + \frac{4\,M\,a\,r}{\Delta}\frac{\partial^2\psi}{\partial t\partial\phi} + \left[\frac{a^2}{\Delta} - \frac{1}{\sin^2\theta}\right]\frac{\partial^2\psi}{\partial\phi^2} + \\
&- \Delta^{-s}\frac{\partial}{\partial r}\left(\Delta^{s+1}\frac{\partial\psi}{\partial r}\right) - \frac{1}{\sin\theta}\frac{\partial}{\partial\theta}\left(\sin\theta\frac{\partial\psi}{\partial\theta}\right) - 2s\left[\frac{a(r-M)}{\Delta} + \frac{i\cos\theta}{\sin^2\theta}\right]\frac{\partial\psi}{\partial\phi} + \\
&- 2s\left[\frac{M(r^2-a^2)}{\Delta} - r - ia\cos\theta\right]\frac{\partial\psi}{\partial t} + \left(s^2\cot^2\theta - s\right)\psi = 4\pi\Sigma T_s, \qquad (4.12)
\end{aligned}$$

where Δ was defined below Eq. (2.4), $\Sigma := r^2 + a^2\cos^2\theta$ and T_s are some source terms, whose explicit expressions for gravitational perturbations can be found, for instance, in [89].

Teukolsky showed that, remarkably, the above equations can be separated by means of the following decomposition

$$\psi = \sum_{\ell\,m} {}_sR_{\ell m}(r)\,{}_sS_{\ell\,m}(\theta)e^{i(m\phi-\omega t)}. \qquad (4.13)$$

If one similarly decomposes the source terms T_s (and denotes by ${}_sT_{\ell m}(r)$ the analogue of ${}_sR_{\ell m}(r)$ in such a decomposition), then Eq.(4.12) can be rewritten as

$$\Delta^{-s}\frac{d}{dr}\left(\Delta^{s+1}\frac{d\,{}_sR_{\ell m}}{dr}\right) + \left[\frac{K^2 - 2is(r-M)K}{\Delta} + 4\,i\,s\omega r - \lambda\right]{}_sR_{\ell m} = {}_sT_{\ell m}, \qquad (4.14)$$

$$\begin{aligned}
&\frac{1}{\sin\theta}\frac{d}{d\theta}\left(\sin\theta\frac{dS}{d\theta}\right) + \Bigg[a^2\omega^2\cos^2\theta - \frac{m^2}{\sin^2\theta} - 2a\omega s\cos\theta + \\
&\qquad - \frac{2\,m\,s\cos\theta}{\sin^2\theta} - s^2\cot^2\theta + E - s^2\Bigg]\,{}_sS_{\ell m} = 0, \qquad (4.15)
\end{aligned}$$

where $K := (r^2+a^2)\omega - a\,m$ and $\lambda := E - s(s+1) + a^2\omega^2 - 2\,a\,m\omega$. The solutions to the angular equation are the so-called spin-weighted spheroidal harmonics. We are interested here in the spin $s = \pm 2$ solutions to Eq. (4.14), which correspond to the quantities ψ_0 ($s=2$) and $\rho^{-4}\psi_4$ ($s=-2$), where $\rho := -(r - ia\cos\theta)^{-1}$, and ψ_0,ψ_4 are the Weyl scalars

defined below

$$\psi_0 := C_{\alpha\beta\gamma\delta} l^\alpha m^\beta l^\gamma m^\delta, \tag{4.16}$$

$$\psi_4 := C_{\alpha\beta\gamma\delta} n^\alpha \bar{m}^\beta n^\gamma \bar{m}^\delta. \tag{4.17}$$

In the above definitions, $C_{\alpha\beta\gamma\delta}$ is the Weyl tensor and l, m belong to a complex null tetrad $w^\mu = \{l^\mu, n^\mu, m^\mu, \bar{m}^\mu\}$, where l^μ, n^μ are the principal null directions of the Kerr spacetime, and $l^\mu n_\mu = -1, m^\mu \bar{m}_\mu = 1$ [90].

Provided that either ψ_0 or ψ_4 are known, it is possible to reconstruct the metric perturbation using an intermediate function called the Hertz potential, which is a homogeneous solution to the Teukolsky radial equation, related to ψ_0 and $\rho^{-4}\psi_4$ by certain fourth-order differential operators. This procedure is sometimes referred to as "CKK metric reconstruction", as it was proposed independently by Chrzanowski and by Cohen and Kegeles [91,92]. A review of the CKK reconstruction in Kerr, whose details will not be important for our analysis, can be found in [93].

We will now illustrate the differences between the two numerical frameworks we took advantage of to solve Eq. (4.14) for a point-like source on a circular orbit in Kerr spacetime. The first calculation is based on method and code developed by A. Shah in Refs. [84, 94], with input from Ref. [85]. In this method, one first numerically integrates in the frequency domain an alternative formulation of the spin-2 radial Teukolsky equation, called the Sasaki-Nakamura equation [95], with "retarded" boundary conditions at infinity and on the event horizon, to obtain the modes of the Weyl scalar ψ_0. An appropriate Hertz potential is then derived, from which the modes of the metric perturbation are reconstructed by applying a certain differential operator [96]. We use a version of the reconstruction procedure that yields the metric perturbation in a regular outgoing radiation gauge[1] anywhere in the vacuum region $r > R$, where R is the Boyer-Lindquist radius of the circular orbit. Finally, a mode-sum regularization procedure is applied to obtain $H^R_{\rm recons}$.

The second calculation was based on a code developed by M. Van de Meent in [86], which follows an approach by Fujita [97], itself based on the semi-analytical formalism of Mano, Suzuki, and Takasugi (MST) [98,99]. In this approach, the Weyl scalar ψ_4 is obtained semi-analytically rather than numerically. In the MST method, the homogeneous solutions to the radial Teukolsky equation are expressed as a series of hypergeometric functions, which are regular at the horizon, but divergent at spatial infinity. This series is then matched to

[1] An outgoing radiation gauge is defined by the conditions $n^\mu h_{\mu\nu} = g^{\mu\nu} h_{\mu\nu} = 0$.

an expansion of the same solutions in terms of Coulomb wave functions, which are instead well-behaved at the horizon, but not at spatial infinity. The expansion coefficients of the two series obey a certain continued-fraction equation, which is solved numerically. The metric reconstruction and mode-sum procedures are essentially as in the first method, but they are implemented using an independent code.

In the MST-based calculation, working near extremality is computationally advantageous. This is due to the improved convergence properties of the MST formalism for circular orbits with $a \sim 1$ and $\Omega \sim 1/2$, highlighted in [86]. In this domain, the series of special functions featuring in MST's solutions for ψ_4 converges faster. Furthermore, the aforementioned continued-fraction equation is both faster convergent and more easily solvable (using the analytically-known extremal solution as an initial guess). As a result, the method is particularly efficient for studying the $\epsilon \to 0$ limit. For our purpose, it was sufficient to apply it in the range $10^{-8} \leq \epsilon \leq 10^{-4}$. Above $\epsilon \sim 10^{-4}$, the analytically-known extremal solution no longer provides an accurate enough initial guess to guarantee finding the solution of the continued-fraction equation for all frequency modes in the spectrum, making our implementation of the MST formalism unreliable.

The calculation of $\hat{H}^R(E)$ proceeded as follows. We considered a dense sample of E values in the range $E_{\rm isco} < E < 2$. For each value of E in the sample we obtained a dataset $H^R_{\rm recons}(E,\epsilon)$, where ϵ is sampled (roughly) uniformly in $\log\epsilon$ between $\epsilon = 10^{-1}$ and $\epsilon = 10^{-8}$. We switched from our fully numerical method to our MST-based method at around $\epsilon = 10^{-4}$. $\hat{H}^R(E)$ was then obtained via extrapolation of each of the fixed-E datasets to $\epsilon = 0$.

For each pair $\{E,\epsilon\}$ in our sample, the first 70 multipoles (l-modes) of the metric perturbation has been computed, for use as input in the mode-sum formula. The remaining large-l tail of modes was approximated by fitting an inverse-power-law model, as detailed in [84]. At high values of E, the l-mode distribution becomes skewed towards larger l values, due to what may be interpreted as a beaming effect. A similar behavior near the light-ring of a Schwarzschild black hole was discussed by Akcay *et al.* [41], who pointed out that the implementation of the mode-sum technique can become problematic in that case, because the standard inverse-power-law tail may fail to manifest itself until l values larger than one can feasibly calculate. This effect restricted our calculation here to E values that are not too large—in practice, to $E \lesssim 2$. However, that should suffice for our purpose here, which is simply to determine the ϵ-scaling of $H^R_{\rm recons}$ in the limit $\epsilon \to 0$ at fixed E: it is perfectly reasonable to assume that the ϵ-scaling at any fixed $E > 2$ would be the same as

it is for lower E.

Figure 4.1 shows $H^R_{\rm recons}(E;\epsilon)$ as a function of ϵ for a few E values within our sample. It is evident that $H^R_{\rm recons}(E;\epsilon)$ approaches a finite limit as $\epsilon \to 0$. Figure 4.2 displays the extrapolated values $\hat{H}^R$ as a function of E, using the numerical data provided by A. Shah and M. Van de Meent. We remind that the details of the function $\hat{H}^R(E)$ are unimportant to us; we needed only establish here that $\hat{H}^R$ is finite for any finite E.

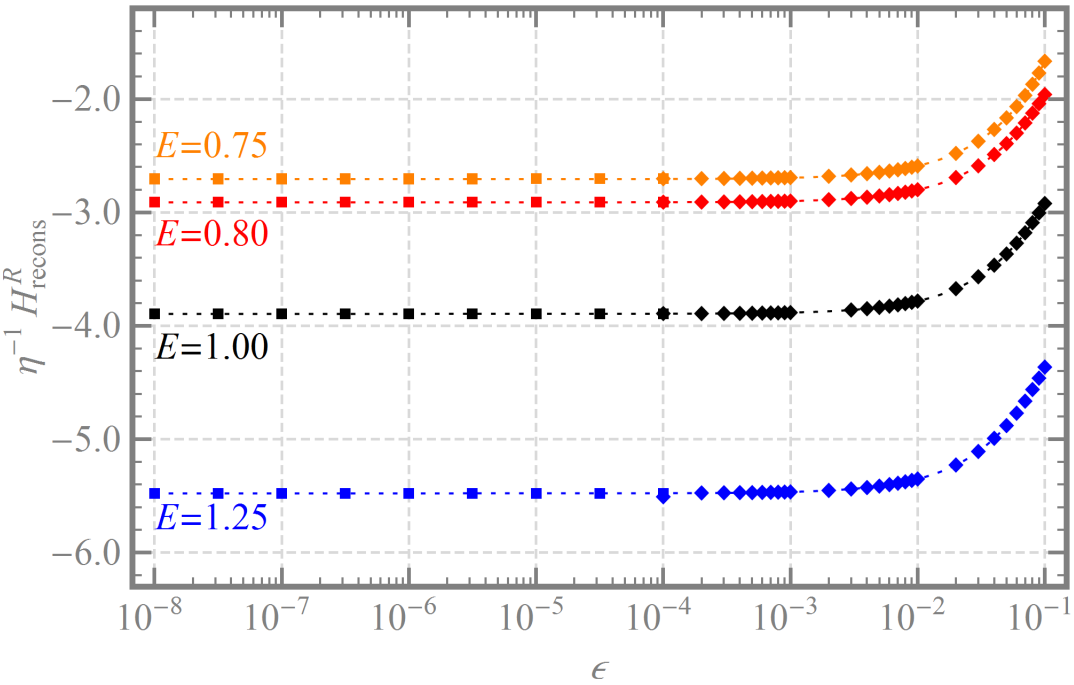

Figure 4.1: $H^R_{\rm recons}$ as a function of ϵ, for a sample of E values. Data points for $\epsilon \geq 10^{-4}$ (diamonds) are from the fully numerical computation, while points for $\epsilon \leq 10^{-4}$ (squares) are from the semi-analytical, MST-based method (there is an overlapping data point at $\epsilon = 10^{-4}$). Error bars are in all cases too small to be resolved in this figure. Curves (dotted line) are quartic polynomial fits. At each fixed E, $H^R_{\rm recons}(E;\epsilon)$ appears to approach a constant value in the extremal limit $\epsilon \to 0$.

4.3 Effect of strong fine-tuning

We have shown that, within our first-order GSF approximation, any weakly fine-tuned capture produces a precisely extremal geometry. Can strong fine-tuning push the system beyond extremality? To answer that question we need to evaluate the condition (3.56). Any choice of $\{E_i, E_f\}$ (with $E_{\rm isco} \leq E_f < E_i$) violating that condition would imply that overspinning is possible via strong fine-tuning. If, on the other hand, we can show that (3.56) applies for any $\{E_i, E_f\}$, then censorship holds even allowing for strong fine-tuning.

The evaluation of (3.56) requires the angular-momentum shift $\delta\breve{L}^{\rm cons}_\infty(E_i)$ and the flux

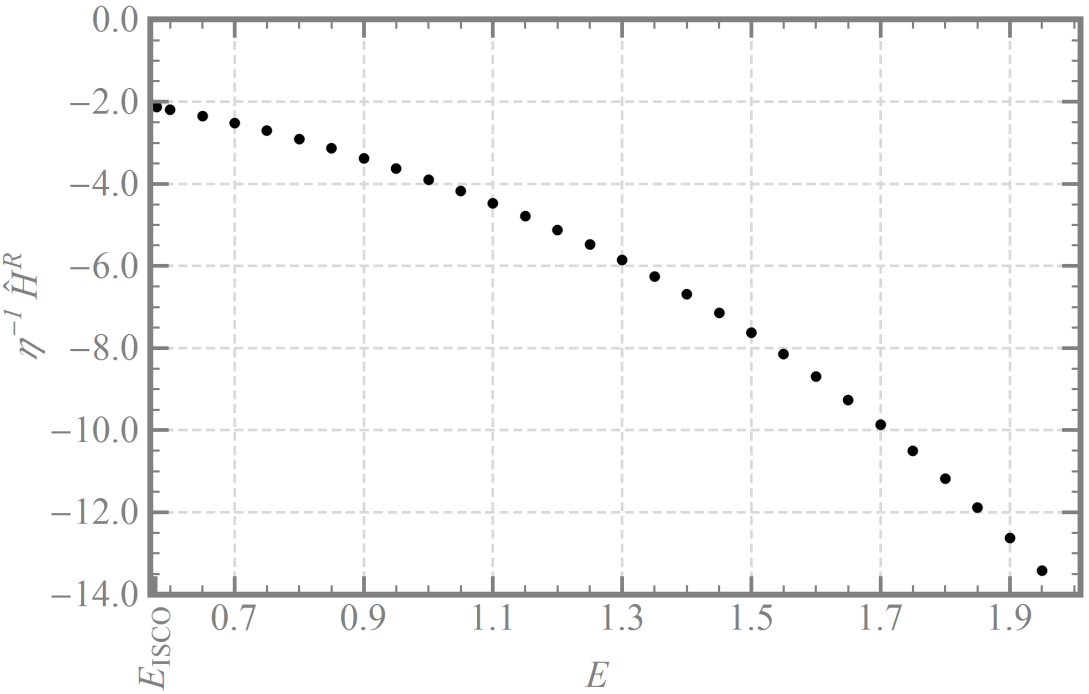

Figure 4.2: The function $\hat{H}^R(E)$, obtained by extrapolating our numerical data for $H^R_{\rm recons}$ to $\epsilon \to 0$ at each fixed E. The actual value of $\hat{H}^R(E)$ is not needed in our analysis, only the fact that it is finite for each finite E.

ratio $\mathcal{R}(E)$. For the former we use Eq. (3.47) and our result (4.10). For the latter we will perform a numerical calculation, to be presented in section 4.5 below. However, much of what we need to know about $\mathcal{R}$ can be deduced from simple analytic considerations, to be presented first. We will show that it is sufficient to require that $\mathcal{R}$ is bounded from below by $-1/3$ over the range $E_{\rm isco} \le E < \frac{2}{\sqrt{3}}$ in order to guarantee that the censorship condition (3.56) always holds. Our actual calculation will later show that $\mathcal{R}$ lies very comfortably above that bound.

4.4 Strongly fine-tuned orbits: analytical considerations

4.4.1 Superradiant domain

First, we consider the sign of $\mathcal{R}(E)$. We recall that this function, defined for circular equatorial geodesics, is the ratio of energy flux through the horizon to the energy flux at infinity. A gravitational-wave mode of the form $\sim e^{-i\omega t}e^{im\phi}$ is known to be superradiant if and only if $0 < \omega < m\Omega_H$, where $\Omega_H = a/(2Mr_+)$ is the horizon's angular velocity, with $r_+ = M + (M^2 - a^2)^{1/2}$. For circular equatorial orbits the gravitational-wave spectrum is simple: $\omega = m\Omega$, where Ω is the orbital angular velocity. Thus, all modes of the radiation

are superradiant for $\Omega < \Omega_H$, giving $\mathcal{R} < 0$ in that case. For $\Omega > \Omega_H$ all modes are instead non-superradiant, giving $\mathcal{R} > 0$.

Let us now specialize to a near-extremal geometry, and reexpress the above in terms of a condition on the specific energy E of the circular geodesic. For $\epsilon \ll 1$, $M\Omega_H = \frac{1}{2} - \frac{1}{\sqrt{2}}\epsilon + O(\epsilon^2)$. Combining this with Eq. (3.63) translates the superradiance condition $\Omega < \Omega_H$ to $E(6E^2-2)^{-1/2} > \sqrt{2}/3$ (at leading order in ϵ), leading to

$$E < \frac{2}{\sqrt{3}} =: E_{\rm sr} \tag{4.18}$$

as the superradiant domain in the extremal limit. Thus

$$\mathcal{R} \;<\; 0 \quad \text{for} \quad E_{\rm isco} \leq E < E_{\rm sr}, \tag{4.19}$$

$$\mathcal{R} \;>\; 0 \quad \text{for} \quad E > E_{\rm sr}. \tag{4.20}$$

This will be confirmed numerically in section 4.5.

4.4.2 Sufficient lower bound for $\mathcal{R}(E)$

We now show that the censorship condition (3.56) is satisfied for all $E_i > E_f \geq \frac{1}{\sqrt{3}}$ if $\mathcal{R}(E)$ is bounded from below by $-1/3$. The condition involves $\bar{F}$ and $\bar{H}$, given in Eqs. (3.49), where we now replace $\delta L_\infty^{\rm cons}(E_i)$ by $\delta \breve{L}^p_{\rm ADM}(E_i)$ (using Eq. (3.47)) and take advantage of Eq. (4.10). We do not know the sign of $\bar{F}$ (for given E_i, E_f) a priori, so we proceed by considering the two options $\bar{F} \geq 0$ and $\bar{F} < 0$ in turn.

Case $\bar{F} \geq 0$:— The censorship condition (3.56) becomes

$$\bar{H} = -\frac{1}{2}(1-E_i^2) + (E_i - \breve{\mathcal{E}}^+_{\rm (qc)})^2 \geq 0. \tag{4.21}$$

This is trivially satisfied for $E_i \geq 1$, so it remains to consider $E_i < 1$, in which case the condition becomes

$$\breve{\mathcal{E}}^+_{\rm (qc)} \leq E_i - \sqrt{(1-E_i^2)/2} =: \nu_1(E_i). \tag{4.22}$$

Recalling (3.59), we may bound $\breve{\mathcal{E}}^+_{\rm (qc)}$ from above using

$$\breve{\mathcal{E}}^+_{\rm (qc)} \leq \int_{\frac{1}{\sqrt{3}}}^{E_i} \frac{dE}{1+\mathcal{R}(E)} \leq \frac{E_i - \frac{1}{\sqrt{3}}}{1+\mathcal{R}_m} =: \nu_2(E_i), \tag{4.23}$$

where in the first inequality we used the positivity of the integrand together with $E_f \geq \frac{1}{\sqrt{3}}$, and in the second inequality we assumed $\mathcal{R}$ is bounded from below by some number $\mathcal{R}_m(> -1)$. Since $\nu_1 = \nu_2(= 0)$ at $E_i = \frac{1}{\sqrt{3}}$, establishing the inequality in (4.22) requires only showing that $\nu_1'(E_i) \geq \nu_2'(E_i) = (1+\mathcal{R}_m)^{-1}$ for all $\frac{1}{\sqrt{3}} < E_i < 1$. But the minimal value of ν_1' over this domain is 3/2, so the condition becomes $(1+\mathcal{R}_m)^{-1} \leq \frac{3}{2}$, or $\mathcal{R}_m \geq -\frac{1}{3}$. We have thereby shown that the censorship condition (4.21) holds for any $E_i > E_f \geq \frac{1}{\sqrt{3}}$ with $\bar{F}(E_i, E_f) \geq 0$, under the sole assumption

$$\mathcal{R}(E) \geq -\frac{1}{3}. \tag{4.24}$$

Case $\bar{F} < 0$:— The censorship condition (3.56) becomes $\bar{H} \geq \bar{F}^2/4$, or, explicitly,

$$\begin{aligned} 0 &\leq -\frac{1}{4}\breve{\mathcal{W}}^+_{(\mathrm{qc})}\left(\breve{\mathcal{W}}^+_{(\mathrm{qc})} - 2\phi(E_i)\right) + \breve{\mathcal{E}}^+_{(\mathrm{qc})}\left(\breve{\mathcal{E}}^+_{(\mathrm{qc})} - 2E_i\right) \\ &=: \Delta(E_i, E_f), \end{aligned} \tag{4.25}$$

where $\phi(E_i) = -(6E_i^2 - 2)^{1/2}$. Since $\breve{\mathcal{W}}^+_{(\mathrm{qc})} = 0 = \breve{\mathcal{E}}^+_{(\mathrm{qc})}$ for $E_i = E_f$, we have $\Delta(E, E) = 0$ for all $E \geq \frac{1}{\sqrt{3}}$. Thus, to establish $\Delta \geq 0$ it suffices to show $\partial\Delta(E_i, E_f)/\partial E_i \geq 0$ for all $E_i \geq E_f \geq \frac{1}{\sqrt{3}}$.

With the aid of Eqs. (3.59) and (3.64), we find

$$[1+\mathcal{R}(E_i)]\frac{\partial\Delta}{\partial E_i} = E_i + \mathcal{R}(E_i)\left[\frac{3E_i\breve{\mathcal{W}}^+_{(\mathrm{qc})}}{\phi(E_i)} - 2\breve{\mathcal{E}}^+_{(\mathrm{qc})}\right]. \tag{4.26}$$

Consider the cases $\mathcal{R}(E_i) \leq 0$ and $\mathcal{R}(E_i) > 0$ separately. For $\mathcal{R}(E_i) \leq 0$, we use $\breve{\mathcal{W}}^+_{(\mathrm{qc})} > \phi(E_i)$ (following from $\bar{F} < 0$) to bound the right-hand side of (4.26) from below by $E_i[1 + 3\mathcal{R}(E_i)] - 2\mathcal{R}(E_i)\breve{\mathcal{E}}^+_{(\mathrm{qc})}$. Since the last term here is non-negative, it is sufficient to require $\mathcal{R}(E_i) \geq -\frac{1}{3}$ in order to guarantee $\partial\Delta/\partial E_i > 0$ and hence $\Delta(E_i, E_f) \geq 0$. If, instead, $\mathcal{R}(E_i) > 0$, one can first use $-2\breve{\mathcal{E}}^+_{(\mathrm{qc})} > \breve{\mathcal{W}}^+_{(\mathrm{qc})}$ [which follows from Eqs. (3.59) and (3.64), noting $b(E) > 2$], then again $\breve{\mathcal{W}}^+_{(\mathrm{qc})} > \phi(E_i)$, to bound the right-hand side of (4.26) from below by $E_i + \mathcal{R}(E_i)\,[\phi(E_i) + 3E_i]$. This is non-negative for all $E_i \geq \frac{1}{\sqrt{3}}$ if and only if $\mathcal{R}(E_i) \geq -\frac{1}{3}$. Thus, the condition (4.24) always implies $\Delta \geq 0$ and, in turn, that the censorship condition (3.56) holds also for $\bar{F} < 0$.

We conclude that it is sufficient to show that the flux ratio $\mathcal{R}$ is bounded from below by $-\frac{1}{3}$ in order to guarantee that the censorship condition (3.56) is always satisfied. In fact, recalling (4.20), we see that it is sufficient to obtain such a bound for $\mathcal{R}$ on the restricted

superradiant domain $E_{\rm isco} \leq E < E_{\rm sr}$. Our numerical calculation, to be presented below, shows that $\mathcal{R}$ is comfortably bounded above the value of $-1/3$.

4.5 Numerical input

To compute the flux ratio $\mathcal{R}$ one can use the MST-based method described above, as implemented in [86]. The gravitational-wave energy fluxes to infinity and down the horizon are obtained directly from the semi-analytical solutions for ψ_4, with no need to reconstruct the metric perturbation. Thanks to the improved convergence properties (already mentioned above) of the MST formalism at $\epsilon \ll 1$ and $\Omega \sim 1/2$, one can obtain the energy fluxes to essentially any accuracy we desire using arbitrary-precision computer algebra.

To determine $\mathcal{R}$ for a given E, the ratio between the flux down the horizon and the flux to infinity has been calculated for a sequence of fixed-E orbits with ϵ values that decrease to 10^{-8} in exponential steps. The value of $\mathcal{R}(E)$ was then found by extrapolating to $\epsilon = 0$. The results, which have been computed by M. Van de Meent, are presented in Fig. 4.3. As expected, $\mathcal{R}(E)$ is negative only in the range $E_{\rm isco} \leq E < E_{\rm sr}$. The minimum of $\mathcal{R}(\mathcal{E})$ appears to be attained at $E_{\rm isco}$ with a value of $-0.13744 \pm 3 \cdot 10^{-5}$. This is comfortably above the value of $-1/3$ required to assure that the censorship condition (3.56) is satisfied and therefore conclude that strongly fine-tuned orbits cannot overspin.

4.5.1 Zoom-whirl orbits

We have implicitly excluded from our discussion orbits exhibiting a zoom-whirl type behaviour, i.e. orbits that reach the strong-field region, whirl, and then zoom out to some finite radius (possibly repeating this multiple times before plunging). In fact, we assumed that (near-)critical orbits would plunge immediately after their whirling phase. Let us now consider instead a small mass coming from infinity that joins the global attractor, emits enough radiation so that its specific energy drops to some value $E < 1$, and then zooms out to a finite radius. Until the moment it leaves the attractor, such an orbit will be equivalent to a strongly fine-tuned one (because the effects related to the transition and plunge are negligible at first order) and thus our analysis indicates that, during this part of the evolution, the orbit cannot overspin. After leaving the attractor the orbit will be bound. Bound orbits were not in position to overspin in the geodesic approximation and we assume here that the self-force will not favour overspinning. Under this assumption it then appears safe to conclude that zoom-whirl orbits are not in position to overspin.

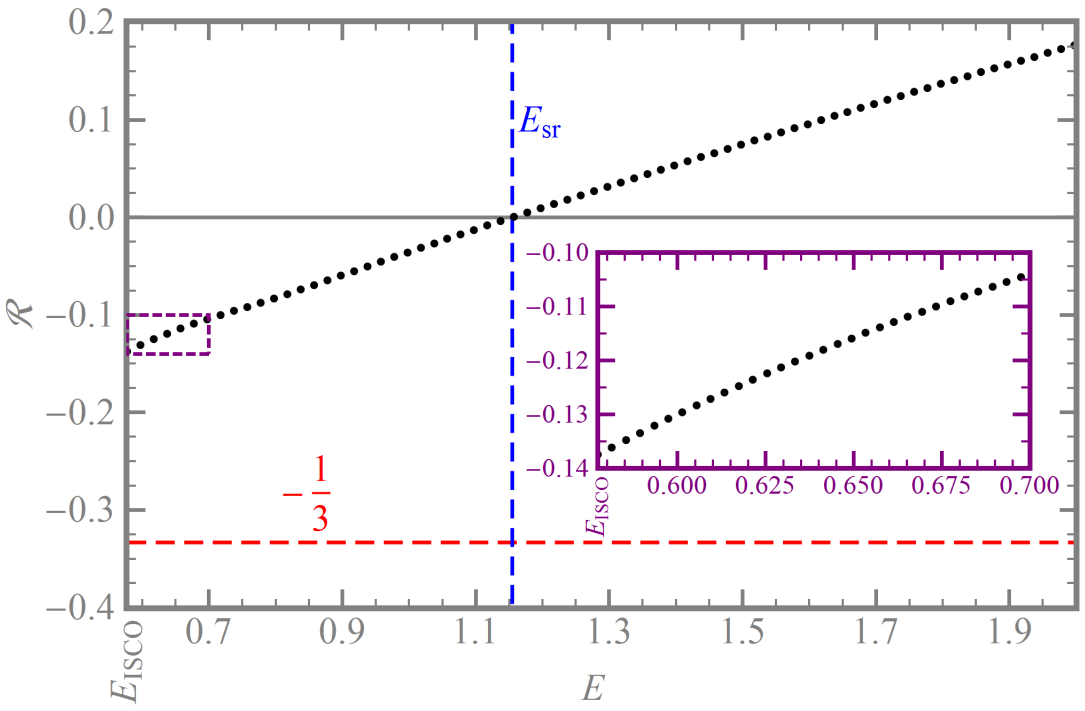

Figure 4.3: Numerical values for the flux ratio $\mathcal{R}$, as a function of specific energy E, for unstable circular equatorial geodesic orbits in the extremal Kerr limit. Each dot represents a numerical measurement, with error bars being much smaller than the size of the dots. Orbits with $E < E_{\rm sr} = 2/\sqrt{3}$ are superradiant, with $\mathcal{R} < 0$. The inset expands the area around the minimum at $E_{\rm isco} = 1/\sqrt{3}$. We find a minimum value of $\mathcal{R} = -0.13744 \pm 3 \cdot 10^{-5}$, safely above what is required for the censorship condition (3.56) to hold (dashed red line).

Chapter 5

Gravitational self-force along MBMS orbits

In Sec. 3.9 we took advantage of some relations obtained using the Hamiltonian formalism of [36] to conveniently reformulate our overspinning conditions. The underlying assumption was that a spacetime containing a critical, unbound orbit has the same Bondi energy and angular momentum of one containing the corresponding unstable circular orbits. We also mentioned that it would be important to verify that the results obtained following this method can be exactly reproduced by a full self-force calculation along unbound orbits.

A numerical computation of the gravitational self-force is now well established for eccentric orbits in Kerr spacetime [100], but is currently unavailable for unbound orbits. On the other hand, a framework to numerically compute the self-force along generic orbits in Schwarzschild was elaborated several years ago by Sago and Barack [101], and it is therefore suited to perform a first self-force calculation along unbound orbits in the simpler environment provided by the Schwarzschild spacetime. A future development of the work present here would be an extension of the calculation to Kerr spacetime, which would have direct applications to the overspinning problem.

In this chapter we will focus, in particular, on marginally bound, marginally stable orbits (MBMS), i.e. zero-binding-energy orbits that asymptote to the IBCO (which has specific energy $E = 1$) either in the infinite future or in the infinite past. There are two MBMS orbits that share the same conserved energy and angular momentum and are distinguished by the initial conditions imposed on their motion: we will call "inbound" an orbit starting from rest at past timelike infinity, and "outbound" its time-reversed counterpart.

Until recently, a direct computation of the GSF along unbound orbits had been hindered

by the gauge-instability affecting the time-domain evolution of certain non-radiative modes of the metric perturbation. However, we will show that, in the specific case of MBMS orbits, it is possible to cure this problem following a strategy based on work by Dolan and Barack [102] who dealt with a similar issue in the case of circular orbits.

In Sec. 5.1 we will give a formal definition of MBMS orbit, while in Sec. 5.2 we will illustrate the effects of the conservative GSF on this type of motion. In particular, we will present numerical results for two GSF effects that have never been examined in the literature, namely the shift in the azimuthal frequency of the IBCO and the correction to the critical value of the angular momentum at infinity of a MBMS orbit. We will show how our computation can be used to establish a comparison with the first law of binary black-hole mechanics.

An additional bonus of our calculation is that it also allows to calibrate the conservative sector of the so-called effective one-body theory (EOB)[1], a semi-analytical framework devised to model gravitational wave emission from compact binaries. EOB offers the advantage of interpolating across the domains of validity of several schemes: in practice, this can be achieved by calibrating some free parameters of the model using information coming from Numerical Relativity, the post-Newtonian approximation and the self-force scheme. In Sec. 5.6, we will show how a computation of the GSF along a MBMS orbit can inform EOB, and describe future applications of our framework.

5.1 Marginally bound geodesics in Schwarzschild spacetime

The motion of a test mass moving on the equatorial plane of a Schwarzschild background with ADM mass M is governed by the following equations:

$$u^t = \frac{E}{f(r)}, \tag{5.1}$$

$$(u^r)^2 = E^2 - V(r, L), \tag{5.2}$$

$$u^\phi = \frac{L}{r^2}, \tag{5.3}$$

$$u^\theta = 0, \tag{5.4}$$

$$\dot{E} = \dot{L} = 0, \tag{5.5}$$

[1]The name stems from the fact that the two-body dynamics is replaced with that of a point particle moving in a certain "effective" geometry. We will come back to this point in Sec. 5.6.

where we defined $V(r,L) := f(r)\left(1+\frac{L^2}{r^2}\right)$, $f(r) := (1-2M/r)$ and an overdot denotes differentiation with respect to proper time. As in Sec. 2.1, E and L represent the conserved specific energy and angular momentum of the test body. From Eq. (5.2) it follows that the radial acceleration has the simple form

$$\ddot{r} = -\frac{\partial_r V(r,L)}{2}. \tag{5.6}$$

A MBMS orbit is defined by the conditions that the particle is at rest when $r \to \infty$ and that its motion approaches circularity either in the infinite past (for the outbound MBMS orbit) or future (for the inbound MBMS orbit). Note that, given that $u^\theta = 0$ and $\lim_{r\to\infty} u^\phi = 0$, the first condition is equivalent to requiring that the particle has zero radial velocity when $r \to \infty$. Hence, a MBMS orbit needs to satisfy the following constraints

$$u^r(r\to\infty) = 0, \tag{5.7}$$

$$u^r(R) = 0, \tag{5.8}$$

$$\ddot{r}(R) = 0, \tag{5.9}$$

where R denotes the radius of the IBCO.

Making use of Eqs.(5.1)-(5.3), one obtains

$$E_0 = 1, \quad L_0 = 4M, \quad R_0 = 4M, \tag{5.10}$$

where a subscript "0" denotes that these parameters characterise a MBMS in the geodesic approximation. Plugging the above results into Eqs. (5.1) and (5.3), it is straightforward to compute the azimuthal frequency of the IBCO in the geodesic case:

$$\Omega_0 := \left.\frac{d\phi}{dt}\right|_{r=4M} = \frac{1}{8M}. \tag{5.11}$$

5.2 Marginally bound orbits in the self-force approximation

We turn next to examining the behaviour of a MBMS orbit when the first-order gravitational self-field exerted by the mass μ is taken into account. In what follows we will focus on *conservative* effects (see Sec. 1.1.4) and for brevity we will denote the conservative GSF simply by F^α. As we did in Ch. 3, we choose to normalise the four-velocity with respect to the background metric, so that Eqs. (5.1)-(5.3) remain unchanged, and again we define

$\hat{E} := -\hat{u}_t, \hat{L} := \hat{u}_\phi$. $\hat{E}$ and $\hat{L}$ evolve according to Eq. (3.4) and (5.6) becomes

$$\ddot{r} = -\frac{\partial_r V(r, L)}{2} + \tilde{F}^r, \tag{5.12}$$

where we adopted the notation $\tilde{F}^\alpha := F^\alpha/\mu$.

We can now define a MBMS orbit in the *perturbed* spacetime along the lines of Sec. 5.1, by imposing the conditions (5.7)–(5.9), with the only difference that the circularity conditions (5.7)–(5.8) will have to be evaluated at some perturbed radius $R = R_0 + \delta R$. Expanding the energy and angular momentum of the orbit around their background values $\hat{E} = E_0 + \delta E(r(\tau)))$, $\hat{L} = L_0 + \delta L(r(\tau))$, and taking the first-order variation of (5.7)–(5.9) with respect to the small mass μ, one obtains

$$2E_0\delta E(\infty) - \partial_r V(\infty, L_0)\delta R - \partial_L V(\infty, L_0)\delta L(\infty) = 0, \tag{5.13}$$

$$2E_0\delta E(R_0) - \partial_r V(R_0, L_0)\delta R - \partial_L V(R_0, L_0)\delta L(R_0) = 0, \tag{5.14}$$

$$\partial_r^2 V(R_0, L_0)\delta R + \partial_L\partial_r V(R_0, L_0)\delta L(R_0) = 2\tilde{F}^r(R_0). \tag{5.15}$$

The above equations imply

$$\delta E(\infty) = 0, \tag{5.16}$$

$$\delta E(R_0) = \Omega_0\delta L(R_0), \tag{5.17}$$

$$\delta R + \delta L(R_0) = -32M^2\tilde{F}^r(R_0). \tag{5.18}$$

Two extra constraints can be formulated by integrating Eqs. (3.4) along an inbound MBMS orbit:

$$\delta E(R_0) - \delta E(\infty) = -\int_\infty^{R_0} \tilde{F}_t \frac{dr}{\dot{r}} := \Delta E, \tag{5.19}$$

$$\delta L(R_0) - \delta L(\infty) = \int_\infty^{R_0} \tilde{F}_\phi \frac{dr}{\dot{r}} := \Delta L. \tag{5.20}$$

Eqs. (5.16)-(5.20) represent a closed system of equations for the unknown variables $\delta E(R_0)$, $\delta E(\infty)$, $\delta L(R_0)$, $\delta L(\infty)$, δR. It is easy to see that Eqs. (5.16)–(5.20) imply

$$\delta R = -8M\Delta E - 32M^2\tilde{F}^r(R_0), \tag{5.21}$$

$$\delta L(\infty) = 8M\Delta E - \Delta L. \tag{5.22}$$

Plugging $R = R_0 + \delta R$ into Eq. (1.31) and expanding in η, the azimuthal frequency of a circular orbit in the perturbed spacetime can be written as

$$\Omega^2 = \Omega_0^2 \left(1 - \frac{3\delta R}{4M} - 8M\tilde{F}^r(4M)\right), \tag{5.23}$$

where the radial self-force can be evaluated, in our case, at the unperturbed radius $4M$, as we are only keeping linear in η corrections. Using Eq. (5.21) the above result can be rewritten in the convenient form

$$\Omega^2 = \Omega_0^2 \left(1 + 6\Delta E + 16M\tilde{F}^r(4M)\right). \tag{5.24}$$

Eq. (5.24) tells us that the IBCO frequency shift can be directly computed from two complementary pieces of information: one is the local radial self-force acting on the IBCO, and the other is an integral of the conservative self-force along an inbound MBMS orbit. Both quantities can be extracted from the self-force code we will describe later on.

Note that, as an inbound MBMS orbit is nothing but a time-reversed outbound MBMS orbit, the time-symmetric part of the self-force acting on it can be easily constructed as follows

$$F^{t/\phi}_{\rm cons}(r) = \frac{\left(F^{t/\phi}_{ret,{\rm in}}(r) - F^{t/\phi}_{ret,{\rm out}}(r)\right)}{2}, \tag{5.25}$$

where "ret" stands for retarded, "in" denotes the inbound orbit and "out" the outbound one. In practice then, one needs to compute the self-force along two distinct orbits, and construct $F^{t/\phi}_{cons}(r)$ using the above formula. In the next section, we will describe the self-force code that has been developed to obtain the numerical input required by Eqs. (5.22) and (5.24).

5.3 A time-domain code for generic orbits in Schwarzschild

Our numerical scheme is largely based on work by Barack and Sago [101] but, while their framework is specifically designed to deal with bound orbits, ours is capable of handling generic orbits. The local self-force acting on the particle is computed in the time-domain, after solving the linearised Einstein's field equations in Lorenz gauge (1.1). The gauge constraints

$$Z_\alpha := \bar{h}_{\alpha\beta}^{\ \ ;\beta} = 0 \tag{5.26}$$

are guaranteed to be satisfied in the continuum limit, provided that they are satisfied initially: in fact, for a Ricci-flat spacetime, taking the divergence of Eq. (1.1) gives $\Box Z_\alpha = 0$, which implies that, if the gauge conditions are initially satisfied, i.e. $Z_\alpha = 0$, then they will be for the entire evolution. However, in the discrete case, round-off and truncation errors will eventually give rise to gauge violations that will propagate over the numerical grid. To tackle this problem, Barack and Lousto [103] added to Eq. (1.1) a constraint damping term in the form

$$\nabla^\mu \nabla_\mu \bar{h}_{\alpha\beta} + 2R^\sigma_{\ \alpha\ \beta}^{\ \ \tau} \bar{h}_{\sigma\tau} - \kappa(r)\left(t_\alpha Z_\beta + t_\beta Z_\alpha\right) = -16\pi T_{\alpha\beta}, \tag{5.27}$$

where t_μ is a future-directed vector field and $\kappa = 2M/r^2$. It can be verified that the gauge constraints evolve now according to a damped wave equation $\Box Z_\alpha - \kappa \nabla^\beta \left(t_\alpha Z_\beta + t_\beta Z_\alpha\right) = 0$; thus, one can expect that any gauge violation produced by discretization errors will be eventually suppressed.

In the Barack-Sago implementation, the retarded (trace-reversed) metric perturbation is first decomposed onto a basis of tensor harmonics

$$\bar{h}_{\alpha\beta} = \frac{\mu}{r} \sum_{l,m} \sum_{i=1}^{10} a^i_l \bar{h}^{i,l\,m}(t,r) Y^{i,l\,m}_{\alpha\beta}(\theta,\phi); \tag{5.28}$$

the numerical coefficients a^i_l and the tensor harmonics $Y^{i,l\,m}_{\alpha\beta}$ were originally given in [101, 103] and are listed in Appendix C. The above decomposition has the effect of decoupling the two-dimensional evolution of the $\bar{h}^{i,l\,m}(t,r)$ from the angular part of the field equations. By taking linear combinations of the metric components (5.28), the field equations can be recast in the form

$$\left(\partial_{uv} + U^l(r)\right) \bar{h}^{i,lm} + \mathcal{M}^{i,l}_j \bar{h}^{j,lm} = S^{i,lm}(r_p(\tau), \phi_p(\tau)) \delta(r - r_p(\tau)), \tag{5.29}$$

$$U^l(r) := \frac{f}{4r^2}\left(l(l+1) + \frac{2M}{r}\right), \tag{5.30}$$

where we introduced the null coordinates $u := t - r^*$ and $v := t + r^*$, with $r^* := r + 2M \log(r/2M - 1)$. In the above equation, $i = 1...10$ and $r_p(\tau), \phi_p(\tau)$ denote the particle's radial and angular positions in Schwarzschild coordinates. The quantities $\mathcal{M}^{i,l}_j$ are certain linear differential operators acting on the metric perturbation and the $S^{i,lm}$ are source terms that depend on the particle's position (both are explicitly defined in Appendix D).

The form of (5.29) is particularly convenient from a numerical point of view, as the

first two terms on the left hand side also appear in the field equation for the spherical harmonics modes of a scalar field: thus, for each index i, Eq. (5.29) corresponds to a scalar wave equation with additional coupling terms. It follows that one can test the robustness of a gravity code by switching off these couplings and comparing the results with scalar codes, which are typically developed first, as a stepping stone towards the electro-magnetic and gravitational problems.

The ten equations of (5.29) split into two subsets of coupled PDE's: the first set includes equations $i = 1...7$, and the second equations $i = 8...10$. The two groups are referred to as the even and odd parity sectors respectively.[2].

We chose to evolve the field equations (5.29) on a two-dimensional grid of null coordinates. In this formulation, one does not need to impose boundary conditions, but only initial ones. The initial data need to decay sufficiently fast both at the horizon and at infinity (a convenient choice is that of setting $\bar{h}^{i,lm} = 0$); also, they do not need to be solutions of the constraint equations, as any spurious radiation resulting from incorrect initial data is going to be dissipated away at late time. As our numerical setup is largely based on the one devised in [101], we will outline here only some essential features of the scheme, and refer the reader to [101] for a more detailed description of its construction.

The first step is that of integrating equations (5.29) over each grid cell[3], and then solving them iteratively using a fourth-order convergent finite-difference scheme, which is derived by approximating the field and its derivatives with some suitable Taylor expansions. To exemplify how this works, let us suppose the field equations are being solved in the top cell of Fig. 5.1, which will be denoted by $\mathcal{C}$. Then, for a single l, m mode (in what follows we will suppress these two indices, for convenience), an integration of Eq. (5.29) over $\mathcal{C}$ gives

$$\bar{h}^i(0) = \bar{h}^i(4) + \bar{h}^i(1) - \bar{h}^i(5) + \int_{\mathcal{C}} \left(-\tilde{\mathcal{M}}^i_j \bar{h}^j + S^i \delta(r - r_p(\tau))\right) du\, dv, \tag{5.31}$$

where the $\tilde{\mathcal{M}}^i_j$ include now also the potential term $U^l(r)$ of Eq.(5.38) and the numbers in brackets denote the grid point at which the field is evaluated. The sources are known exactly and can thus be integrated numerically in a straightforward manner; the terms $\tilde{\mathcal{M}}^i_j \bar{h}^j$ can be Taylor-expanded around the centre of $\mathcal{C}$ and then integrated semi-analytically, as we show in Appendix E.

[2]In black hole perturbation theory, the two subsets are sometimes denoted as "polar" and "axial", as perturbations belonging to the first group are invariant under $\phi \to -\phi$, while those belonging to the second are not, and are related to frame-dragging effects.

[3]This conveniently solves the problem of dealing directly with distributional sources. The strategy was proposed for the first time by Lousto and Price [104].

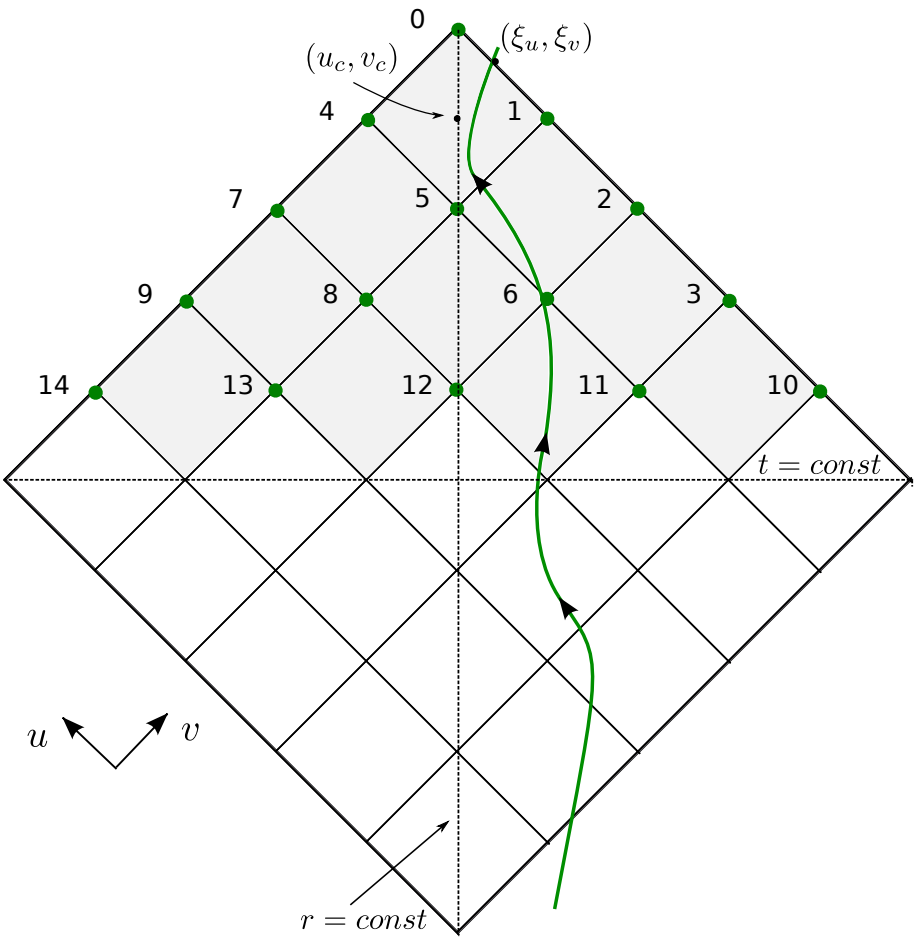

Figure 5.1: Illustration of a portion of the numerical domain of our time-domain code. The green curvy line represents a timelike geodesic crossing the null grid. The numerical scheme used to integrate the field equations over the top cell with vertices $0 - 1 - 4 - 5$ takes input from all the grid points 1-14. Hypersurfaces of constant radius are represented by vertical lines, whereas horizontal lines represent $t = const$ slices.

As the numerical variables $\bar{h}^i$ are only C^0, one has to deal with a non-smooth problem whenever the particle's worldline crosses the integration domain. In [101], this problem was circumvented by defining two different Taylor expansions, one in the region $r > r_p(\tau)$ and one in the region $r < r_p(\tau)$. In our implementation we chose to follow a slightly different strategy. This relies on the fact that the jumps in the $\bar{h}^i$ and their derivatives can be computed analytically, by integrating the field equations along null rays in a neighbourhood of the worldline. To exemplify how this can be done, let us rewrite Eq. (5.29) in the form

$$\left(\partial_{uv} + U^l(r)\right)\bar{h}^i + \mathcal{M}^{i,l}_j \bar{h}^j = \int_{-\infty}^{\infty} \frac{2E}{f^2} S^i \delta(u - u_p(\tau))\delta(v - v_p(\tau))d\tau, \tag{5.32}$$

where we used Eq. (5.1) and the definitions of u, v. First, we write the solution to the field equations in the form $\bar{h}^i = \bar{h}^i_+\theta(r - r_p) + \bar{h}^i_-\theta(r_p - r)$, where a subscript "+" denotes a homogeneous solution valid in the domain $r > r_p(\tau)$ and a subscript "−" denotes a solution valid in the domain $r < r_p(\tau)$. Direct substitution of this expression into (5.32) gives $\bar{h}^i_+ = \bar{h}^i_-$, i.e. in Lorenz gauge the metric is *continuous* across the worldline. Now suppose one wants to compute the junction conditions on the $u-$derivatives of the field variables, i.e. the quantities $[\bar{h}^i_{,u}] := \partial_u\left(\bar{h}^i_+ - \bar{h}^i_-\right)|_{r=r_p}$. This can be achieved by integrating Eq.(5.32) along a null ray $u = u_p$, over an interval $(v_p - \epsilon, v_p + \epsilon)$, with $\epsilon \ll 1$:

$$\begin{aligned}\bar{h}^i_{,u}|^{v_p+\epsilon}_{v_p-\epsilon} + \int_{v_p-\epsilon}^{v_p+\epsilon}\left(U^l(r)\bar{h}^i + \mathcal{M}^{i,l}_j\bar{h}^j\right) = \\ = \int_{v_p-\epsilon}^{v_p+\epsilon} dv \int_{-\infty}^{\infty}\frac{2E}{f^2}S^i\delta(u - u_p(\tau))\delta(v - v_p(\tau))d\tau,\end{aligned} \tag{5.33}$$

which, in the limit $\epsilon \to 0$, gives

$$[\bar{h}^i_{,u}] = \left[2E\frac{S^i}{f^2\dot{u}}\right]_p, \tag{5.34}$$

where we used the facts that all the functions linear in $\bar{h}^i$ are bounded at the particle's location and the metric perturbation is continuous there.

Higher order junction conditions can be similarly computed and this information can be directly incorporated in the finite-difference scheme, as suggested in [105]. In fact, suppose that one wishes to approximate a non-smooth function, say $g(u, v)$, in the neighbourhood of a point (u_c, v_c), knowing that the grid is intersected at the point (ξ_u, ξ_v) by the worldline

(see Fig. 5.1). Then, if the jumps

$$J_{a\,b} := \lim_{\epsilon\to 0}\left(\partial_u^a\partial_v^b g(\xi_u,\xi_v+\epsilon) - \partial_u^a\partial_v^b g(\xi_u,\xi_v-\epsilon)\right)$$

are known, it can be shown that g can be written as a piecewise series

$$g(u,v) = \sum_{a+b=0}^{N-1}\left(\partial_a\partial_b g(u_c,v_c)\frac{(u-u_c)^a(v-v_c)^b}{a!b!} + \right.$$
$$\left. + \left(\theta(v-u-\xi_v+\xi_u) - \theta(v_c-u_c-\xi_v+\xi_u)\right) J_{ab}\frac{(u-\xi_u)^a(v-\xi_v)^b}{a!b!}\right) + O(h^N), \tag{5.35}$$

where N depends on the convergence rate that is being sought (in our case, $N \leq 5$); in [101] one has instead

$$g(u,v) = \sum_{a+b=0}^{N-1}\left(\partial_a\partial_b g^{\pm}(u_c,v_c)\frac{(u-u_c)^a(v-v_c)^b}{a!b!}\right) + O(h^N), \tag{5.36}$$

where $\partial_a\partial_b g^{+}(u_c,v_c)$ are expansion coefficients valid in the $r > r_p(\tau)$ region while $\partial_a\partial_b g^{-}(u_c,v_c)$ are the ones to be used in the $r < r_p(\tau)$ domain. In both cases, the function g and its derivatives at the point (u_c,v_c) need to be determined by numerically solving a suitable linear system of algebraic equations that follows from applying Eq. (5.35) to the grid points $0-14$. It is clear that the use of Eq. (5.35) halves the dimension of the system's unknown variables ($N(N+1)/2$, compared to the $N(N+1)$ required by Eq. (5.36)), and should thus be advantageous from a computational point of view.

Once the field has been computed along the orbit, the local gravitational self-force can be obtained using Eq. (1.14) and subsequently regularised, following the procedure described in Sec. 1.1.3.

5.4 Treatment of non-radiative modes

Typically, the correct initial conditions for Eq. (5.27) are not known, and the simplest choice is to set the field to zero on the initial null surfaces, which will result in a burst of "junk" radiation in the numerical evolution. This does not represent an issue for radiative modes ($\ell > 1$) as in this case the spurious radiation is completely radiated away in the course

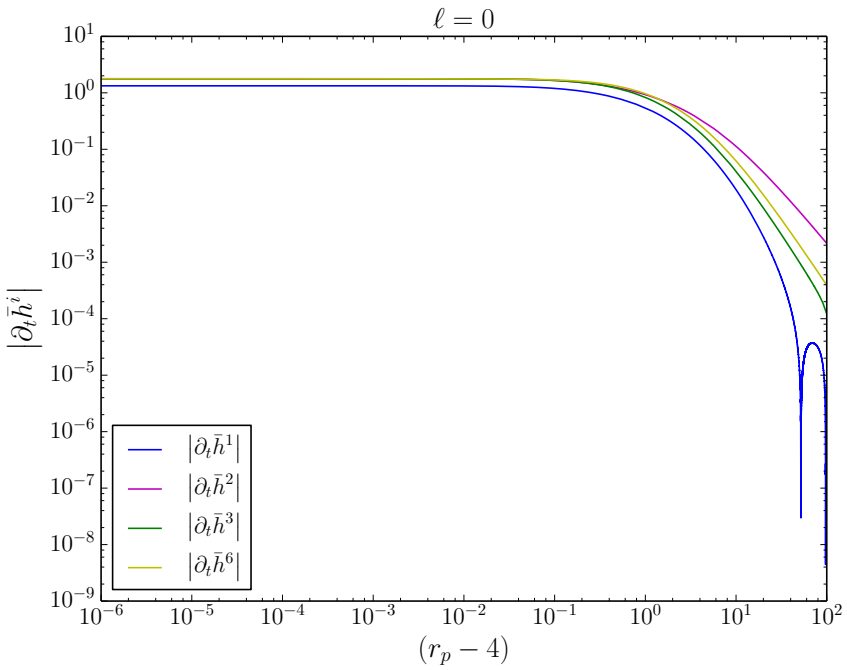

Figure 5.2: Time-derivatives of the monopole, retarded field along an inbound MBMS orbit. In the region $r_p \sim 4$ the physical metric perturbation should approach stationarity: what we observe is instead a solution with constant time-derivatives, which suggests the evolution here is dominated by a linear-in-time homogeneous gauge mode. Note that we set $M = 1$ for convenience.

of the numerical evolution [4]. Furthermore, all the regular, homogeneous gravitational perturbations with $\ell > 1$ are known to decay at late time like $\sim t^{-2\ell+3}$, and thus growing-in-time behaviour are a priori excluded [106]. However, time-dependent instabilities are known to affect the evolution of the modes $\ell = 0, 1$ [35]: in our numerical implementation, we find that the full retarded fields solving the $\ell = 0$ and the $\ell = 1, m = 1$ equations are contaminated by spurious Lorenz-gauge solutions, which are globally regular and exhibit a linear-in-time behaviour (see Fig. 5.2). This issue was extensively explored by Dolan and Barack [102] in the context of the time-evolution of circular orbits [5]. The authors proposed two different approaches to tackle this problem. The first is a numerical filtering procedure: as we will describe in Subsecs. 5.4.1 and 5.4.2, for the modes $\ell = 0$ and $\ell = 1, m = 1$ it is

[4] The issue is problematic only for highly relativistic objects, as junk radiation will closely trail the orbit along its evolution.

[5] The numerical framework used by Dolan is quite different from ours: in fact, it relies on the so-called "puncture scheme", where instead of dealing with the full, retarded metric perturbation, one evolves a regularised field, obtained by subtracting from the full field an analytical approximation of the singular field. Also, while we solve the field equations in $1 + 1$ dimensions, taking advantage of the spherical symmetry of the Schwarzschild background, Dolan's code makes use of a $2 + 1$ scheme, where the field is decomposed in azimuthal m-modes. However, the gauge instabilities we are describing in this section have been observed in several independent self-force codes and appear to be generic features of time-domain evolutions.

possible to find analytical, homogeneous solutions with a linearly growing in time behaviour, on the basis of simple symmetry and regularity arguments. These solutions come with two degrees of freedom that can be fixed using numerical data, provided one can disentangle the physical metric perturbation from any spurious gauge excitation. The task is relatively straightforward whenever the physical metric perturbation is known to be stationary: in this case, any time dependence in the data is a clear signature of homogeneous gauge modes. Along MBMS orbits, the physical perturbation is not, in general, stationary; however, it closely approaches stationarity as the orbit asymptotes to the IBCO. Thus, the numerical filtering technique described above can be applied to our case (and, in general, to any critical unbound orbit).

A complementary approach is that of stabilising the evolution of the field equations, in order to prevent ab initio the excitation of non-physical solutions. A first way to achieve this is that of imposing correct initial conditions, when these are known analytically. We verified that this method can be successfully applied to evolve the monopole equations for an outbound MBMS orbit; however, analytical initial conditions are not known in general, and thus this strategy has a limited domain of applicability. A second approach relies on the use of a generalised Lorenz gauge, i.e. a gauge of the form $\nabla^\alpha \bar{h}_{\alpha\beta} = H_\beta$, where the right hand side is generically different from zero, but such that $H_\beta \to 0$ when $t \gg M$. This method was also tested in [102] with partial, but not complete success and we will not investigate it further in what follows.

5.4.1 Monopole solution

The Lorenz-gauge monopole perturbation sourced by a circular orbit is known analytically [107] and we observed that it provides sufficiently accurate initial conditions for an outbound MBMS: in fact, gauge instabilities are efficiently suppressed.

The same method cannot be applied to an inbound MBMS, which starts off at $r \gg M$, and so we proceeded to apply a numerical filtering technique that will be now described in detail. The gauge metric perturbation contaminating our numerical evolution grows linearly in time, but has a constant trace: We then seek Lorenz-gauge solutions of the form

$$h_{\alpha\beta} = \xi_{\alpha;\beta} + \xi_{\beta;\alpha}, \tag{5.37}$$

where $\xi_\alpha = \partial_\alpha \phi(t, r)$, with $\phi(t, r)$ featuring at most quadratic terms in t. It can be shown

that this choice implies $\partial_\alpha h = 0$ [6] and guarantees that the metric components grow at most linearly in time, consistently with the behaviour of our numerical solution. Our ansatz for $\phi(t, r)$ is the following:

$$\phi(t, r) = a_0 t^2 + \int F(r) dr + tG(r), \tag{5.38}$$

where F and G are two arbitrary functions, to be determined by imposing the Lorenz gauge conditions $\nabla^\alpha \bar{h}_{\alpha\beta} = 0$. Fixing the gauge gives two separate second order differential equations for F and G, which can be solved to give

$$G(r) = c_0 + \frac{c_1}{2} \log(f), \tag{5.39}$$

$$F(r) = \frac{c_2}{r^2 f} + \frac{c_3 r}{f} + \frac{2a_0(8^2 + 12r + 3r^2 + 24\log(-2 + r))}{3r^2 f}, \tag{5.40}$$

where we set $M = 1$ for convenience. The trace of the metric perturbation generated by the potential (5.38) is found to be $h = -4a_0$. We set c_3 to zero to prevent the gauge vector ξ_α from diverging when $r \to \infty$, which will then result in a severe pathological behaviour of the metric at infinity [7]. Further constraints on the free parameters left can be obtained by imposing metric regularity at the horizon. As the Schwarzschild coordinates are ill-behaved at $r = 2$, we require the ingoing Eddington-Finkelstein components of the metric to remain finite as the horizon is approached. The only non-zero components in this case are

$$\begin{aligned} h^{EF}_{vv} &= h_{tt}, \\ h^{EF}_{vr} &= -\frac{h_{tt}}{f} + h_{tr}, \\ h^{EF}_{rr} &= \frac{h_{tt}}{f^2} - 2\frac{h_{tr}}{f} + h_{rr}. \end{aligned}$$

The above components take a finite value at the horizon provided that

$$c_1 = -2h, \quad c_2 = \frac{2}{3}(6c_0 + h(11 + \log 64)).$$

It follows that the non-zero components of the trace-reversed gauge metric perturbation

[6] To see this, note that the Lorenz-gauge conditions implies $\Box\xi_\alpha = 0$, and that $h_{,\alpha} = 2(\Box\phi)_{,\alpha} = 2\Box\xi_\alpha$.

[7] With this choice, our gauge solution will only have $h_{tt} \to const$: this does not constitute a major problem though, as the metric can be "flattened" at infinity by a suitable gauge transformation away from Lorenz, which results in a translation of the asymptotic coordinate time. This observation will be relevant for our calculation of the IBCO frequency shift.

can be written as

$$
\begin{aligned}
h^G_{tt} &= \frac{-a_1 + h\left(r\left(r^3 - r - 4\right) - 4t + 12 + 8\log 2 - 8\log(r-2)\right)}{2r^4}, \\
h^G_{tr} &= \frac{-\frac{a_1}{4} + h(2\log f + t - 4)}{2r(2-r)}, \\
h^G_{rr} &= \frac{(a_1 + 8h\log(r-2))(3-2r) + h(r(-5r - 8t + 36 + 16\log(2)))}{2(r-2)^2 r^2} + \\
&\quad + \frac{12h(t - 3 - \log(4))}{2(r-2)^2 r^2}, \\
h^G_{\phi\phi} &= \frac{a_1 + h(r(r+4) + 4(t - 3 - \log(4))) + 8h\log(r-2)}{2r},
\end{aligned}
\tag{5.41}
$$

where we defined $a_1 := 8c_0$.

We will now describe how to extract a_1 and h from the numerical data. In order to do so, we will look at the metric perturbation and its time-derivatives on a $t = const$ hypersurface along the final whirl of an inbound MBMS, where the metric should be, with a very good approximation, a superposition of the circular orbit solution and of the gauge perturbation (5.41). Numerical experiments suggest that, in order to extract the free parameters a_1, h of the gauge perturbation, it is advantageous to look at the metric in the near-horizon region, as this yields a more accurate fit.

If we denote by r_p the radius of the circular orbit, the metric perturbation sourced by the particle is of the form $h^C_{\alpha\beta} = h^{C,+}_{\alpha\beta}\theta(r - r_p) + h^{C,-}_{\alpha\beta}\theta(r_p - r)$ (we refer the reader to [102] for a thorough discussion of the analytical construction of this solution). To carry out a near-horizon expansion, we only need $h^{C,-}_{\alpha\beta}$: in terms of our evolution variables this reads

$$
\bar{h}^{(1)}_C = \frac{2\sqrt{\pi}(r-2)^3(r+2)(1+\log(2))}{3r^3}, \tag{5.42}
$$

$$
\bar{h}^{(3)}_C = \frac{4\sqrt{\pi}\left(r^3 - 8\right)(1+\log(2))}{3r^2}, \tag{5.43}
$$

$$
\bar{h}^{(6)}_C = -\frac{2\sqrt{\pi}\left(r^3 + 16\right)(1+\log(2))}{3r^2}, \tag{5.44}
$$

with all the other components being identically zero. We then fit our numerical $\bar{h}^{(i)}$ to a solution of the form $\bar{h}^{(i)}_S = \bar{h}^{(i)}_C + \bar{h}^{(i)}_G$, where the $\bar{h}^{(i)}_G$ are obtained from Eq. (5.41) using

the reconstruction formulae given in Appendix A of [101]. The non-zero $\bar{h}^i_S$ are

$$\bar{h}^{(1)}_S = \frac{\sqrt{\pi}}{3r^3}\left[3\left(h\left(8(r-1)(\log 4 - t + 2\log(-2+r)) - 24 + r\left(r^3 - 6r - 8t + 32\right)\right)\right) + \right.$$
$$\left. +2(r-2)^3(r+2)(1+\log(2)) - 6a_1(r-1)\right], \tag{5.45}$$
$$\bar{h}^{(2)}_S = -\frac{2\sqrt{\pi}(\frac{a_1}{4} + 2h\log(r-2) - 2h\log(r) + h(t-4))}{r}, \tag{5.46}$$
$$\bar{h}^{(3)}_S = \frac{2\sqrt{\pi}}{3r^2}\left(3(a_1 + h(r(r+4) + 4(t-3-\log(4))) + 8h\log(r-2)) + \right.$$
$$\left. +2\left(r^3 - 8\right)(1+\log(2))\right), \tag{5.47}$$
$$\bar{h}^{(6)}_S = \frac{\sqrt{\pi}}{3r^2}\left(6a_1 + 3h(r(r(r+2)+8) + 8(t-3-\log(4))) + 48h\log(r-2) + \right.$$
$$\left. -2\left(r^3 + 16\right)(1+\log(2))\right), \tag{5.48}$$

Conveniently, in the limit $r \to 2$, the time-derivatives of the $\bar{h}^{(i)}$ approach a set of constants

$$\lim_{r\to 2}\left(\frac{\partial\bar{h}^{(1)}}{\partial t}, \frac{\partial\bar{h}^{(2)}}{\partial t}, \frac{\partial\bar{h}^{(3)}}{\partial t}, \frac{\partial\bar{h}^{(6)}}{\partial t}\right) = \sqrt{\pi}\,(-h, -h, 2\,h, 2\,h)\,. \tag{5.49}$$

Thus, one can estimate h by fitting the time-derivatives of the numerical metric perturbation; subsequently, the field itself can be used to estimate a_1. Once the spurious gauge mode has been identified, we subtract it from our numerical data. In Fig. 5.3, we show the results of this numerical filtering procedure, for an inbound MBMS orbit evolved with a numerical grid step of $h_s = 0.025$. We fitted the four metric variables $\bar{h}^{(1)}, \bar{h}^{(2)}, \bar{h}^{(3)}, \bar{h}^{(6)}$ independently, in order to have an internal consistency check of our method, and averaged the corresponding values of a_1,h. Our numerically filtered metric could potentially accumulate large errors at late time ($t \gg M$), due to the imperfect estimation of the gauge parameters. To estimate such effects, we compared the values of the field and its derivatives computed at two different resolutions, $h_1 = 0.05$ and $h_2 = 0.025$. We found that the relative differences between the two data sets are typically $\sim 10^{-4}$ for the field and its derivatives, which is acceptable for our purposes.

5.4.2 Dipole solution

When studying the $\ell = 1, m = \pm 1$ mode, one can again take advantage of the background's symmetry properties to write down a parametric form for a generic linear-in-time homogeneous solution. Static solutions of the dipole equations can be straightforwardly obtained by solving once again $\Box\phi = 0$, this time using the ansatz $\phi = F(r)Y^{11}$, and then look-

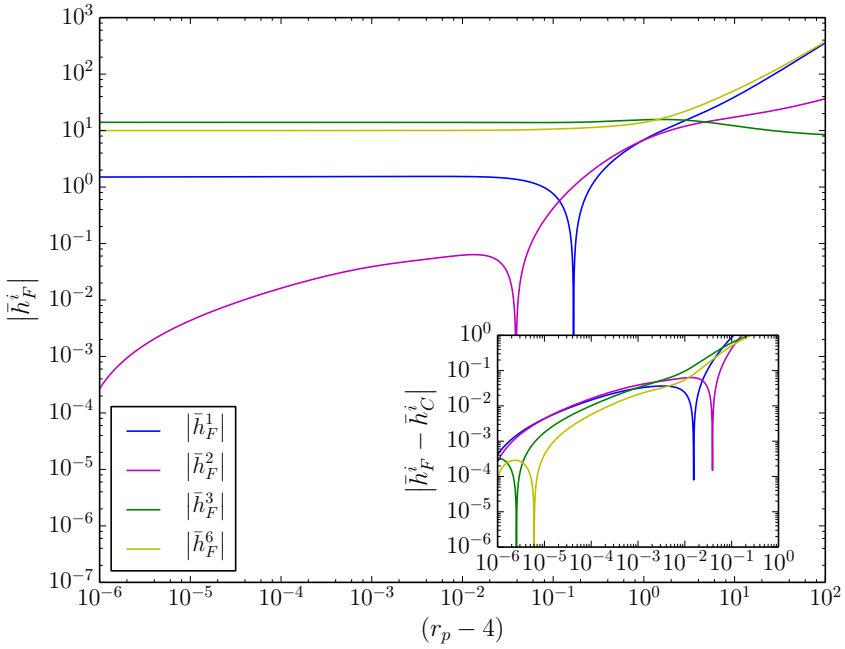

Figure 5.3: Numerical filtering of the monopole solution along an inbound MBMS orbit. The main plot shows our numerical variables, after subtraction of a suitable linear-in-t gauge mode ($\bar{h}^{(i)}_F$). The inset shows the difference between our numerically filtered solution and an exactly circular one. As the orbit approaches circularity, this quantity should converge to zero: however, we observe fluctuations due to the numerical error affecting our fit.

ing at the metric perturbation generated by $\xi_\alpha = \partial_\alpha \phi$. The wave equation admits two independent solutions, $F(r)^+ = c_0(r-1)$, which is regular at the horizon but diverges for $r \to \infty$ and $F(r)^- = c_1(2 + (r-1)\log f)$, which is regular at spatial infinity but diverges at the horizon. One might then try to construct a linear-in-t solution from a potential of the form $\phi = F(r)^+(1 + k_1 t) + F(r)^-(1 + k_2 t)$: however, this fails to produce a globally regular metric perturbation. It turns out that this can be achieved by adding to the ansatz for ξ_μ a term of the form $G(r)\delta^t_\mu Y^{11}$, which corresponds to one of the static homogeneous solutions obtained by Ori [108]. Our full ansatz for ξ_μ will thus be

$$\xi_\mu = \partial_\mu \left(\left(F(r)^+(1 + k_1 t) + F(r)^-(1 + k_2 t) \right) Y^{11} \right) + G(r)\delta^t_\mu Y^{11}. \tag{5.50}$$

Imposing the Lorenz-gauge condition, as well as global regularity, gives $G(r) = -c_1 r f$, $k_1 = \frac{c_1}{2c_0}$, $k_2 = 0$.

It follows that the most general linear-in-t, globally regular Lorenz-gauge solution to the dipole equations reads

$$\begin{aligned}
\bar{h}^{(1)}_G &= -\frac{8c_1}{r^3}, \\
\bar{h}^{(2)}_G &= \frac{2\,c_1(-3+r)}{r}, \\
\bar{h}^{(3)}_G &= -\frac{2\left(2c_0 r + c_1 r t + 2c_1 r \log\left(\frac{r-2}{r}\right) + 4c_1\right)}{r^2}, \\
\bar{h}^{(4)}_G &= 4\,c_1, \\
\bar{h}^{(5)}_G &= \frac{4\left(2c_0 r - 4c_0 + c_1 r t - 4c_1 \log\left(\frac{r-2}{r}\right) + 2c_1 r \log\left(\frac{r-2}{r}\right) - 2c_1 t + 4c_1\right)}{r^2}, \\
\bar{h}^{(6)}_G &= -\frac{2\left(2c_0 r + c_1 r t + 2c_1 r \log\left(\frac{r-2}{r}\right) + 4c_1\right)}{r^2}, \\
\bar{h}^{(7)}_G &= 0,
\end{aligned} \tag{5.51}$$

where c_0, c_1 are two complex parameters.

In analogy with the monopole case, we compare our numerical results in the region $r \sim 4$ to a solution of the form $\bar{h}^{(i)}_S = \bar{h}^{(i)}_C + \bar{h}^{(i)}_G$, where by $\bar{h}^{(i)}_C$ we denote the circular orbit solution, which we computed semi-analytically, following work by Poisson and Detweiler [107]. The construction of a circular orbit solution proceeds as follows: starting from an analytical, asymptotically flat, singular solution to the dipole equations $h^S_{\alpha\beta}$ [109], one numerically calculates the gauge vector ξ_μ such that $h_{\alpha\beta} = h^S_{\alpha\beta} - \xi_{\alpha;\beta} - \xi_{\beta;\alpha}$ is a Lorenz gauge solution, i.e. satisfies $\nabla^\alpha \bar{h}_{\alpha\beta} = 0$. Due to the symmetry of the background, the sought gauge vector

can be written as

$$\xi^m_\mu = \{\xi^m_t(t,r), \xi^m_r(t,r), \xi^m(t,r)\partial_\theta, \xi^m(t,r)\partial_\phi\}\, Y^{11}, \tag{5.52}$$

where the superscript m denotes the sign of the magnetic mode considered ($m = \pm 1$). If one introduces the complex functions $A^m(r), B^m(r), C^m(r)$ defined through

$$\begin{aligned}
\xi^m_t(t,r) &= -\mu E\sqrt{\frac{8\pi}{12}}\, \iota\Omega R \frac{A^m(r)}{r} e^{-\mathrm{sgn}(m)\, i\Omega t},\\
\xi^m_r(t,r) &= -\mathrm{sgn}(m)\, \mu E\sqrt{\frac{8\pi}{12}}\, \frac{B^m(r)}{r-2} e^{-\mathrm{sgn}(m) i\Omega t},\\
\xi^m(t,r) &= -\mathrm{sgn}(m)\, \mu E\sqrt{\frac{8\pi}{12}} \frac{C^m(r)}{r} e^{-\mathrm{sgn}(m) i\Omega t},
\end{aligned}$$

the problem of finding ξ_μ reduces to that of numerically solving a set of ODE's for the unknown functions A^m, B^m, C^m. Once these are known, the corresponding metric variables $\bar{h}^i$ read

$$\begin{aligned}
\bar{h}^{(1)}_C &= \frac{2\sqrt{\frac{2\pi}{3}} E e^{-i(\Omega\, t-\phi)} \left(r\, R\, \Omega^2 A^m(r) + (r-2)\partial_r B^m(r) - B^m(r)\right)}{r},\\
\bar{h}^{(2)}_C &= -\frac{2i\sqrt{\frac{2\pi}{3}} E\Omega e^{-i(\Omega\, t-\phi)} \left(-(r-2)R\partial_r A^m(r) + r_0 A^m(r) + r B^m(r)\right)}{r},\\
\bar{h}^{(3)}_C &= \frac{4\sqrt{\frac{2\pi}{3}} E e^{-i(\Omega\, t-\phi)} (B^m(r) - C^m(r))}{r},\\
\bar{h}^{(4)}_C &= \frac{4i\sqrt{\frac{2\pi}{3}} E\Omega e^{-i(\Omega\, t-\phi)} (R\, A^m(r) - r\, C^m(r))}{r},\\
\bar{h}^{(5)}_C &= \frac{4\sqrt{\frac{2\pi}{3}} E e^{-i(\Omega\, t-\phi)} \left(r B^m(r) + (r-2)\left(r\, \partial_r C^m(r) - 2C^m(r)\right)\right)}{r^2},\\
\bar{h}^{(6)}_C &= \frac{2\sqrt{\frac{2\pi}{3}} E e^{-i(\Omega\, t-\phi)} \left(r^2\, R\, \Omega^2\, A^m(r) + (r-2)\left(B^m(r) - r\, \partial_r B^m(r)\right)\right)}{(r-2)r},
\end{aligned} \tag{5.53}$$

where Ω represents in our case the frequency of the IBCO. In practice, since the physical solution on the whirl has a purely harmonic time-dependence, the linear-in-t gauge mode can be identified by looking at the linear combination $\bar{h}^{(i)} - i/\omega\partial_t \bar{h}^{(i)}$. In fact, this is identically zero on a circular orbit and thus will not encode any information about the physical metric perturbation in the limit $r \to 4$. By fitting our numerical data, we can estimate c_0, c_1, and subsequently subtract the mode of Eq. (5.51) from our full retarded solution. After the subtraction, the field approaches stationarity along the whirl, an indication that our numerical filtering has been successful (see Fig. 5.4). [8]

[8] In analogy with the monopole case, we tried to evolve the dipole equations starting from the semi-

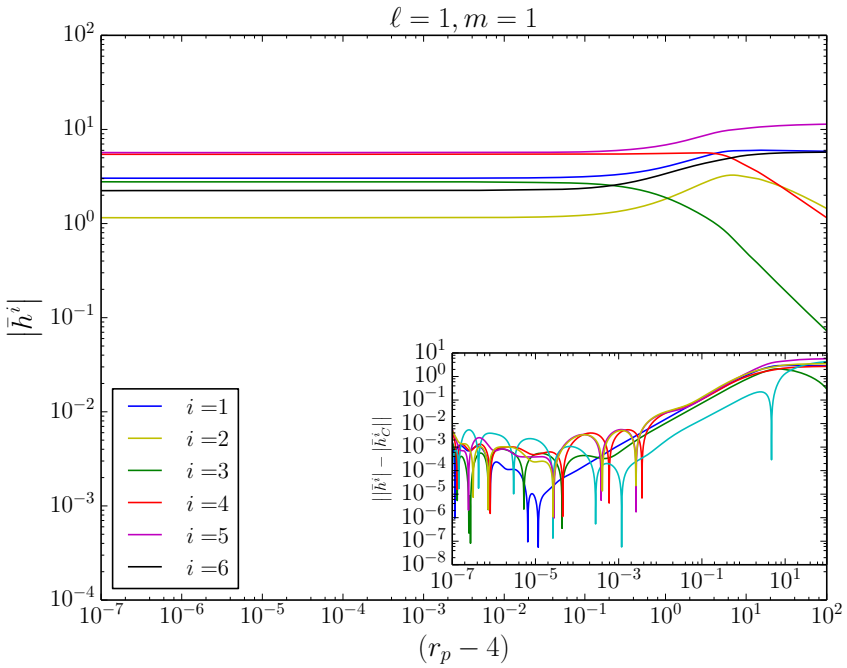

Figure 5.4: Numerical filtering of the dipole mode for an outgoing MBMS orbit. The plot shows the dipole field along the orbit, after subtraction of a gauge mode of the form (5.51), where c_0, c_1 have been extracted from data in the region $10^{-7} \lesssim r_p - 4 \lesssim 10^{-4}$. As shown in the inset, the filtered solution approaches the circular one in the limit $r_p \to 4$.

5.5 Results

We will now provide results obtained by applying the numerical framework described in the previous sections to the study of a MBMS orbit. The data presented in this section have been computed at a maximal resolution of $h_3 = 0.0125M$[9]. We used data at lower resolutions ($h_1 = 0.05M$, $h_2 = 0.025M$) for convergence tests and error estimates. We evolved both an ingoing MBMS orbit starting off at $r = 150M$ and an outgoing one starting from $r = (4 + 10^{-13})M$ and subsequently computed the conservative GSF using Eq.(5.25).

As we explained in Sec.1.1.4, the conservative self-force acting on the particle is obtained by an infinite sum of suitably regularised spherical harmonics modes. It is clear that, in practice, such an infinite sum will be truncated at some $\ell = \ell_{max}$ (in this work, for instance, we take $\ell_{max} = 15$). To account for the contribution of higher modes (the so-called "tail"), we implement a point-wise fitting procedure, following, for instance, [101]. We approximate the infinite sum in Eq.(1.28) as

$$F^{\mu}_{cons} \approx \sum_{l=0}^{\ell_{max}} F^{\mu\ell}_{R} + \sum_{l=\ell_{max}+1}^{\infty} F^{\mu\ell}_{tail}, \tag{5.54}$$

where by $F^{\mu\ell}_{R}$ we denote the conservative, regularised GSF obtained from our numerical data, and by $F^{\mu\ell}_{tail}$ we denote an approximation of the higher modes of $F^{\mu\ell}_{R}$ obtained by fitting the modes $10 \leq \ell \leq 15$ to a function of the form $a_0/(\ell+1/2)^2 + a_1/(\ell+1/2)^4$, where a_0, a_1 are two numerical coefficients, to be determined numerically. Such an expansion, in fact, captures the large-ℓ behaviour of the singular field, as shown in [110]. The tail-fitting leaves one with an error on the GSF of order $\sim \sum_{l=\ell_{max}+1}^{\infty} \ell^{-6} = O(\ell_{max}^{-5})$: given that in our computation $\ell_{max} = 15$, this translates into an absolute error $\sim O(10^{-6})$.

The integrals of Eqs.(5.19)-(5.20) formally extend over an infinite domain, but of course numerical data are available only over a finite range. Therefore, we integrated the GSF along the orbit semi-analytically, as explained below. Denoting by R_{min} and R_{max} the minimum and maximum radii for which we have robust numerical data, we approximate ΔE as follows

$$\Delta E \approx -\int_{R_{max}}^{R_{min}} \tilde{F}_t^{num} \frac{dr_p}{\dot{r_p}} - \int_{\infty}^{R_{max}} \tilde{F}_t^{far} \frac{dr_p}{\dot{r_p}}, \tag{5.55}$$

analytical solutions given in [107], but we could not successfully stabilise our numerical evolution: whether or not this might be achieved remains an open question.

[9] In this section we reintroduce M, for the sake of clarity.

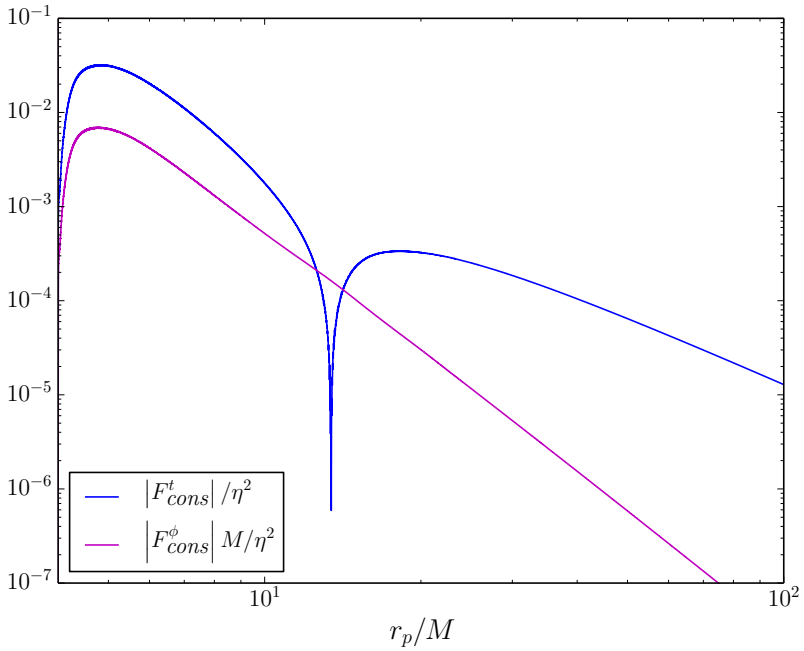

Figure 5.5: The conservative GSF along a MBMS orbit. The plot shows the t and ϕ components of the force (in blue and magenta respectively). As the IBCO is approached, both components tend to zero, in line with Eq.(3.9). In the weak field, the force exhibits a simple power-law behaviour, whose leading order terms are given in Eqs.(5.56)-(5.57).

Here, $\tilde{F}_t^{num}$ denotes a function interpolating among our numerical data for $\tilde{F}_t$ between $R_{min} = (4 + 10^{-6})M$ and $R_{max} = 100M$, while $\tilde{F}_t^{far}$ denotes an extrapolation of the GSF obtained by fitting our data in the range $100M < r < 130M$. Since for the conservative part of the GSF one has $\lim_{r\to R_0} \tilde{F}_{t/\phi} = 0$, we neglect the term $\int_{R_{min}}^{4M} \tilde{F}_{t/\phi} dr_p/\dot{r_p}$: with our choice of $R_{\rm min}$, one can see, using Eq. (3.10), that this produces an error of order $O(10^{-6})$, comparable to the one coming from the large-ℓ tail fitting. We proceed in an analogous way to compute ΔL.

We find that, in the far field, the conservative GSF behaves, at leading order, like the following inverse powers of r:

$$\tilde{F}^{t}_{far} \sim \frac{-1.25}{\tilde{r}^{5/2}} \frac{\eta}{M}, \tag{5.56}$$

$$\tilde{F}^{\phi}_{far} \sim \frac{27.75}{\tilde{r}^{9/2}} \frac{\eta}{M^2}, \tag{5.57}$$

where $\tilde{r} := r/M$. Fig. 5.5 shows the numerical conservative GSF along a MBMS orbit, as a function of the orbital radius.

The last piece of information needed in order to compute the conservative shift to the

IBCO frequency is $\tilde{F}^r(4M)$: we report here the most accurate result we have up to date, which has been computed by Sago [111]:

$$\tilde{F}^r(4M) = -0.00309(3)\frac{\eta}{M}. \tag{5.58}$$

Before proceeding further, we shall return to the observation made in Sec. 5.4 regarding the asymptotic properties of the Lorenz gauge: as we have already mentioned, the tt component of the monopole metric perturbation tend to a constant for $r \to \infty$. For circular orbits, there exists a unique Lorenz-gauge perturbation $h_{\alpha\beta}$ which possesses the correct mass and is regular both at infinity and at the horizon. This solution is such that [107, 112]

$$\lim_{r\to\infty} h_{tt} = -\frac{2\mu}{\sqrt{R_0(R_0-3M)}} := -2\alpha. \tag{5.59}$$

Since a MBMS orbit approaches a circular orbit either in the infinite future or infinite past and the above result is time-independent, we expect the metric sourced by a MBMS orbit to exhibit the same asymptotic behaviour. We verified this statement by examining our data: although our growing-in-time solution is asymptotically flat, the gauge metric perturbation that needs to be subtracted from it (see Eq.(5.41)) is indeed such that $\lim_{r\to\infty} h^G_{tt} = 2\alpha$.

Therefore, in order to obtain the conservative shift to Ω in physical units, i.e. within the class of asymptotically flat gauges, we need to asymptotically "flatten out" our gauge. As explained in [112], this can be achieved by means of a gauge transformation, away from Lorenz gauge, of the form $x^\mu \to x'^\mu = x^\mu + \delta^\mu_t t\alpha$: in fact, this generates a metric perturbation that asymptotically tends to 2α, as can be seen by inspecting Eq. (5.37). It is easy to see that such a gauge transformation shifts the azimuthal frequency $d\phi/dt$ by an amount $-\alpha\Omega_0$. It then follows from Eq.(5.24) that the self-force corrected frequency in an asymptotically flat gauge, which we will denote by Ω_F satisfies

$$\Omega_F^2 = \Omega_0^2\left(1 - \eta + 6\Delta E + 16M\tilde{F}^r(4M)\right), \tag{5.60}$$

where we used the fact that, for a MBMS orbit, $\alpha = 1/2$. We can then evaluate the first-order self-force corrections to the critical angular momentum at fixed energy at infinity and

azimuthal frequency as given by Eqs.(5.22) and (5.24):

$$\delta L(\infty) = -3.22(2)\mu, \tag{5.61}$$

$$\delta\Omega := \Omega_F - \Omega_0 = 0.069(2)\frac{\eta}{M}. \tag{5.62}$$

To estimate the error affecting our results, we compared data computed at two different resolutions ($h_3 = 0.0125M$ and $h_2 = 0.025M$).

5.5.1 IBCO frequency shift: comparison with the first law

We now proceed to compare our result for $\delta\Omega$ with the one obtained using the first law of binary black-hole mechanics. Let us introduce the dimensionless parameter ("invariant mass over distance")

$$x := ((1+\eta)M\Omega)^{2/3}. \tag{5.63}$$

Then the shifts in x and Ω, for a fixed value of an arbitrary orbital parameter B, are related via

$$\delta x(B) = \frac{2}{3}\left(\eta\Omega_0 + \frac{\delta\Omega(B)}{\Omega_0^{1/3}}\right), \tag{5.64}$$

whence it follows, in particular, that

$$\delta\Omega(x) = -\Omega_0\eta. \tag{5.65}$$

We also note that the frequency shift at fixed energy can be computed once the shift at fixed x is known, given that $\delta\Omega(E) = \delta\Omega(x) - \frac{\partial\Omega}{\partial E}\delta E(x)$. For a MBMS orbit, this gives

$$\delta\Omega(E) = -\frac{1}{8M}\left(\eta + 3\delta E(1/4)\right), \tag{5.66}$$

where we used Eq.(5.65), together with $\Omega_0 = 1/(8M)$. Ref. [81] provides an explicit expression for the conservative first-order correction to the binary's (binding) energy, at fixed x, which relies on the use of the first law:

$$\delta E(x) = \frac{z_1(x)}{2} - \frac{1}{3}x\frac{\partial z_1(x)}{\partial x} + \frac{x(7-24x)}{6(1-3x)^{3/2}} + \sqrt{1-3x} - 1, \tag{5.67}$$

where $z_1(x)$ denotes the first-order correction to the redshift variable (see Eq.(3.67)). We extract the value of $z_1(1/4)$ and $dz_1/dx(1/4)$ implementing the fitting procedure described in [41], where knowledge of the metric perturbation along a sequence of circular orbits in the range $1/150 < x < 1/3$ was used to fit $z_1(x)$ to a global analytical model incorporating constraints coming from the post-Newtonian approximation. Combining Eqs. (5.66) and (5.67) we get

$$\delta\Omega(E) = 0.0692008\frac{\eta}{M}, \tag{5.68}$$

which is consistent with our numerical result (Eq.(5.62)). We wish to stress the fact that the agreement obtained here is far from trivial, as the first law has been shown to rigorously apply only in the *weak* field regime, whereas our self-force computation tests the *strong* field one. Furthermore, Eq. (5.68) receives input exclusively from the metric perturbation computed along circular orbits, whereas our numerical result (5.62) rests on an integration of the conservative GSF along a MBMS orbit. Thus, our work provides a strong check of the validity of the first law in the strong field regime.

5.6 Calibration of EOB

We will now explain how our computation can assist in calibrating the EOB model [15]. In the EOB formalism, the two-body problem is replaced by that of a particle of effective mass $m := \mu M/(\mu + M)$, moving in a deformed Schwarzschild metric

$$ds^2_{eff} = -A(r;\nu)dt^2 + \bar{B}(r;\nu)dr^2 + r^2\left(d\theta^2 + \sin\theta^2\, d\phi^2\right), \tag{5.69}$$

where $\nu = \mu M/(\mu + M)^2$ and $A(r;\nu)$ and $\bar{B}(r;\nu)$ are two a priori unspecified functions. The total energy of the system, defined as the sum of the rest masses μ, M plus their binding energy, is given by the EOB Hamiltonian

$$H_{EOB} = (M + \mu)\sqrt{1 + 2\nu\left(\hat{H}_{eff} - 1\right)}, \tag{5.70}$$

where $\hat{H}_{eff} := H_{eff}/m$ represents a (specific) effective Hamiltonian that governs the particle's motion, as we will see below. Its explicit form is

$$\hat{H}_{eff} = \sqrt{A(\hat{r};\nu)\left(1 + \frac{j^2}{\hat{r}^2} + \frac{\hat{p}_r^2}{\bar{B}(r;\nu)} + \hat{Q}(\hat{r},\hat{p}_r)\right)}, \tag{5.71}$$

where we introduced the rescaled quantities $\hat{r} := r/(\mu + M), \hat{p}_r := p_r/m$ (p_r being the effective radial momentum of the particle) and $j := J/(\mu M)$, where J can be identified with the total conserved angular momentum of the system. The function $\hat{Q}(\hat{r},\hat{p}_r) := Q(r,p_r)/m^2$ represents a deformation of the mass-shell condition, defined through

$$0 = m^2 + g^{\mu\nu}_{eff} p_\mu p_\nu + Q(r,p_r), \tag{5.72}$$

and is at least quartic in $\hat{p}_r$. Knowledge of the precise form of the functions $A, \bar{B}$ can be obtained by comparing their expansions, either in $1/\hat{r}$ or ν, with results coming from the post-Newtonian and self-force approximations respectively.

To illustrate how this works, we will review a strategy proposed by Damour [13] to obtain information about the EOB effective metric using a GSF calculation along a MBMS orbit. This is, by definition, a zero-binding-energy orbit and thus $H_{EOB} = (M+\mu)$, whence it follows that $\hat{H}_{eff} = 1$. On the whirl, $\hat{r} \to \hat{r}_{IBCO}$ and $\hat{p}_r \to 0$. Then, using Eq. (5.71), one has $A(\hat{r}_{IBCO};\nu)(1+j^2/\hat{r}^2_{IBCO}) = 1$, as well as $A'(\hat{r}_{IBCO};\nu)+j^2(A'(\hat{r}_{IBCO};\nu)/\hat{r}^2_{IBCO} - 2A(\hat{r}_{IBCO};\nu)/\hat{r}^3_{IBCO}) = 0$, where we denoted with a prime differentiation with respect to $\hat{r}$. It is easy to see that these two conditions imply

$$A^2(\hat{r}_{IBCO};\nu) = A(\hat{r}_{IBCO};\nu) - \hat{r}_{IBCO}\frac{A'(\hat{r}_{IBCO};\nu)}{2}. \tag{5.73}$$

In the limit $\mu \ll M$, ν is a small parameter, and thus one can write $A(\hat{r};\nu) = 1 - 2/\hat{r} + a(\hat{r})\nu + O(\nu^2)$, where $a(\hat{r})$ is an unknown function. Inserting this expansion into Eq.(5.73) gives

$$\frac{4 - \hat{r}_{IBCO}}{\hat{r}^2_{IBCO}} + \frac{\hat{r}_{IBCO}}{2}\, a'(\hat{r}_{IBCO})\nu = 0. \tag{5.74}$$

In the EOB literature results are most often expressed in terms of the inverse distance

$\hat{u} := 1/\hat{r}$. Changing variables in the above equation and using $\hat{u}_{IBCO} = 1/4 + O(\nu)$ gives

$$\hat{u}_{IBCO} = \frac{1}{4}\left(1 + \frac{\nu}{2}\partial_u a(1/4)\right). \tag{5.75}$$

Damour showed that, for a zero-binding-energy orbit, the invariant mass over distance defined in Eq. (5.63) is given by

$$x(u) = u\left(\frac{-\partial_u A(u)}{2}\right)^{1/3}. \tag{5.76}$$

Plugging into the above equation an expansion in ν of $A(u)$ and using (5.75), together with (5.63), the above result can be translated into a shift in the IBCO frequency Ω which, when expressed in an asymptotically flat gauge, reads

$$\Omega_F^2 = \Omega_0^2\left(1 + \nu\left(\partial_u a(1/4) - 2\right)\right). \tag{5.77}$$

Noting that, when $\mu \ll M$, $\nu \sim \eta$, we can compare Eq.(5.77) with Eq.(5.60), obtaining

$$\partial_u a(1/4) = 2\left(1 + \frac{\delta\Omega}{\eta\Omega_0}\right) = 3.10(8). \tag{5.78}$$

We can compare the above result with the one obtained in [41], where a fit for $a(u)$ was computed by interpolating self-force data on unstable circular orbits:

$$\partial_u a(1/4) = 3.10720606064. \quad \text{(Akcay et al.)}$$

The calculation relied on results by Barausse *et al.* [113], which establish a simple relationship between the redshift z and the function $a(u)$, by making use of the first law of binary black-hole mechanics. Our framework does not rely at any point on this law and thus represents a completely independent tool to calibrate the EOB model.

5.6.1 Future directions

An interesting extension of the work presented here would be a computation of $\delta L^{\rm p}_{\rm ADM}$ for a MBMS orbit: however, the task is not as straightforward as it might seem, as the notion of angular momentum is intrinsically ambiguous in General Relativity. In Sec. 3.2 we provided expressions to compute an ADM-like angular momentum under the assumption that, when the two bodies are at an infinite distance, the system can be modelled as a

pair of relativistic point-particles in flat spacetime. We also assumed that the gauge used to carry out our self-force computation could be somehow considered "black-hole-centred" (whereas ADM quantities are computed in a centre-of-mass frame). However, there are several aspects under which the Lorenz gauge appears to violate these assumptions: the metric perturbation is not asymptotically flat and it is not clear a priori where the system's centre of mass lies. Furthermore, the dipole solution for a static particle in Lorenz gauge does not reduce, in the limit $r \to \infty$ to the flat-space solution, as it was pointed out in [114]. We are currently investigating these aspects in order to gain a full understanding of how to convert our result (5.61) into a conserved, gauge-invariant quantity suitable to be compared with Refs. [36, 81].

A possible future application of our numerical framework is the computation of deflection angles $\chi(E_{ADM}, L_{ADM}) := \phi(\tau \to \infty) - \phi(\tau \to -\infty) - \pi$ for hyperbolic-like orbits scattered off Schwarzschild black holes. Elastic scattering of equal-mass black holes in the strong field region has been recently investigated to establish a cross-comparison between EOB and Numerical Relativity [14]. A similar study could be carried out for extreme-mass-ratio binaries, such as the ones modelled by the self-force approximation, once a rigorous method to compute E_{ADM}, L_{ADM} has been established (knowledge of these quantities is in fact necessary to identify in an unambiguous manner an orbit in the perturbative problem).

Chapter 6

Conclusions

We studied the scenario in which a massive particle is thrown into a nearly-extremal Kerr black hole on an equatorial trajectory, working consistently in the first-order self-force approximation, i.e. taking into account all finite-η effects (radiative and other) to one order in η beyond the geodesic approximation. In our work, we focussed on two types of captured orbits near the capture–scatter separatrix: (i) weakly fine-tuned orbits, which execute $O(\ln \eta)$ quasi-circular revolutions below the ISCO prior to falling into the black hole, radiating $O(\eta^2 \ln \eta)$ of gravitational-wave energy in the process; and (ii) strongly fine-tuned orbits, which execute $O(\eta^{-1})$ revolutions and emit $O(\eta)$ of energy. Proceeding under the assumption that the self-force should disfavour overspinning, we focused on orbits coming from infinity, as these appear to threaten the cosmic censorship conjecture in the geodesic approximation. We also restricted our attention to non-spinning bodies, in order to simplify our analysis.

In Sec. 4.1 we found that, within our first-order GSF approximation, any weakly fine-tuned capture leads to a precisely extremal geometry. This implies that "generic" captures produce *sub*-extremal geometries. In Sec. 4.3 we further established that *strong fine-tuning promotes censorship*: all strongly fine-tuned captures produce subextremal geometries. Thus, one can at best reach extremality, using weakly fine-tuned orbits (any such orbit would do), but there is no way of overspinning the black hole. In summary:

> Within the first-order self-force approximation (and excluding deeply bound orbits), *equatorial captures generically result in a subextremal post-capture geometry. One can at best achieve extremality, through weak fine-tuning, but overspinning is not possible.*

That overspinning appears to be possible in the geodesic approximation [55] is simply

an artefact of ignoring important GSF terms that appear *already at leading order* in the relevant overspinning conditions.

We note that the above conclusions were arrived at almost entirely via analytical considerations. We required only two pieces of numerical input, one confirming the boundedness of the extremal limit in Eq. (4.11), and another establishing the bound (4.24) for the flux ratio. Both numerical computations involve only circular geodesic orbits, and neither requires particularly high precision. The above general conclusions are entirely robust with respect to numerical error.

However, it is important to remember that here we have been working strictly within the framework of the first-order GSF approximation, with no control whatsoever over high-order GSF corrections. Since the first-order analysis appeared to allow for an exact saturation of the overspinning condition, higher-order effects may qualitatively change the outcome. A second-order analysis may potentially yield any possible result: that the final geometry is always subextremal, or that overspinning is possible, or (once again) that the black hole can at most be brought to extremality. In that respect, *our first-order GSF analysis—just like the geodesic analysis of Ref. [55]—does not provide a conclusive answer to the question of overspinning.* It is not clear if the question can be fully resolved at second-order or at any other finite order in perturbation theory.

It would be desirable to repeat the calculation of the angular momentum shift $\delta\breve{L}_\infty^{\rm cons}$ using a direct integration of the GSF, via Eq. (3.45). This would eliminate our reliance [in deriving Eq. (3.76)] on the effective Hamiltonian formulation of Refs. [36, 80, 115], which is axiomatic in nature. In fact, an explicit demonstration of agreement between the direct formula (3.45) and redshift formula (3.76) (related by Eq. (3.47)) would constitute an important test of the Hamiltonian formulation.

In Ch. 5 we started developing the computational tools to achieve this. In the simplified context of the Schwarzschild geometry, we provided strong evidence in support of the applicability of the first law of binary black-hole mechanics to the calculation of invariants in the strong field regime. We presented a first numerical computation of the full self-force along marginally bound, marginally stable orbits, i.e. orbits that start off at rest at $r \to \infty$ and asymptote to a marginally stable circular orbit of radius $r = 4M$ either in the infinite future or the infinite past. In particular, we computed for the first time a new strong-field, gauge-invariant quantity, namely the conservative shift to the azimuthal frequency of the innermost bound circular orbit (Eq. (5.62)). This required, in particular, computing the integral of the conservative GSF along a MBMS orbit: the calculation presented here is

thus analogous to the one required in the overspinning problem. We verified that the our numerical result is consistent with the one obtained relying on the first law: the latter only requires knowledge of the metric perturbation along circular orbits and thus the agreement between the two calculations is highly non-trivial.

As we mentioned in Subsec. 5.6.1, work is under way to extract from our numerical data the total conserved angular momentum of a spacetime containing a MBMS orbit. Once a rigorous procedure to do so is in place, our framework could be exploited to calculate new strong-field gauge invariant quantities, such as scattering angles for hyperbolic-like orbits. This would create new possibilities for the the self-force scheme to inform semi-analytical frameworks modelling compact binary systems.

Appendix A

ADM energy and angular momentum

This appendix gives a detailed derivation of Eqs. (3.11) and (3.12). We consider two relativistic point particles in flat space, representing the black hole–particle system at an infinite separation. We are given the two rest masses, M and μ, and the particle's energy $\mu E_\infty (> \mu)$ and angular momentum μL_∞ in a reference frame attached to the mass M. The mass M has an intrinsic spin Ma perpendicular to the orbital plane, and the mass μ is spinless. Our goal is to obtain the system's total energy and angular momentum in a center-of-mass (CoM) frame.

First, we note that, in the limit of infinite separation, both black-hole frame and CoM frame are inertial, and they are related via a simple Lorentz boost. Let $x^\alpha = (t, x, y, z)$ be a Cartesian frame centred at M, so that the spin of M is aligned with the z direction, and the particle's orbit lies in the x–y plane. Denote the four-momenta of μ and M in the black-hole frame by

$$\begin{aligned} p^\alpha_{(\mu)} &= (\mu E_\infty, p^x_{(\mu)}, p^y_{(\mu)}, 0), \\ p^\alpha_{(M)} &= (M, 0, 0, 0). \end{aligned} \tag{A.1}$$

The magnitude of particle's 3-momentum satisfies

$$|\mathbf{p}_{(\mu)}|^2 = (p^x_{(\mu)})^2 + (p^y_{(\mu)})^2 = \mu^2 (E_\infty^2 - 1). \tag{A.2}$$

The CoM system $\tilde{x}^\alpha$ is related to x^α via a Lorentz boost $\Lambda^\alpha{}_\beta$ in the x–y plane. Let $\tilde{p}^\alpha_{(\mu)} = \Lambda^\alpha{}_\beta p^\beta_{(\mu)}$ and $\tilde{p}^\alpha_{(M)} = \Lambda^\alpha{}_\beta p^\beta_{(M)}$ denote the 4-momenta of μ and M in $\tilde{x}^\alpha$. The CoM

condition,

$$\tilde{\mathbf{p}}_{(M)} + \tilde{\mathbf{p}}_{(\mu)} = 0, \tag{A.3}$$

yields two nontrivial equations for the two boost parameters $\beta^x = v^x/c$ and $\beta^y = v^y/c$ (where v^x and v^y are components of the boost velocity). One finds $\beta^i = p^i_{(\mu)}(M + \mu E_\infty)^{-1}$ for $i = x, y$. Thus, using (A.2),

$$\beta = [(\beta^x)^2 + (\beta^y)^2]^{1/2} = \frac{\eta(E_\infty^2 - 1)^{1/2}}{1 + \eta E_\infty}, \tag{A.4}$$

where $\eta = \mu/M$.

Now that we have at hand the boost $\Lambda^\alpha{}_\beta(\beta)$, the relativistic energies of μ and M in the CoM system are obtained as $\tilde{p}^0_{(\mu)} = \Lambda^0{}_\beta p^\beta_{(\mu)}$ and $\tilde{p}^0_{(M)} = \Lambda^0{}_\beta p^\beta_{(M)}$. The sum of these two energies is the total, ADM energy of the system. A short calculation gives

$$E_{\rm ADM} = \tilde{p}^0_{(\mu)} + \tilde{p}^0_{(M)} = M(1 + 2\eta E_\infty + \eta^2)^{1/2}. \tag{A.5}$$

This result is valid for any mass ratio η. For $\eta \ll 1$, an expansion in η through $O(\eta)$ gives Eq. (3.11).

To obtain the total angular momentum in the CoM system, we need first to relate the particle's CoM position $\tilde{\mathbf{x}}_{(\mu)}$ and black hole's CoM position $\tilde{\mathbf{x}}_{(M)}$ to their separation $\mathbf{x}$ in the black-hole frame. This is achieved by solving the CoM condition

$$\tilde{\mathbf{x}}_{(\mu)}\tilde{p}^0_{(\mu)} + \tilde{\mathbf{x}}_{(M)}\tilde{p}^0_{(M)} = 0, \tag{A.6}$$

simultaneously with $|\tilde{\mathbf{x}}_{(\mu)}| + |\tilde{\mathbf{x}}_{(M)}| = |\tilde{\mathbf{x}}|$, where $\tilde{x}^i = \Lambda^i{}_\beta x^\beta$ $(i = x, y)$ is the separation in the CoM frame. The particle's CoM orbital angular momentum is then given by $\tilde{L}_{(\mu)} = \tilde{x}_{(\mu)}\tilde{p}^y_{(\mu)} - \tilde{y}_{(\mu)}\tilde{p}^x_{(\mu)}$, and similarly for the mass M. The total, ADM angular momentum of the system (with respect to the CoM) is the sum of $\tilde{L}_{(\mu)}$, $\tilde{L}_{(M)}$ and the spin angular momentum. A short calculation, using Eqs. (A.2) and (A.4) and the relation $\mu L_\infty = x p^y_{(\mu)} - y p^x_{(\mu)}$, gives

$$L_{\rm ADM} = M\left(a + \mu L_\infty / E_{\rm ADM}\right). \tag{A.7}$$

This is valid for any η. Substituting for $E_{\rm ADM}$ and expanding through $O(\eta^2)$ produces Eq. (3.12).

Appendix B

Radiation from transition to plunge and final plunge

In this appendix we argue that the term $\mathcal{W}^+_{(\mathrm{end})}$ in Eq. (3.39) is subdominant for $\eta, \epsilon \ll 1$ and may therefore be dropped within our leading-order analysis. Recall $\mathcal{W}^+_{(\mathrm{end})} = 2\mathcal{E}^+_{(\mathrm{end})} - \mathcal{L}^+_{(\mathrm{end})}$, where $\mathcal{E}^+_{(\mathrm{end})}$ and $\mathcal{L}^+_{(\mathrm{end})}$ are the energy and angular momentum radiated out to infinity during the transition from adiabatic inspiral along the attractor to a final plunge into the black hole, and during the plunge itself.

Critical orbits may transit into plunge in one of two ways: If the orbit is perfectly fine-tuned, the transition will occur around the location of the ISCO, and will then be similar to the transition at the end of a physical adiabatic inspiral (on a *stable* orbit) that has already been studied in detail [75, 76, 78, 116]. With any less than perfect fine-tuning, the particle will slide off the peak of the effective potential and into the black hole before the ISCO is reached (cf. Fig. 3.1). It is reasonable to expect the former scenario (transition through the ISCO) to yield the maximal radiation output, because (i) orbits linger much longer around the ISCO location, where the potential is very flat, than they do around the peak of the potential; and (ii) the remaining distance to the horizon is maximal when the transition is at the ISCO. Below we start by looking at the "worse case" scenario of transition through the ISCO, and argue that, even in that case, $\mathcal{W}^+_{(\mathrm{end})}$ is negligible in Eq. (3.39). We then also examine the more generic scenario of a transition from an unstable orbit, and, as expected, arrive at a similar conclusion.

B.1 Plunge from the ISCO

For a transition through the ISCO, we use results by Ori and Thorne [75], who studied radiation from the transition regime at the end of a quasi-circular inspiral. An inspection of their analysis reveals that the main results are insensitive to whether the particle arrives the transition regime along stable or unstable orbits. In particular, their equation (3.26) for the deficits in (specific) energy and angular moment over the entire transition should hold in either case. We write it here in the form

$$\begin{aligned} (\Delta L)_{\rm trans} &= -\mathcal{A}(a)\eta^{4/5}, \\ (\Delta E)_{\rm trans} &= -\Omega_{\rm isco}\mathcal{A}(a)\eta^{4/5}, \end{aligned} \tag{B.1}$$

where $\mathcal{A}(a)$ is a certain (positive) function of the spin a only, given explicitly in [75]. These expressions hold for any a, at leading order in $\eta \ll 1$. The factor $\eta^{4/5}$ arises, essentially, from the fact that the transiting orbit spends an amount of proper time $\propto \eta^{-1/5}$ whirling around the ISCO location on a nearly circular orbit [cf. Eq. (3.20) of [75]].

The function $\mathcal{A}(a)$ involves a certain a-dependent dimensionless factor, denoted $\dot{\mathcal{E}}$ in [75] (not to be confused with our $\mathcal{E}^{\pm}$), which describes corrections to the leading-order quadrupole emission formula for circular orbits, and is to be determined numerically. Kesden [76] used numerical data by Hughes (from a code presented in [117]) to estimate, in the near-extremal case, $\dot{\mathcal{E}} \propto \epsilon^{2/3}$, a scaling previously suggested by Chrzanowski [118]. We have confirmed this scaling using much more accurate numerical results by M. van de Meent [119]. We also note that the scaling $\dot{\mathcal{E}} \propto \epsilon^{2/3}$ follows simply from a regularity assumption, namely that $dE/d\tau$ must remain bounded (and nonzero) even in the limit $\epsilon \to 0$: Noting that the Ori-Thorne function $\dot{\mathcal{E}}$ is defined with respect to coordinate time t (not proper time τ), and that $(d\tau/dt)_{\rm isco} \propto \epsilon^{2/3}$, we obtain $\dot{\mathcal{E}} \propto (dE/d\tau)(d\tau/dt)_{\rm isco} \propto \epsilon^{2/3}$. Assuming this scaling, and expanding the remaining a-dependence of $\mathcal{A}(a)$ in ϵ, we obtain, at leading order in ϵ,

$$\begin{aligned} (\Delta L)_{\rm trans} &= -a_0\epsilon^{-2/15}\eta^{4/5}, \\ (\Delta E)_{\rm trans} &= -a_0\Omega_{\rm isco}\epsilon^{-2/15}\eta^{4/5}, \end{aligned} \tag{B.2}$$

with some (positive) numerical coefficient a_0 whose explicit value will not be needed here.

Refs. [76,78] discuss the reason for the non-physical divergence of $(\Delta E)_{\rm trans}$ and $(\Delta L)_{\rm trans}$ when $\epsilon \to 0$ is taken with a fixed η, but this will not concern us here. We are in-

stead interested in the combination $(\Delta W)_{\rm trans} := 2(\Delta E)_{\rm trans} - (\Delta L)_{\rm trans}$, which, noting $\Omega_{\rm isco} = \frac{1}{2} + O(\epsilon^{2/3})$ and keeping only the leading term, reads

$$(\Delta W)_{\rm trans} = b_0 \epsilon^{8/15} \eta^{4/5}, \tag{B.3}$$

with some (positive) numerical coefficient b_0. Assuming the usual balance between the local dissipative GSF and the flux of energy and angular momentum in gravitational waves emitted during the transition, we have $\mathcal{W}^+_{\rm trans} = -\eta (\Delta W)_{\rm trans}$ and thus

$$\mathcal{W}^+_{\rm trans} = -b_0 \epsilon^{8/15} \eta^{9/5}. \tag{B.4}$$

Now examine the magnitude of $\mathcal{W}^+_{\rm trans}$ compared to that of other terms in the censorship condition (3.39). If $\epsilon > \eta$, we have $\epsilon^{8/15}\eta^{9/5} < \epsilon^{7/3}$, which, for $\epsilon \ll 1$, is smaller than the ϵ^2 term in Eq. (3.39). If instead we have $\epsilon \leq \eta$, then $\epsilon^{8/15}\eta^{9/5} \leq \eta^{7/3}$, which, for $\eta \ll 1$, is smaller than the $O(\eta^2)$ terms in that equation. The conclusion is that the contribution to $\mathcal{W}^+_{\rm (end)}$ from the transition regime, $\mathcal{W}^+_{\rm trans}$, is always subdominant in Eq. (3.39) for $\eta, \epsilon \ll 1$.

It remains to assess the contribution to $\mathcal{W}^+_{\rm plng}$ from the final plunge into the hole. In general (when the black hole is not near-extremal) one identifies a final stage, extending smoothly from the transition regime, where radiation reaction is negligible and the orbit plunges into the black hole on a nearly geodesic trajectory [75,77]. The picture may change a little in the near-extremal case, because the radial velocity remains small, $|\dot{r}| \propto \epsilon \ll 1$, all the way to the horizon. This can mean that the conditions that define the transition regime never quite break down before the the horizon is reached. In other words, there is a possibility that the particle crosses the horizon while still in the transition regime.[1]

That possibility can be assessed using Eq. (3.20) of [75], according to which the radial extent $(\Delta r)_{\rm trans}$ of the transition regime, in the near-extremal case, is $\propto \epsilon^{4/15}\eta^{2/5}$, with a coefficient of order unity. This should be compared with the radial distance from the ISCO to the horizon, $\Delta r \simeq (2\epsilon)^{2/3}$. It follows that for ϵ/η smaller than a number of order unity, the transition regime extends to the horizon. In such cases, the amplitude of $\mathcal{W}^+_{\rm trans}$ in Eq. (B.4) serves as an upper bound for the amplitude of $\mathcal{W}^+_{\rm (end)}$, and it follows immediately that the entire term $\mathcal{W}^+_{\rm (end)}$ is negligible in Eq. (3.39).

Let us then consider the case where the transition ends before the horizon is reached, so that a plunge regime is identifiable. In the plunge regime, by definition, the motion is very

[1] This possibility was studied in some detail in Ref. [76]; see, in particular, Fig. 5 therein, in which 'δ' is equivalent to our ϵ^2.

nearly geodesic, and the near-horizon analysis of Mino and Brink [77] should be applicable. Ref. [77] obtained (among other things) an analytic expression for the energy output from the final plunge, by analyzing solutions to Teukolsky equation in the near-horizon, low-frequency, quadrupole approximations. They find (in our notation)[2,3]

$$\mathcal{E}^+_{\rm plung} \propto \eta^2 \epsilon^5 (r_{\rm init} - r_{\rm eh})(E - \Omega_H L)^{-2} \tag{B.5}$$

at leading order in ϵ, where $r_{\rm init}$ is the radius at the start of the plunge, and $r_{\rm eh}$ is the horizon's radius (denoted $R_{\rm eh}$ in the main text). For a plunge following a transition at the ISCO, $r_{\rm init} - r_{\rm eh} = O(\epsilon^{2/3})$ and $E - \Omega_H L = O(\epsilon)$, giving $\mathcal{E}^+_{\rm plung} = O(\eta^2 \epsilon^{11/3})$. Thus $\mathcal{E}^+_{\rm plung}$ is strongly suppressed at small ϵ. Since the motion is nearly circular even during the plunge, we have $\mathcal{L}^+_{\rm plung} \simeq \Omega^{-1} \mathcal{E}^+_{\rm plung} \simeq 2\mathcal{E}^+_{\rm plung}$ and the radiated angular momentum is similarly suppressed. The combination $\mathcal{W}^+_{\rm plung} := 2\mathcal{E}^+_{\rm plung} - \mathcal{L}^+_{\rm plung}$ is even more strongly suppressed at small ϵ, and clearly contributes negligibly to $\mathcal{W}^+_{\rm (end)}$.

In conclusion, we have found that, for a transition through the ISCO, $\mathcal{W}^+_{\rm (end)} = \mathcal{W}^+_{\rm trans} + \mathcal{W}^+_{\rm plunge} \simeq \mathcal{W}^+_{\rm trans}$ is always negligible in Eq. (3.39) for $\eta, \epsilon \ll 1$. That radiation from the transition to plunge should have a negligible effect on the conditions for overspinning was previously suggested by Kesden [76] and Harada and Kimura [78].

B.2 Plunge from an unstable circular orbit

This scenario is rather different from—and much simpler than—a transition through the ISCO. As the orbit is perturbed away from unstable equilibrium, its subsequent evolution is almost immediately controlled by the "geosedic" radial force (proportional to the derivative of the effective potential), and back-reaction corrections become negligible. Let us state this point more precisely. Suppose $r = r_{\rm end}$ is the radius at which the particle leaves the attractor (for concreteness, this may be chosen as the radius of the last turning point along the attractor). Note that the radial acceleration due to the geodesic potential is $\propto (r - r_{\rm end})$, with a coefficient of order unity [since the second derivative of the effective potential at $r_{\rm end}$ is of $O(\epsilon^0)$]. Since $r_{\rm end} - r_{\rm eh} = O(\epsilon)$, the magnitude of the geodesic radial acceleration is of $O(\epsilon)$ throughout much of the plunge. This should be compared with the magnitude of

[2] See Eq. (4.3) of [77], noting their κ is $\sqrt{2}\,\epsilon$ in our notation. The discussion following that equation seems to ignore the ϵ dependence implicit in the factors $\exp[-\kappa(T - t_0)/r_+] \sim (r_{\rm init} - r_+)/r_+$ and $(E - \Omega_H L)$.

[3] It is not clear to us whether the low-frequency and quadrupole approximations, introduced in [77] to enable analytic calculation, are justifiable for near-horizon orbits in the near-extremal case (where the dimensionless angular velocity is $\sim 1/2$). We prefer to regard the form of Eq. (B.5) as indicative only, but this should suffice for our purpose.

the radial self-acceleration, which is of $O(\eta\epsilon)$.[4] We may *define* the onset of plunge as the point where the geodesic acceleration takes over from the GSF in controlling the motion; this happens near a radius $r = r_{\rm plng}$ satisfying $r_{\rm plng} - r_{\rm end} = O(\eta\epsilon)$. For $r \lesssim r_{\rm plng}$, the motion is governed by the geodesic equation of motion (2.3) to a good approximation.

We wish to bound the magnitude of $\mathcal{W}^{+}_{\rm (end)}$ sufficiently well to show that it contributes negligibly in Eq. (3.39). Let us first consider the contribution to $\mathcal{W}^{+}_{\rm (end)}$ from the pre-plunge orbital segment $r_{\rm plng} \leq r \leq r_{\rm end}$. The proper-time interval along this segment is $\Delta\tau \sim (r_{\rm end} - r_{\rm plng})/\dot{r} = O(\eta^0\epsilon^0)$ (at most), since $\dot{r} = O(\eta\epsilon)$ along the attractor, where the evolution is driven by radiation reaction. Hence, the change experienced by the specific energy and angular momentum along this segment is $\Delta E \simeq \Omega\Delta L = O(\eta)$. Recalling $\Omega = 1/2 + O(\epsilon)$, this gives $\Delta W = O(\epsilon\eta)$ and thus a contribution of $O(\epsilon\eta^2)$ to $\mathcal{W}^{+}_{\rm (end)}$, negligible compared to the $O(\eta^2)$ terms in Eq. (3.39).

Next consider the contribution to $\mathcal{W}^{+}_{\rm (end)}$ from the plunge segment $r_{\rm eh} \leq r < r_{\rm plng}$. Using the geodesic equation of motion (2.3), one finds that the proper-time interval along that segment is $\propto \ln[(r_{\rm end} - r_{\rm eh})/(r_{\rm end} - r_{\rm plng})] \sim \ln\eta$. The corresponding change in specific energy is $\Delta E = O(\eta \ln\eta)$. Since the radial velocity remains small, $\dot{r} = O(\epsilon)$, throughout the entire plunge, we have $\Delta L \simeq \Omega^{-1}\Delta E$, giving $\Delta W = O(\epsilon\eta\log\eta)$ and a contribution of $O(\epsilon\eta^2\log\eta)$ to $\mathcal{W}^{+}_{\rm (end)}$. Once again, this is negligible compared to the $O(\eta^2)$ terms in Eq. (3.39), assuming only $\epsilon \ll 1/|\ln\eta|$.

We conclude that, whether the plunge from the attractor occurs at the ISCO or earlier, the term $\mathcal{W}^{+}_{\rm (end)}$ in Eq. (3.39) is always sub-dominant and negligible for $\epsilon, \eta \ll 1$. Within our approximation, the energy the particle carries with it as it crosses the horizon is the energy with which it has left the attractor.

[4] This can be seen in one of two ways. First, by noting that the shift in the radial location of the unstable equilibrium due to the GSF is of $O(\epsilon\eta)$ [see the discussion below Eq. (3.15)]; and, second, by using the regularity argument presented below Eq. (3.22) to show that F^r must be $\propto \epsilon$ (in addition to being $\propto \eta^2$).

Appendix C

Metric decomposition: basis of tensor harmonics

We provide here explicit expressions for the basis of tensor harmonics appearing in Eq. (5.28):

$$Y^1_{\alpha\beta} = \frac{1}{\sqrt{2}} \begin{pmatrix} 1 & 0 & 0 & 0 \\ 0 & f^{-2} & 0 & 0 \\ 0 & 0 & 0 & 0 \\ 0 & 0 & 0 & 0 \end{pmatrix} Y^{l\,m}, \quad Y^2_{\alpha\beta} = \frac{f^{-1}}{\sqrt{2}} \begin{pmatrix} 0 & 1 & 0 & 0 \\ 1 & 0 & 0 & 0 \\ 0 & 0 & 0 & 0 \\ 0 & 0 & 0 & 0 \end{pmatrix} Y^{l\,m},$$

$$Y^3_{\alpha\beta} = \frac{1}{\sqrt{2}} \begin{pmatrix} f & 0 & 0 & 0 \\ 0 & -f^{-1} & 0 & 0 \\ 0 & 0 & 0 & 0 \\ 0 & 0 & 0 & 0 \end{pmatrix} Y^{l\,m}, \quad Y^4_{\alpha\beta} = \frac{r}{\sqrt{2l(l+1)}} \begin{pmatrix} 0 & 0 & \partial_\theta & \partial_\phi \\ 0 & 0 & 0 & 0 \\ \partial_\theta & 0 & 0 & 0 \\ \partial_\phi & 0 & 0 & 0 \end{pmatrix} Y^{l\,m},$$

$$Y^5_{\alpha\beta} = \frac{r\,f^{-1}}{\sqrt{2l(l+1)}} \begin{pmatrix} 0 & 0 & 0 & 0 \\ 0 & 0 & \partial_\theta & \partial_\phi \\ 0 & \partial_\theta & 0 & 0 \\ 0 & \partial_\phi & 0 & 0 \end{pmatrix} Y^{l\,m}, \quad Y^6_{\alpha\beta} = \frac{r^2}{\sqrt{2}} \begin{pmatrix} 0 & 0 & 0 & 0 \\ 0 & 0 & 0 & 0 \\ 0 & 0 & 1 & 0 \\ 0 & 0 & 0 & s^2 \end{pmatrix} Y^{l\,m},$$

$$Y^7_{\alpha\beta} = \frac{r^2}{\sqrt{2\lambda\,l(l+1)}} \begin{pmatrix} 0 & 0 & 0 & 0 \\ 0 & 0 & 0 & 0 \\ 0 & 0 & D_2 & D_1 \\ 0 & 0 & D_1 & -s^2 D_2 \end{pmatrix} Y^{l\,m},$$

$$Y^{8}_{\alpha\beta} = \frac{r}{\sqrt{2l(l+1)}} \begin{pmatrix} 0 & 0 & s^{-1}\partial_\phi & -s\partial_\theta \\ 0 & 0 & 0 & 0 \\ s^{-1}\partial_\phi & 0 & 0 & 0 \\ -s\partial_\theta & 0 & 0 & 0 \end{pmatrix} Y^{l\,m},$$

$$Y^{9}_{\alpha\beta} = \frac{r}{\sqrt{2l(l+1)}} \begin{pmatrix} 0 & 0 & \frac{\partial_\phi}{s} & -s\partial_\theta \\ 0 & 0 & 0 & 0 \\ \frac{\partial_\phi}{s} & 0 & 0 & 0 \\ -s\partial_\theta & 0 & 0 & 0 \end{pmatrix} Y^{l\,m},$$

$$Y^{10\,lm}_{\alpha\beta} = \frac{r^2}{\sqrt{2\lambda l(l+1)}} \begin{pmatrix} 0 & 0 & 0 & 0 \\ 0 & 0 & 0 & 0 \\ 0 & 0 & \frac{D_1}{s} & -s\,D_2 \\ 0 & 0 & -s\,D_2 & -s\,D_1 \end{pmatrix} Y^{l\,m},$$

where $\lambda := (l+2)(l-1)$, $s := \sin\theta$, $D_1 := 2(\partial_\theta - \cot\theta)\partial_\phi$ and $D_2 := \partial_{\theta\theta} - \cot\theta\partial_\theta - s^{-2}\partial_{\phi\phi}$. The functions $r, f(r) = (1-2M/r)$ were introduced to guarantee regularity at infinity and at the horizon of the numerical variables $\bar{h}^{i,l\,m}$.

The coefficients $a^{(i)l}$ in Eq. (5.28) read

$$a^{(i)l} = \frac{1}{\sqrt{2}} \times \begin{cases} 1, & i = 1,2,3,6, \\ [l(l+1)]^{-1/2}, & i = 4,5,8,9, \\ [\lambda l(l+1)]^{-1/2}, & i = 7,10. \end{cases} \tag{C.1}$$

Appendix D

Coupling terms and sources in the field equations

We provide here the coupling terms and sources appearing in Eq.(5.29), as given in [101]. In what follows, a prime will denote differentiation with respect to r, so that $f' = 2M/r^2$.

The coupling terms $\mathcal{M}^{i,l}_{j}\bar{h}^{j,lm}$ read (we will omit the indices l, m for the sake of brevity):

$$\mathcal{M}^{1}_{j}\bar{h}^{j} = \frac{\partial}{\partial r^*}\left(\frac{1}{2}ff'\bar{h}^3\right) + \frac{(r-4M)f}{2r^3}(\bar{h}^1 - \bar{h}^5) - \frac{(r^2-10Mr+20M^2)f}{2r^4}\bar{h}^3 + \\ - \frac{(r-6M)f^2}{2r^3}\bar{h}^6, \tag{D.1}$$

$$\mathcal{M}^{2}_{j}\bar{h}^{j} = \frac{\partial}{\partial r^*}\left(\frac{1}{2}ff'\bar{h}^3\right) + \frac{\partial}{\partial v}\left[f'(\bar{h}^2 - \bar{h}^1)\right] - \frac{3Mf}{r^3}\bar{h}^1 + \frac{(r+2M)f}{2r^3}\bar{h}^2 + \\ + \frac{(3r-8M)Mf}{r^4}\bar{h}^3 - \frac{f^2}{2r^2}\bar{h}^4 + \frac{ff'}{2r}\bar{h}^5 + \frac{f^2f'}{r}\bar{h}^6, \tag{D.2}$$

$$\mathcal{M}^{3}_{j}\bar{h}^{j} = -\frac{f}{2r^2}\left[\bar{h}^1 - \bar{h}^5 - \left(1-\frac{4M}{r}\right)\left(\bar{h}^3 + \bar{h}^6\right)\right], \tag{D.3}$$

$$\mathcal{M}^{4}_{j}\bar{h}^{j} = \frac{\partial}{\partial v}\left[\frac{f'}{2}(\bar{h}^4 - \bar{h}^5)\right] - \frac{l(l+1)f}{2r^2}\bar{h}^2 - \frac{Mf}{2r^3}\bar{h}^4 - \frac{2Mf}{r^3}\bar{h}^5 - \frac{l(l+1)ff'}{4r}\bar{h}^6 + \frac{ff'}{4r}\bar{h}^7, \tag{D.4}$$

$$\mathcal{M}^{5}_{j}\bar{h}^{j} = \frac{f}{r^2}\left[\left(1-\frac{9M}{2r}\right)\bar{h}^5 - \frac{1}{2}l(l+1)\left(\bar{h}^1 - f\bar{h}^3\right) + \frac{1}{2}\left(1-\frac{3M}{r}\right)\left(l(l+1)\bar{h}^6 - \bar{h}^7\right)\right], \tag{D.5}$$

$$\mathcal{M}^6_j\bar{h}^j = -\frac{f}{2r^2}\left[\bar{h}^1 - \bar{h}^5 - \left(1-\frac{4M}{r}\right)\left(\bar{h}^3+\bar{h}^6\right)\right], \tag{D.6}$$

$$\mathcal{M}^7_j\bar{h}^j = -\frac{f}{2r^2}\left(\bar{h}^7+\lambda\,\bar{h}^5\right), \tag{D.7}$$

$$\mathcal{M}^8_j\bar{h}^j = \frac{\partial}{\partial v}\left[\frac{f'}{2}(\bar{h}^8-\bar{h}^9)\right] - \frac{Mf}{2r^3}\bar{h}^8 - \frac{2Mf}{r^3}\bar{h}^9 + \frac{Mf}{2r^3}\bar{h}^{10}, \tag{D.8}$$

$$\mathcal{M}^9_j\bar{h}^j = \frac{f}{r^2}\left(1-\frac{9M}{2r}\right)\bar{h}^9 - \frac{f}{2r^2}\left(1-\frac{3M}{r}\right)\bar{h}^{10}, \tag{D.9}$$

$$\mathcal{M}^{10}_j\bar{h}^j = -\frac{f}{2r^2}\left(\bar{h}^{10}+\lambda\,\bar{h}^9\right). \tag{D.10}$$

Below we give the source terms appearing on the right hand side of Eq.(5.29). E and L denote the particle's energy and angular momentum and a subscript p indicates that the corresponding quantities need to be evaluated along the worldline. Y^{lm} are the standard spherical harmonics and an asterisk denotes complex conjugation.

$$S^1 = \frac{4\pi f_{\rm p}^2}{E r_{\rm p}^3}\left(2E^2r_{\rm p}^2 - f_{\rm p}r_{\rm p}^2 - L^2 f_{\rm p}\right)Y^*_{lm}(\pi/2,\phi_{\rm p}), \tag{D.11}$$

$$S^2 = -\frac{8\pi f_{\rm p}^2}{r_{\rm p}}u^r Y^*_{lm}(\pi/2,\phi_{\rm p}), \tag{D.12}$$

$$S^3 = \frac{4\pi}{E r_{\rm p}^3}f_{\rm p}^2(r_{\rm p}^2+L^2)Y^*_{lm}(\pi/2,\phi_{\rm p}), \tag{D.13}$$

$$S^4 = \frac{8\pi i m f_{\rm p}^2 L}{r_{\rm p}^2}Y^*_{lm}(\pi/2,\phi_{\rm p}), \tag{D.14}$$

$$S^5 = -\frac{8\pi i m f_{\rm p}^2 u^r L}{r_{\rm p}^2 E}Y^*_{lm}(\pi/2,\phi_{\rm p}), \tag{D.15}$$

$$S^6 = \frac{4\pi f_{\rm p}^2 L^2}{r_{\rm p}^3 E}Y^*_{lm}(\pi/2,\phi_{\rm p}), \tag{D.16}$$

$$S^7 = \left[l(l+1)-2m^2\right]S^6, \tag{D.17}$$

$$S^8 = \frac{8\pi f_{\rm p}^2 L}{r_{\rm p}^2}Y^*_{lm,\theta}(\pi/2,\phi_{\rm p}), \tag{D.18}$$

$$S^9 = -\frac{8\pi f_{\rm p}^2 u^r L}{r_{\rm p}^2 E}Y^*_{lm,\theta}(\pi/2,\phi_{\rm p}), \tag{D.19}$$

$$S^{10} = \frac{8\pi i m f_{\rm p}^2 L^2}{r_{\rm p}^3 E}Y^*_{lm,\theta}(\pi/2,\phi_{\rm p}). \tag{D.20}$$

Appendix E

Semi-analytical integration of piece-wise continuous series

Let us suppose that the field equations are being integrated on a cell crossed by the particle as shown in Fig. E.1. The orbit enters and leaves the cell from two different $u = const$ lines, splitting the integration domain in two regions: if we denote by $r_p(\tau)$ the orbit's position, then one has $r > r_p(\tau)$ in the L region and $r < r_p(\tau)$ in the R region. Eq.(5.35) contains terms of the form $\sim (u-u_0)^a (v-v_0)^b$ which need to be integrated separately in the two domains. In the L region:

$$I_L := \int_{v_\gamma(u)}^{v_c+h} \int_{u_c-h}^{u_c+h} (u-u_0)^a \, (v-v_0)^b \, du \, dv = P(v_c+h; x_0) - NI(x_0), \tag{E.1}$$

where $x_0 := (u_0, v_0)$, and we introduced

$$P(x; x_0) := \frac{\left((h-u_0+u_c)^{a+1} - (-h-u_0+u_c)^{a+1}\right)(x-v_0)^{b+1}}{(a+1)(b+1)}, \tag{E.2}$$

as well as

$$NI(x_0) := \int_{u_c-h}^{u_c+h} (u-u_0)^a \, \frac{(v_\gamma(u)-v_0)^{b+1}}{b+1} du. \tag{E.3}$$

In the R region a similar calculation returns $I_R = NI(x_0) - P(v_c-h; x_0)$. As one of the Heaviside functions in Eq.(5.35) is sensitive to the position of the cell's centre, one needs to consider two distinct cases, i.e. $(u_c, v_c) \in L$ and $(u_c, v_c) \in R$. Denoting by g_{ab} the terms

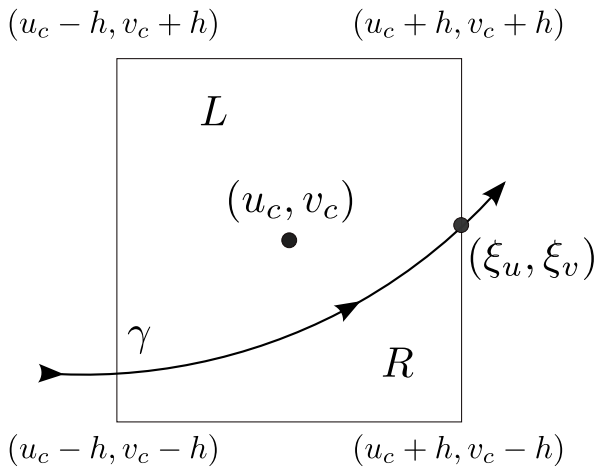

Figure E.1: Grid cell crossed by a worldline: the particle enters the cell from a $u = u_c - h$ line and leaves from a $u = u_c + h$ line. There are three more configurations that need to be taken into account in the numerical implementation: in fact, the orbit could 1) enter from a $u = u_c - h$ line and leave from a $v = v_c + h$ line; 2) enter from a $v = v_c - h$ line and leave from a $v = v_c + h$ one; 3) enter from a $v = v_c - h$ line and leave from a $u = u_c + h$. Other configurations are forbidden as they would violate causality.

appearing between brackets in Eq.(5.35), the integration of g_{ab} over the cell $\mathcal{C}$ gives

$$\int_{\mathcal{C}} g_{ab} du\, dv = \partial_a \partial_b g^{\pm}(u_c, v_c)\, h^{a+b+2} \frac{(1+(-1)^a)\left(1+(-1)^b\right)}{(a+1)(b+1)} + J_{ab}\left(P(v_c \mp h, \xi) - NI(\xi)\right), \tag{E.4}$$

where by ξ we denote the particle's position at the time where the orbit leaves the cell, and in $P(v_c \mp h, \xi)$ the upper sign refers to the case $(u_c, v_c) \in L$ and the lower to the case $(u_c, v_c) \in R$. The integral $NI(\xi)$ needs to be approximated numerically and, to achieve fourth-order convergence, the truncation error on the approximation has to be at most $O(h^6)$. In our implementation, we approximate $NI(\xi)$ using Boole's rule, which gives a $O(h^7)$ truncation error. Similar expressions can be obtained for the remaining configurations, where the orbit either leaves or enter the cell from a $v = const$ line.

Bibliography

[1] B. P. Abbott *et al.*, "Observation of gravitational waves from a binary black hole merger," *Phys. Rev. Lett.*, vol. 116, p. 061102, Feb 2016.

[2] B. D. Lackey and L. Wade, "Reconstructing the neutron-star equation of state with gravitational-wave detectors from a realistic population of inspiralling binary neutron stars," *Phys. Rev. D*, vol. 91, p. 043002, Feb 2015.

[3] J. R. Gair, *Gravitational Wave Astrophysics: Proceedings of the Third Session of the Sant Cugat Forum on Astrophysics*, ch. The Scientific Potential of Space-Based Gravitational Wave Detectors, pp. 225–243. Springer International Publishing, 2015.

[4] M. Wade, J. D. E. Creighton, E. Ochsner, and A. B. Nielsen, "Advanced LIGO's ability to detect apparent violations of the cosmic censorship conjecture and the no-hair theorem through compact binary coalescence detections," *Phys. Rev. D*, vol. 88, p. 083002, Oct 2013.

[5] L. Barack and C. Cutler, "Using LISA extreme-mass-ratio inspiral sources to test off-Kerr deviations in the geometry of massive black holes," *Phys. Rev. D*, vol. 75, p. 042003, Feb 2007.

[6] K. Glampedakis and S. Babak, "Mapping spacetimes with LISA: inspiral of a test body in a 'quasi-Kerr' field," *Classical and Quantum Gravity*, vol. 23, no. 12, p. 4167, 2006.

[7] J. R. Gair, C. Li, and I. Mandel, "Observable properties of orbits in exact bumpy spacetimes," *Phys. Rev. D*, vol. 77, p. 024035, Jan 2008.

[8] R. Geroch, "Multipole moments. ii. curved space," *Journal of Mathematical Physics*, vol. 11, no. 8, 1970.

[9] E. Barausse and T. P. Sotiriou, "Perturbed Kerr black holes can probe deviations from general relativity," *Phys. Rev. Lett.*, vol. 101, p. 099001, Aug 2008.

[10] B. P. Abbott *et al.*, "Tests of general relativity with GW150914." arXiv:1602.03841 [gr-qc].

[11] J. L. Friedman, K. Uryū, and M. Shibata, "Thermodynamics of binary black holes and neutron stars," *Phys. Rev. D*, vol. 65, p. 064035, 2002.

[12] A. Le Tiec, L. Blanchet, and B. F. Whiting, "The first law of binary black hole mechanics in General Relativity and post-Newtonian theory," *Phys. Rev. D*, vol. 85, p. 064039, 2012.

[13] T. Damour, "Gravitational self-force in a Schwarzschild background and the effective one-body formalism," *Phys. Rev. D*, vol. 81, p. 024017, Jan 2010.

[14] T. Damour, F. Guercilena, I. Hinder, S. Hopper, A. Nagar, and L. Rezzolla, "Strong-field scattering of two black holes: Numerics versus analytics," *Phys. Rev. D*, vol. 89, p. 081503, Apr 2014.

[15] A. Buonanno and T. Damour, "Effective one-body approach to general relativistic two-body dynamics," *Phys. Rev. D*, vol. 59, p. 084006, Mar 1999.

[16] R. Geroch and J. Traschen, "Strings and other distributional sources in general relativity," *Phys. Rev. D*, vol. 36, pp. 1017–1031, Aug 1987.

[17] Y. Mino, M. Sasaki, and T. Tanaka, "Gravitational radiation reaction to a particle motion," *Phys. Rev. D*, vol. 55, pp. 3457–3476, Mar 1997.

[18] T. C. Quinn and R. M. Wald, "Energy conservation for point particles undergoing radiation reaction," *Phys. Rev. D*, vol. 60, p. 064009, 1999.

[19] E. Poisson, A. Pound, and I. Vega, "The motion of point particles in curved spacetime," *Living Rev. Rel.*, vol. 14, pp. 1–162, 2011.

[20] A. I. Harte, "Motion in classical field theories and the foundations of the self-force problem." arXiv:1405.5077 [gr-qc].

[21] S. L. Detweiler and B. F. Whiting, "Self-force via a Green's function decomposition," *Phys. Rev.*, vol. D67, p. 024025, 2003.

[22] A. Pound, "Motion of small objects in curved spacetimes: An introduction to gravitational self-force," *Fund. Theor. Phys.*, vol. 179, pp. 399–486, 2015.

[23] S. E. Gralla and R. M. Wald, "A rigorous derivation of gravitational self-force," *Class. Quant. Grav.*, vol. 25, p. 205009, 2008.

[24] A. Pound, "Self-consistent gravitational self-force," *Phys. Rev. D*, vol. 81, p. 024023, 2010.

[25] A. I. Harte, "Mechanics of extended masses in general relativity," *Class. Quant. Grav.*, vol. 29, no. 5, p. 055012, 2012.

[26] A. Pound, "Second-order perturbation theory: Problems on large scales," *Phys. Rev. D*, vol. 92, p. 104047, Nov 2015.

[27] L. Barack and A. Ori, "Gravitational self-force and gauge transformations," *Phys. Rev. D*, vol. 64, p. 124003, Oct 2001.

[28] L. Barack, "Gravitational self force in extreme mass-ratio inspirals," *Class. Quant. Grav.*, vol. 26, p. 213001, 2009.

[29] L. Barack and A. Ori, "Gravitational self-force on a particle orbiting a Kerr black hole," *Phys. Rev. Lett.*, vol. 90, p. 111101, Mar 2003.

[30] B. Wardell and N. Warburton, "Applying the effective-source approach to frequency-domain self-force calculations: Lorenz-gauge gravitational perturbations," *Phys. Rev. D*, vol. 92, p. 084019, Oct 2015.

[31] A. Heffernan, A. Ottewill, and B. Wardell, "High-order expansions of the Detweiler-Whiting singular field in Kerr spacetime," *Phys. Rev. D*, vol. 89, p. 024030, Jan 2014.

[32] A. Pound, C. Merlin, and L. Barack, "Gravitational self-force from radiation-gauge metric perturbations," *Phys. Rev. D*, vol. 89, p. 024009, 2014.

[33] L. Barack and N. Sago, "Beyond the geodesic approximation: Conservative effects of the gravitational self-force in eccentric orbits around a Schwarzschild black hole," *Phys. Rev. D*, vol. 83, p. 084023, Apr 2011.

[34] S. R. Dolan, N. Warburton, A. I. Harte, A. Le Tiec, B. Wardell, and L. Barack, "Gravitational self-torque and spin precession in compact binaries," *Phys. Rev. D*, vol. 89, p. 064011, Mar 2014.

[35] L. Barack and N. Sago, "Gravitational self-force correction to the innermost stable circular orbit of a Schwarzschild black hole," *Phys. Rev. Lett.*, vol. 102, p. 191101, May 2009.

[36] S. Isoyama, L. Barack, S. R. Dolan, A. Le Tiec, H. Nakano, A. G. Shah, T. Tanaka, and N. Warburton, "Gravitational self-force correction to the innermost stable circular equatorial orbit of a Kerr black hole," *Phys. Rev. Lett.*, vol. 113, p. 161101, 2014.

[37] S. R. Dolan, P. Nolan, A. C. Ottewill, N. Warburton, and B. Wardell, "Tidal invariants for compact binaries on quasicircular orbits," *Phys. Rev. D*, vol. 91, p. 023009, Jan 2015.

[38] T. Hinderer and F. E. E. *Phys. Rev. D*, vol. 78, p. 064028, 2008.

[39] S. Detweiler, "Consequence of the gravitational self-force for circular orbits of the Schwarzschild geometry," *Phys. Rev. D*, vol. 77, p. 124026, Jun 2008.

[40] N. K. Johnson-McDaniel, A. G. Shah, and B. F. Whiting, "Experimental mathematics meets gravitational self-force," *Phys. Rev. D*, vol. 92, p. 044007, Aug 2015.

[41] S. Akcay, L. Barack, T. Damour, and N. Sago, "Gravitational self-force and the effective-one-body formalism between the innermost stable circular orbit and the light ring," *Phys. Rev. D*, vol. 86, p. 104041, 2012.

[42] L. Barack and N. Sago, "Gravitational self-force on a particle in circular orbit around a Schwarzschild black hole," *Phys. Rev. D*, vol. 75, p. 064021, Mar 2007.

[43] J. R. Oppenheimer and H. Snyder, "On continued gravitational contraction," *Phys. Rev.*, vol. 56, pp. 455–459, Sep 1939.

[44] S. W. Hawking and G. F. R. Ellis, *The Large Scale Structure of Space-Time*. Cambrige University Press, 1973.

[45] R. Geroch, "What is a singularity in general relativity?," *Annals of Physics*, vol. 48, pp. 526–540, 1968.

[46] R. Penrose, "Gravitational Collapse: the Role of General Relativity," *Rivista del Nuovo Cimento*, vol. 1, p. 242, 1969.

[47] M. Dafermos, "Stability and instability of the Cauchy horizon for the spherically symmetric Einstein-Maxwell-scalar field equations," *Ann. of Math.*, vol. 158, pp. 875–928, 2003.

[48] P. Yodzis, H.-J. Seifert, and H. Müller zum Hagen, "On the occurrence of naked singularities in general relativity," *Comm. Math. Phys.*, vol. 34, no. 2, pp. 135–148, 1973.

[49] M. W. Choptuik, "Universality and scaling in gravitational collapse of a massless scalar field," *Phys. Rev. Lett*, vol. 70, p. 9, 1993.

[50] D. Christodoulou, "The instability of naked singularities in the gravitational collapse of a scalar field," *Ann. of Math.*, vol. 149, pp. 183–217, 1999.

[51] S. Klainerman, "Cosmic censorship and other great mathematical challenges of general relativity," 2009.

[52] R. Wald, "Gravitational collapse and cosmic censorship." arXiv:gr-qc/9710068.

[53] R. Wald, "Gedanken experiments to destroy a black hole," *Ann. Phys.*, vol. 82, p. 548, 1974.

[54] V. E. Hubeny, "Overcharging a Black Hole and Cosmic Censorship," *Phys. Rev. D*, vol. 59, p. 064013, 1999.

[55] T. Jacobson and T. P. Sotiriou, "Over-spinning a black hole with a test body," *Phys. Rev. Lett.*, vol. 103, p. 141101, 2009.

[56] A. Saa and R. Santarelli, "Destroying a near-extremal Kerr-Newman black hole," *Phys. Rev. D*, vol. 84, p. 027501, 2011.

[57] S. Isoyama, N. Sago, and T. Tanaka, "Cosmic censorship in overcharging a Reissner-Nordström black hole via charged particle absorption," *Phys. Rev. D*, vol. 84, p. 124024, 2011.

[58] P. Zimmerman, I. Vega, E. Poisson, and R. Haas, "Self-force as a cosmic censor," *Phys. Rev. D*, vol. 87, p. 041501, Feb 2013.

[59] P. Zimmerman and E. Poisson, "Gravitational self-force in nonvacuum spacetimes," *Phys. Rev. D*, vol. 90, p. 084030, 2014.

[60] T. M. Linz, J. L. Friedman, and A. G. Wiseman, "Combined gravitational and electromagnetic self-force on charged particles in electrovac spacetimes," *Phys. Rev. D*, vol. 90, p. 084031, 2014.

[61] E. Barausse, V. Cardoso, and G. Khanna, "Test bodies and naked singularities: is the self-force the cosmic censor?," *Phys. Rev. Lett.*, vol. 105, p. 261102, 2010.

[62] E. Barausse, V. Cardoso, and G. Khanna, "Testing the Cosmic Censorship Conjecture with point particles: the effect of radiation reaction and the self-force," *Phys. Rev. D*, vol. 84, p. 104006, 2011.

[63] U. Ruangsri, S. J. Vigeland, and S. A. Hughes, "Gyroscopes orbiting black holes: A frequency-domain approach to precession and spin-curvature coupling for spinning bodies on generic Kerr orbits," 2015.

[64] L. M. Burko and G. Khanna, "Self-force gravitational waveforms for extreme and intermediate mass ratio inspirals. ii. importance of the second-order dissipative effect," *Phys. Rev. D*, vol. 88, p. 024002, Jul 2013.

[65] L. M. Burko and G. Khanna, "Self-force gravitational waveforms for extreme and intermediate mass ratio inspirals. iii. spin-orbit coupling revisited," *Phys. Rev. D*, vol. 91, p. 104017, May 2015.

[66] K. Glampedakis and D. Kennefick, "Zoom and whirl: Eccentric equatorial orbits around spinning black holes and their evolution under gravitational radiation reaction," *Phys. Rev. D*, vol. 66, p. 044002, 2002.

[67] J. M. Bardeen, W. H. Press, and S. A. Teukolsky, "Rotating black holes: locally nonrotating frames, energy extraction, and scalar synchrotron radiation," *Astrophys. J.*, vol. 178, p. 347, 1972.

[68] T. Jacobson, "Where is the extremal Kerr ISCO?," *Classical and Quantum Gravity*, vol. 28, no. 18, p. 187001, 2011.

[69] L. M. Burko, A. I. Harte, and E. Poisson, "Mass loss by a scalar charge in an expanding universe," *Phys. Rev. D*, vol. 65, p. 124006, May 2002.

[70] S. Detweiler, "Consequence of the gravitational self-force for circular orbits of the Schwarzschild geometry," *Phys. Rev. D*, vol. 77, p. 124026, Jun 2008.

[71] E. E. Flanagan, S. A. Hughes, and U. Ruangsri, "Resonantly enhanced and diminished strong-field gravitational-wave fluxes," *Phys. Rev. D*, vol. 89, p. 084028, 2014.

[72] C. Gundlach, S. Akcay, L. Barack, and A. Nagar, "Critical phenomena at the threshold of immediate merger in binary black hole systems: The extreme mass ratio case," *Phys. Rev. D*, vol. 86, p. 084022, Oct 2012.

[73] W. Israel, "Third law of black-hole dynamics: A formulation and proof," *Phys. Rev. Lett.*, vol. 57, pp. 397–399, 1986.

[74] G. Chirco, S. Liberati, and T. P. Sotiriou, "Gedanken experiments on nearly extremal black holes and the third law," *Phys. Rev. D*, vol. 82, p. 104015, Nov 2010.

[75] A. Ori and K. S. Thorne, "Transition from inspiral to plunge for a compact body in a circular equatorial orbit around a massive, spinning black hole," *Phys. Rev. D*, vol. 62, p. 124022, 2000.

[76] M. Kesden, "Transition from adiabatic inspiral to plunge into a spinning black hole," *Phys. Rev. D*, vol. 83, p. 104011, 2011.

[77] Y. Mino and J. Brink, "Gravitational radiation from plunging orbits: Perturbative study," *Phys. Rev. D*, vol. 78, p. 124015, 2008.

[78] T. Harada and M. Kimura, "Collision of an object in the transition from adiabatic inspiral to plunge around a Kerr black hole," *Phys. Rev. D*, vol. 84, p. 124032, 2011.

[79] D. Kennefick, "Stability under radiation reaction of circular equatorial orbits around Kerr black holes," *Phys. Rev. D*, vol. 58, p. 064012, 1998.

[80] S. Isoyama, R. Fujita, A. Le Tiec, H. Nakano, N. Sago, and T. Tanaka. in preparation.

[81] A. Le Tiec, E. Barausse, and A. Buonanno, "Gravitational self-force correction to the binding energy of compact binary systems," *Phys. Rev. Lett.*, vol. 108, p. 131103, Mar 2012.

[82] L. Blanchet, A. Buonanno, and A. Le Tiec, "First law of mechanics for black hole binaries with spins," *Phys. Rev. D*, vol. 87, p. 024030, Jan 2013.

[83] S. E. Gralla and A. Le Tiec, "Thermodynamics of a black hole with moon," *Phys. Rev. D*, vol. 88, p. 044021, Aug 2013.

[84] A. G. Shah, J. L. Friedman, and T. S. Keidl, "Extreme-mass-ratio inspiral corrections to the angular velocity and redshift factor of a mass in circular orbit about a Kerr black hole," *Phys. Rev. D*, vol. 86, p. 084059, 2012.

[85] M. van de Meent and A. G. Shah, "Metric perturbations produced by eccentric equatorial orbits around a Kerr black hole," 2015.

[86] M. van de Meent, "A numerical solver for the Teukolsky equation." (in preparation).

[87] R. M. Wald, "Construction of solutions of gravitational, electromagnetic, or other perturbation equations from solutions of decoupled equations," *Phys. Rev. Lett.*, vol. 41, pp. 203–206, Jul 1978.

[88] S. E. Gralla, A. P. Porfyriadis, and N. Warburton, "Particle on the Innermost Stable Circular Orbit of a Rapidly Spinning Black Hole," 2015.

[89] C. Merlin, *Gravitational self-force from curvature scalars.* PhD thesis, University of Southampton, `http://eprints.soton.ac.uk/384183/1.hasCoversheetVersion/Cesar%20Gonzalez%20thesis.pdf`, 2015.

[90] E. Newman and R. Penrose, "An approach to gravitational radiation by a method of spin coefficients," *Journal of Mathematical Physics*, vol. 3, no. 3, 1962.

[91] P. L. Chrzanowski, "Vector potential and metric perturbations of a rotating black hole," *Phys. Rev. D*, vol. 11, pp. 2042–2062, Apr 1975.

[92] J. Cohen and L. Kegeles, "Space-time perturbations," *Physics Letters A*, vol. 54, no. 1, pp. 5 – 7, 1975.

[93] B. F. Whiting and L. R. Price, "Metric reconstruction from weyl scalars," *Classical and Quantum Gravity*, vol. 22, no. 15, p. S589, 2005.

[94] A. G. Shah, T. S. Keidl, J. L. Friedman, D.-H. Kim, and L. R. Price, "Conservative, gravitational self-force for a particle in circular orbit around a Schwarzschild black hole in a Radiation Gauge," *Phys. Rev.*, vol. D83, p. 064018, 2011.

[95] M. Sasaki and T. Nakamura, "A class of new perturbation equations for the Kerr geometry," *Physics Letters A*, vol. 89, no. 2, pp. 68 – 70, 1982.

[96] T. S. Keidl, A. G. Shah, J. L. Friedman, D.-H. Kim, and L. R. Price, "Gravitational Self-force in a Radiation Gauge," *Phys. Rev.*, vol. D82, no. 12, p. 124012, 2010. [Erratum: Phys. Rev.D90,no.10,109902(2014)].

[97] R. Fujita and H. Tagoshi, "New numerical methods to evaluate homogeneous solutions of the Teukolsky equation," *Prog. Theor. Phys.*, vol. 112, pp. 415–450, 2004.

[98] S. Mano, H. Suzuki, and E. Takasugi, "Analytic solutions of the Teukolsky equation and their low frequency expansions," *Prog. Theor. Phys.*, vol. 95, pp. 1079–1096, 1996.

[99] S. Mano and E. Takasugi, "Analytic solutions of the Teukolsky equation and their properties," *Prog. Theor. Phys.*, vol. 97, pp. 213–232, 1997.

[100] M. Van de Meent. in preparation.

[101] L. Barack and N. Sago, "Gravitational self-force on a particle in eccentric orbit around a Schwarzschild black hole," *Phys. Rev. D*, vol. 81, p. 084021, Apr 2010.

[102] S. R. Dolan and L. Barack, "Self-force via m-mode regularization and 2+1D evolution. iii. gravitational field on Schwarzschild spacetime," *Phys. Rev. D*, vol. 87, p. 084066, 2013.

[103] L. Barack and C. O. Lousto, "Perturbations of Schwarzschild black holes in the lorenz gauge: Formulation and numerical implementation," *Phys. Rev. D*, vol. 72, p. 104026, Nov 2005.

[104] C. O. Lousto and R. H. Price, "Understanding initial data for black hole collisions," *Phys. Rev. D*, vol. 56, pp. 6439–6457, Nov 1997.

[105] C. Markakis and L. Barack, "High-order difference and pseudospectral methods for discontinuous problems." arXiv:1406.4865v1.

[106] L. Barack, "Late time decay of scalar, electromagnetic, and gravitational perturbations outside rotating black holes," *Phys. Rev. D*, vol. 61, p. 024026, Dec 1999.

[107] S. Detweiler and E. Poisson, "Low multipole contributions to the gravitational self-force," *Phys. Rev. D*, vol. 69, p. 084019, Apr 2004.

[108] A. Ori, "Harmonic-gauge dipole metric perturbations for weak-field circular orbits in Schwarzschild spacetime," *Phys. Rev. D*, vol. 70, p. 124027, Dec 2004.

[109] F. J. Zerilli, "Gravitational field of a particle falling in a Schwarzschild geometry analyzed in tensor harmonics," *Phys. Rev. D*, vol. 2, pp. 2141–2160, Nov 1970.

[110] A. Heffernan, A. Ottewill, and B. Wardell, "High-order expansions of the detweiler-whiting singular field in Schwarzschild spacetime," *Phys. Rev. D*, vol. 86, p. 104023, Nov 2012.

[111] N. Sago. (private communication).

[112] N. Sago, L. Barack, and S. Detweiler, "Two approaches for the gravitational self-force in black hole spacetime: Comparison of numerical results," *Phys. Rev. D*, vol. 78, p. 124024, Dec 2008.

[113] E. Barausse, A. Buonanno, and A. Le Tiec, "Complete nonspinning effective-one-body metric at linear order in the mass ratio," *Phys. Rev. D*, vol. 85, p. 064010, Mar 2012.

[114] A. Ori, "Harmonic-gauge dipole metric perturbations for weak-field circular orbits in Schwarzschild spacetime," *Phys. Rev. D*, vol. 70, p. 124027, Dec 2004.

[115] A. L. Tiec, "First Law of Mechanics for Compact Binaries on Eccentric Orbits," 2015.

[116] A. Buonanno and T. Damour, "Transition from inspiral to plunge in binary black hole coalescences," *Phys. Rev. D*, vol. 62, p. 064015, 2000.

[117] S. A. Hughes, "Evolution of circular, nonequatorial orbits of Kerr black holes due to gravitational-wave emission," *Phys. Rev. D*, vol. 61, p. 084004, 2000.

[118] P. L. Chrzanowski, "Applications of metric perturbations of a rotating black hole: distortion of the event horizon," *Phys. Rev. D*, vol. 13, pp. 806–818, 1976.

[119] M. van de Meent. (private communication).